

**Spectroscopic Studies on Refolding of Reduced and Mutant Lysozymes, and
Collagen/Dentin Crosslinking**

By

WEIYING ZHU

B.S., Peking University, Beijing, China, 2006

M.S., University of Illinois at Chicago, Chicago, US, 2011

THESIS

Submitted as partial fulfillment of the requirements
for the degree of Doctor of Philosophy in Chemistry
in the Graduate College of the
University of Illinois at Chicago, 2016

Chicago, Illinois

Defense Committee:

Timothy A. Keiderling, Chair and Advisor

Lawrence W. Miller

Leslie Wo-Mei Fung

Scott A. Shippy

Ana Bedran-Russo, College of Dentistry

This thesis is dedicated to my parents, Wanming Zhu and Xiaolan Zhu, and my wife
Guannan Li, without whom it would never have been accomplished

ACKNOWLEDGEMENT

I would like to thank my Ph.D advisor and mentor Dr. Timothy A. Keiderling for the great opportunity to pursue my Ph.D research in his lab, for his invaluable scientific and intellectual guidance and inspiration throughout my Ph.D studies. I am very grateful for his support, caring advice, and constant patience, which have allowed me to overcome the major challenges to my work.

I would also like to express my thank to my dissertation committee members, Dr. Lawrence W. Miller, Dr. Leslie Wo-Mei Fung, Dr. Scott A. Shippy and Dr. Ana Bedran-Russo, for their support and guidance on my research plan and critical evaluation of this work.

I would like to thank my labmates, Ning Ge, Ling Wu, Heng Chi, Ge Zhang, Martin, Ahmed, Anjan Roy and Fernando Tobias for their friendship and help in my research.

TABLE OF CONTENTS

<u>CHAPTER</u>	<u>PAGE</u>
1. INTRODUCTION	1
1.1 PROTEIN STRUCTURE AND ITS DETERMINATION	1
1.2 PROTEIN FOLDING	8
1.3 THE ROLE OF DISULFIDE BONDS ON PROTEIN FOLDING	12
1.4 SURFACTANT MICELLES AND LIPID VESICLES	14
1.5 THESIS STRUCTURE	17
2. MATERIAL PREPARATIONS AND SPECTROSCOPIC METHODS	18
2.1 ELECTRONIC CIRCULAR DICHROISM (ECD)	18
2.1.1 <i>Theory for Electronic Circular Dichroism</i>	18
2.1.2 <i>ECD of Proteins and Peptides</i>	19
2.1.3 <i>ECD Instrument and Measurements</i>	22
2.2 STOPPED-FLOW MEASUREMENTS.....	23
2.3 FLUORESCENCE SPECTROSCOPY	25
2.4 UV-VIS SPECTROSCOPY.....	25
2.5 ATTENUATED TOTAL REFLECTANCE FOURIER TRANSFORM INFRARED (ATR-FTIR).....	26
3. INTERACTION OF REDUCED LYSOZYME WITH SURFACTANTS: DISULFIDE EFFECTS ON REFORMED PROTEIN STRUCTURE IN MICELLES	28
3.1 INTRODUCTION	28
3.2 EXPERIMENTAL	32
3.2.1 <i>Materials</i>	32
3.2.2 <i>CMC measurement of surfactants</i>	34
3.2.3 <i>CD measurements</i>	39
3.2.4 <i>Fluorescence</i>	39
3.2.5 <i>Stopped-flow measurements</i>	39
3.2.6 <i>Lysozyme activity assay</i>	40
3.3 RESULTS AND DISCUSSION	41
3.3.1 <i>The refolding of reduced HEWL with anionic surfactant micelles</i>	41
3.3.2 <i>The interaction of reduced HEWL with cationic and zwitterionic surfactant micelles</i>	53
3.3.3 <i>The folding of OSS mutant HEWL with anionic and cationic surfactant micelles</i>	57
3.3.4 <i>The refolding of helical structure in reduced HEWL induced with trifluoroethanol (TFE)</i>	57
3.3.5 <i>Thermal stability studies on the refolded state of reduced HEWL in</i>	

<i>surfactant micelles</i>	62
3.3.6 <i>Stopped-flow kinetic study of the refolding of reduced HEWL with surfactant micelles</i>	64
3.3.7 <i>Comparison with refolding of denatured/reduced HEWL by dilution and reformation of disulfide bonds</i>	71
3.4 CONCLUSION	72
3.4.1 <i>Interaction of reduced HEWL in surfactant micelles</i>	72
3.4.2 <i>The role of disulfide bonds on the folding pathway of HEWL</i>	74
4. REFOLDING OF REDUCED AND MUTANT LYSOZYMES IN VESICLES. IMPACT OF DISULFIDE EFFECTS ON REFOLDING EQUILIBRIA AND DYNAMICS	75
4.1 INTRODUCTION	75
4.2 EXPERIMENTAL	76
4.2.1 <i>Materials</i>	76
4.2.2 <i>Lipid vesicles preparation</i>	77
4.2.3 <i>CD measurements</i>	78
4.2.4 <i>Fluorescence</i>	78
4.2.5 <i>Stopped-flow measurements</i>	79
4.2.6 <i>Attenuated Total Reflectance Fourier Transform Infrared (ATR-FTIR)</i>	79
4.3 RESULTS AND DISCUSSION	80
4.3.1 <i>Refolding of reduced HEWL with various lipid vesicles</i>	80
4.3.2 <i>Refolding of HEWL mutants with DMPG vesicles</i>	96
4.3.3 <i>Thermal stability studies</i>	104
4.3.4 <i>Orientation of protein structures in the lipid bilayer</i>	106
4.3.5 <i>Stopped-flow kinetic studies of reduced HEWL refolding with DMPG vesicles</i>	108
4.3.6 <i>Comparison with micelle refolding</i>	111
4.4 CONCLUSION	114
4.4.1 <i>Effects of charges, hydrophobicity and membrane packing</i>	114
4.4.2 <i>Micelles and vesicles as mimics of membrane</i>	116
4.4.3 <i>Role of disulfide bonds on protein folding</i>	117
5. SPECTROSCOPIC STUDY ON COLLAGEN-COLLAGEN INTERACTIONS MEDIATED BY PLANT-DERIVED PROANTHOCYANIDINS	119
5.1 INTRODUCTION	119
5.2 EXPERIMENTAL	121
5.2.1 <i>Materials</i>	121
5.2.2 <i>Fluorescence analysis</i>	121
5.2.3 <i>ATR-FTIR analysis</i>	122
5.3 RESULTS	124
5.3.1 <i>Fluorescence results</i>	124
5.3.2 <i>ATR-FTIR analysis</i>	125
5.4 DISCUSSION	133

5.5 CONCLUSION.....	139
CITED LITERATURE.....	140
APPENDIX.....	147
VITA	149

LIST OF SCHEMES

<u>SCHEME</u>	<u>PAGE</u>
Scheme 3-1. Proposed mechanism for refolding of reduced HEWL, showing the possibility of multiple intermediates.....	68

LIST OF TABLES

<u>TABLE</u>	<u>PAGE</u>
Table 3-1. Measured cmc of surfactants in 20 mM phosphate buffer at pH 4.6	35
Table 3-2. Stopped-flow kinetic parameters from ECD and fluorescence for reduced HEWL mixing with SDS and DTAC	67
Table 4-1. Stopped-flow kinetic parameters from ECD and fluorescence for reduced HEWL mixing with 5 mM DMPG vesicles.....	110

LIST OF FIGURES

<u>FIGURES</u>	<u>PAGE</u>
Figure 1-1. The ϕ , ψ angles in a polypeptide chain.....	3
Figure 1-2. Ramachandran Plot for protein secondary structures.....	4
Figure 1-3. Protein Structure: from primary to quaternary structure.....	6
Figure 1-4. The “folding funnel” free energy landscape scheme.....	10
Figure 1-5. Coupling of disulfide bond formation and conformational folding.....	13
Figure 1-6. Structure of surfactant micelle and lipid vesicle.....	15
Figure 2-1. CD spectra for representative protein secondary structures.....	20
Figure 2-2. A simple scheme for stopped-flow system setup.....	24
Figure 3-1. The structure of native HEWL.....	31
Figure 3-2. Schematic representations of the structures of surfactants.....	33
Figure 3-3. Absorbance spectra of BZA in SDS (a) and absorbance of BZA as a function of concentration of SDS (b) , DTAC (c) , C ₁₂ SO ₃ (d) and C ₁₀ SO ₃ (e)	38
Figure 3-4. The mass spectra of (a) oxidized and (b) reduced lysozyme.....	42
Figure 3-5. (a) Far-UV CD spectra of native HEWL and reduced HEWL, and with addition of different concentrations of SDS at pH 4.6. (b) Calculated secondary structure fractions.....	43
Figure 3-6. (a) Fluorescence spectra of native HEWL and reduced HEWL, and with addition of different concentrations of SDS. (b) Variation of the integrated fluorescence intensity and peak position with addition of SDS.....	44
Figure 3-7. Comparison of effects on native HEWL, (a) ECD and (b) fluorescence spectra of native HEWL and HEWL with addition of SDS and DTAC.....	46
Figure 3-8. Variation of fractional secondary structure for oxidized HEWL on addition of SDS.....	47
Figure 3-9. Near-UV CD spectra of native HEWL, reduced HEWL, native HEWL in 50 mM SDS and reduced HEWL in 50 mM SDS.....	49
Figure 3-10. (a) Variation of fractional secondary structure for reduced HEWL on addition of C ₁₂ SO ₃ . (b) Integrated fluorescence intensity and peak position.....	51
Figure 3-11. (a) Variation of fractional secondary structure for reduced HEWL on addition of C ₁₀ SO ₃ . (b) Integrated fluorescence intensity and peak position.....	52
Figure 3-12. (a) Variation of fractional secondary structure for reduced HEWL on addition of DTAC. (b) Integrated fluorescence intensity and peak position.....	54

Figure 3-13. Variation of fractional secondary structure for reduced HEWL on addition of SB3-10.....	56
Figure 3-14. (a) Calculated fractions of secondary structures. (b) Fluorescence peak intensity and peak position variation with addition of SDS to 0SS mutant HEWL. ...	58
Figure 3-15. (a) Calculated fractions of secondary structures. (b) Fluorescence peak intensity and peak position variation with addition of DTAC to 0SS mutant HEWL. ...	59
Figure 3-16. Variation of reduced HEWL with different concentrations of TFE (a) CD spectra of reduced HEWL with added TFE. (b) Change in fluorescence.....	60
Figure 3-17. Thermal denaturation of native HEWL in buffer, and with DTAC and SDS, and reduced HEWL in buffer, and with DTAC and SDS	63
Figure 3-18. (a) An example of stopped-flow kinetic ECD actual measured data and fitted curve. (b) Expanded view of the short time component of (a).....	65
Figure 3-19. Kinetic variation of reduced HEWL spectral response on mixing with SDS. (a) Fitted curves for the CD signal and (b) Curves for the fluorescence intensity	66
Figure 3-20. Kinetic variation of reduced HEWL spectral response on mixing with DTAC. Fitted curves for (a) the CD signal and (b) the fluorescence intensity.....	70
Figure 4-1. Far-UV CD spectra of native HEWL and reduced HEWL, and with addition of different concentrations of DMPG	81
Figure 4-2. Near-UV CD spectra of native HEWL, reduced HEWL, native HEWL in 5 mM DMPG and reduced HEWL in 5 mM DMPG	84
Figure 4-3. Variation of the integrated intrinsic fluorescence intensity and peak position of reduced HEWL with addition of DMPG	85
Figure 4-4. Fluorescence spectra of reduced HEWL, and reduced HEWL with varying concentrations of DMPG.....	86
Figure 4-5. Far-UV CD spectra of native HEWL and reduced HEWL, and with addition of different concentrations of DMPC.....	88
Figure 4-6. ATR spectra of reduced HEWL, reduced HEWL with 5 mM DMPG and reduced HEWL with 1.5 mM DMPC	90
Figure 4-7. Fluorescence spectra of reduced HEWL, and reduced HEWL with varying concentrations of DMPC.....	91
Figure 4-8. Far-UV CD spectra of native HEWL, and reduced HEWL with addition of different concentrations of DLPG.....	93
Figure 4-9. Far-UV CD spectra of native HEWL, and reduced HEWL with addition of different concentrations of POPG	94
Figure 4-10. Far-UV CD spectra of native HEWL, and reduced HEWL with addition of different concentrations of DOPG	95
Figure 4-11. Far-UV CD spectra of native HEWL, and 0SS mutant with addition of	

different concentrations of DMPG.....	97
Figure 4-12. Far-UV CD spectra of native HEWL, and 1SS mutant with addition of different concentrations of DMPG.....	98
Figure 4-13. Variation of the integrated intrinsic fluorescence intensity and peak position of 0SS mutant with addition of DMPG.....	100
Figure 4-14. Fluorescence spectra of 0SS mutant, and 0SS mutant with varying concentrations of DMPG.	101
Figure 4-15. Variation of the integrated intrinsic fluorescence intensity and peak position of 1SS mutant with addition of DMPG.....	102
Figure 4-16. Fluorescence spectra of 1SS mutant, and 1SS mutant with varying concentrations of DMPG.	103
Figure 4-17. Thermal denaturation of oxidized HEWL and reduced HEWL in DMPG vesicles, native HEWL in buffer only and reduced HEWL in buffer only.	105
Figure 4-18. Polarized ATR-FTIR difference spectra of reduced HEWL, 0SS mutant and 1SS mutant with DMPG vesicles and DMPG only.....	107
Figure 4-19. (a) The CD signal at 222 nm and its fitted curve; (b) The total fluorescence intensity of reduced HEWL mixing with 5 mM DMPG vesicles.	109
Figure 5-1. Collagen fluorescence changes in peak position and fluorescence intensity when treated with different concentrations of GSE, EDC/NHS and GA	127
Figure 5-2. (a) ATR-FTIR spectra of type I collagen treated with 0.065% GSE. (b) ATR-FTIR spectra type I collagen treated with 5.75% EDC/1.4% NHS. (c) ATR-FTIR spectra type I collagen treated with 5% GA.	129
Figure 5-3. (a) ATR-FTIR spectra of dentin treated with GSE. (b) ATR-FTIR spectra of dentin treated with 5.75% EDC/1.4% NHS. (c) Dentin treated with 5% GA.....	131

LIST OF ABBREVIATIONS

0SS	Lysozyme mutant with no disulfide bonds
1SS	Lysozyme mutant with one disulfide bond
ATR	Attenuated total reflectance
BZA	Benzoylacetone or 1-phenyl-1,3-butadione
C ₁₀ SO ₃	Sodium 1-decanesulfonate
C ₁₂ SO ₃	Sodium 1-dodecanesulfonate
CD	Circular dichroism
CMC	Critical micelle concentration
DLPG	Dilauroylphosphatidylglycerol
DLS	Dynaamic light scattering
DMPC	Dimyristoylphosphatidylcholine
DMPG	Dimyristoylphosphatidylglycerol
DOPG	Dioleoylphosphatidylglycerol
DSPG	Distearoylphosphatidylglycerol
DTAC	Dodecyltrimethylammonium chloride
DTT	1,4-dithio-DL-threitol
DW	Distilled water
ECD	Electronic circular dichroism
EDC	1-ethyl-3-[3-dimethylaminopropyl] carbodiimide hydrochloride
FTIR	Fourier transform infrared

GA	Glutaraldehyde
GSE	Grape seed extract
HEWL	Hen egg white lysozyme
IR	Infrared
LUVs	Large unilamellar vesicles
NHS	N-hydroxysuccinimide
NMR	Nuclear magnetic resonance
PACs	Proanthocyanidins
POPG	Palmitoylphosphatidylglycerol
SB3-10	Sulfobetaine
SDS	Sodium dodecyl sulfate
S/N	Signal-to-Noise Ratio
SUVs	Small unilamellar vesicles
TFE	Trifluoroethanol
Trp	Tryptophan
UV-Vis	Ultraviolet-Visible

SUMMARY

The work in this thesis focused on using spectroscopic methods to study the refolding of reduced and mutant lysozymes with surfactant micelles and lipid vesicles, and the cross-linkings of collagen and dentin with highly biocompatible plant-derived proanthocyanidins (PACs).

The reformation of secondary structure for disordered, disulfide reduced hen egg white lysozyme (HEWL) upon interaction with surfactants and lipid vesicles was studied using Circular Dichroism (CD), fluorescence and infrared (IR) spectroscopic techniques. Equilibrium CD studies showed that reduced HEWL when mixed with negatively charged surfactants above critical micelle concentration (CMC), such as sodium dodecyl sulfate (SDS), or with lipid vesicles having negative head groups, such as DMPG at concentration above CMC, can regain helical structure but lose tertiary structure in such environments. Fluorescence studies showed the changes in the local environment of the tryptophan residues. Comparing the results between oxidized HEWL, reduced HEWL and the 0SS and 1SS (with zero and one disulfide bond, respectively) mutants provides an example of the role of disulfide bonds on the protein folding process. With positively charged/zwitterionic surfactants or lipid vesicles, the interactions with reduced HEWL are weaker and thus the degree of helicity recovered is less. Stopped flow dynamics studies showed that both the CD kinetics and the fluorescence kinetics can be fit to two or three exponentials. The faster steps in CD and fluorescence detected kinetics appear to be correlated, which suggests formation of an

intermediate on rapid interaction of the surfactant micelles or lipid vesicles and the protein. The slow steps suggest that the protein further rearrange its structure, continue to gain helical content and relax packing of the tryptophan residues, for which the hydrophobic interactions are the major driving forces.

ATR-FTIR and fluorescence spectroscopic analysis were used to study the mechanism of interactions of PACs with collagen and with dentin. The PACs used are from *vitis vinifera* grape seed extract. Two cross-linking agents, glutaraldehyde and carbodiimide hydrochloride, with known cross-linking mechanisms, were selected for comparative analyses. Both the ATR-FTIR and fluorescence results evidence different mechanisms for these three cross-linking agents. A new feature was observed in the ATR-FTIR spectra in PACs-treated collagen and dentin, suggesting a covalent bond formation between collagen and PACs. PACs-treated collagen also shows different patterns of changes of fluorescence from the chemical cross-linkers, further supporting a different mechanism in dentin.

1. Introduction

1.1 Protein structure and its determination

Proteins are heterogeneous polymers, also known as polypeptides, of amino acids and play various functions in various biological processes in all living organisms on earth. The common monomers, or residues, for proteins are 20 naturally occurring α -amino acids, with the amino and carboxylic acid groups separated by a single carbon, all of which have the chiral L-form except for the non-chiral glycine. Amino acids can link together through the formation of a peptide bond between the carboxyl group (R-COOH) of one amino acid and the amino group (NH₂-R) of the following amino acid, during which the two functional groups would condense and form an amide bond by losing one water molecule. Since each amino acid has both the carboxyl group and the amino group, they can be connected to each other in a sequence and forming a linear polymer known as polypeptide chain. Depending on the length of the polypeptide chain, they are sometimes called peptides for chains under 40 residues and proteins or polypeptides for longer chains.⁽¹⁾ The primary structure of proteins refers to the order in which the amino acids are covalently linked by peptide bonds, or the sequence of amino acids, and the location of covalent linkages such as disulfide bonds between amino acids. The primary structure of a protein is unique to the specific protein and is a fundamental aspect of the structure and function of the protein.

The peptide amide bond has a planar character because it has a partial delocalized double bond nature which favors a planar conformation. Due to the planar peptide bond, the polypeptide chain only twists or rotates at the single bonds on either

side of the α -carbons. The torsion angle ϕ (phi) for rotation about the N-C α bond and ψ (psi) for rotation about the C α -C bond are thus the two main degrees of rotational freedom in the polypeptide chain (ignoring side chain formations), as shown in Figure 1-1. The planar character of peptide amide bonds, and the corresponding dihedral rotation angles (ϕ and ψ), determine the local conformation of the polypeptide chain. Not all ψ and ϕ angle combinations are allowed due to the stereochemical interactions of adjacent residues and stereochemical conflict within the polypeptide chains. A Ramachandran plot (Figure 1-2) shows the favored and excluded conformations of ψ and ϕ angles for simple peptides that result in different protein secondary structures.⁽²⁾ Driven by a number of non-covalent interactions such as hydrogen bonding, ionic interactions, van der Waals forces, and hydrophobic effects, sequential residues in protein polypeptide chains adopt several (ϕ , ψ) repeat patterns in the main chain, which are called protein secondary structure. The most commonly occurring secondary structures are alpha-helices,⁽³⁾ the beta-sheets,⁽⁴⁾ and turns and loops⁽⁵⁾ that can be seen to occupy local minima in the Ramachandran plot.

Tertiary structure is the global 3-dimensional protein structure, assembled from different secondary structure building blocks or segments. Hydrogen bonding, hydrophobic effects, ion pairs and disulfide bonds are the four driving forces for the formation of protein tertiary structure. Hydrogen bonds can be formed between backbone groups, between side chain groups and between backbone groups and side chain groups. Hydrophobic amino acid residues can stabilize the tertiary structure by collapse of their side chains to a compact structure excluding water from that part of

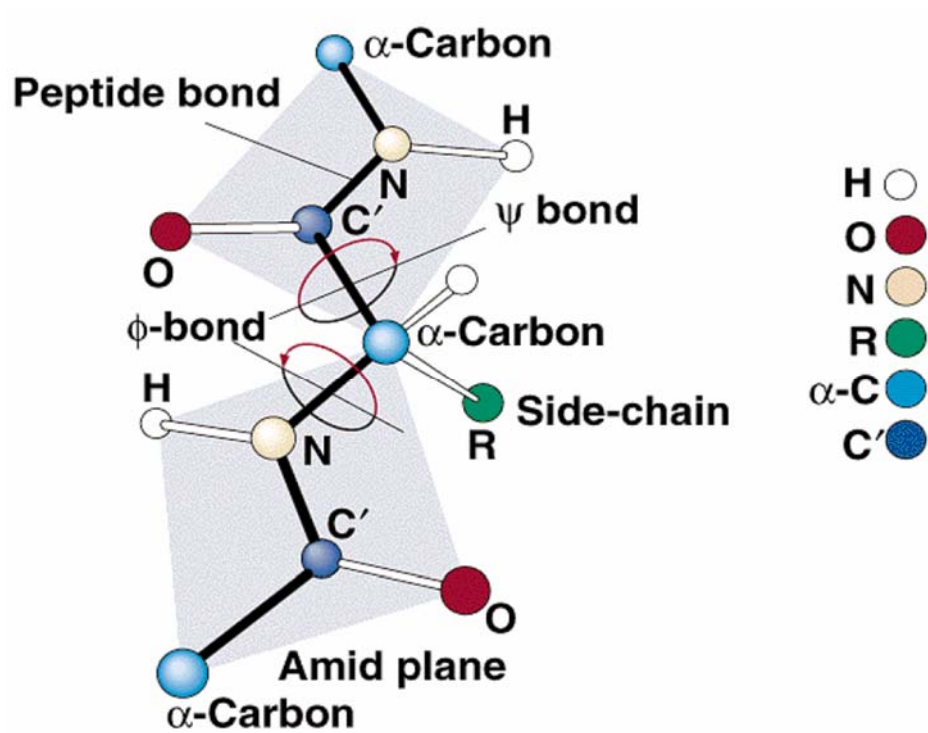


Figure 1-1. The ϕ , ψ angles between two consecutive amino acid residues in a polypeptide chain, indicating direction of positive rotation. The shaded areas represent amide bond planes.

Derived from "Textbook of Biochemistry: With Clinical Correlations" 4th edition by Thomas M. Delvin.

The Ramachandran Plot.

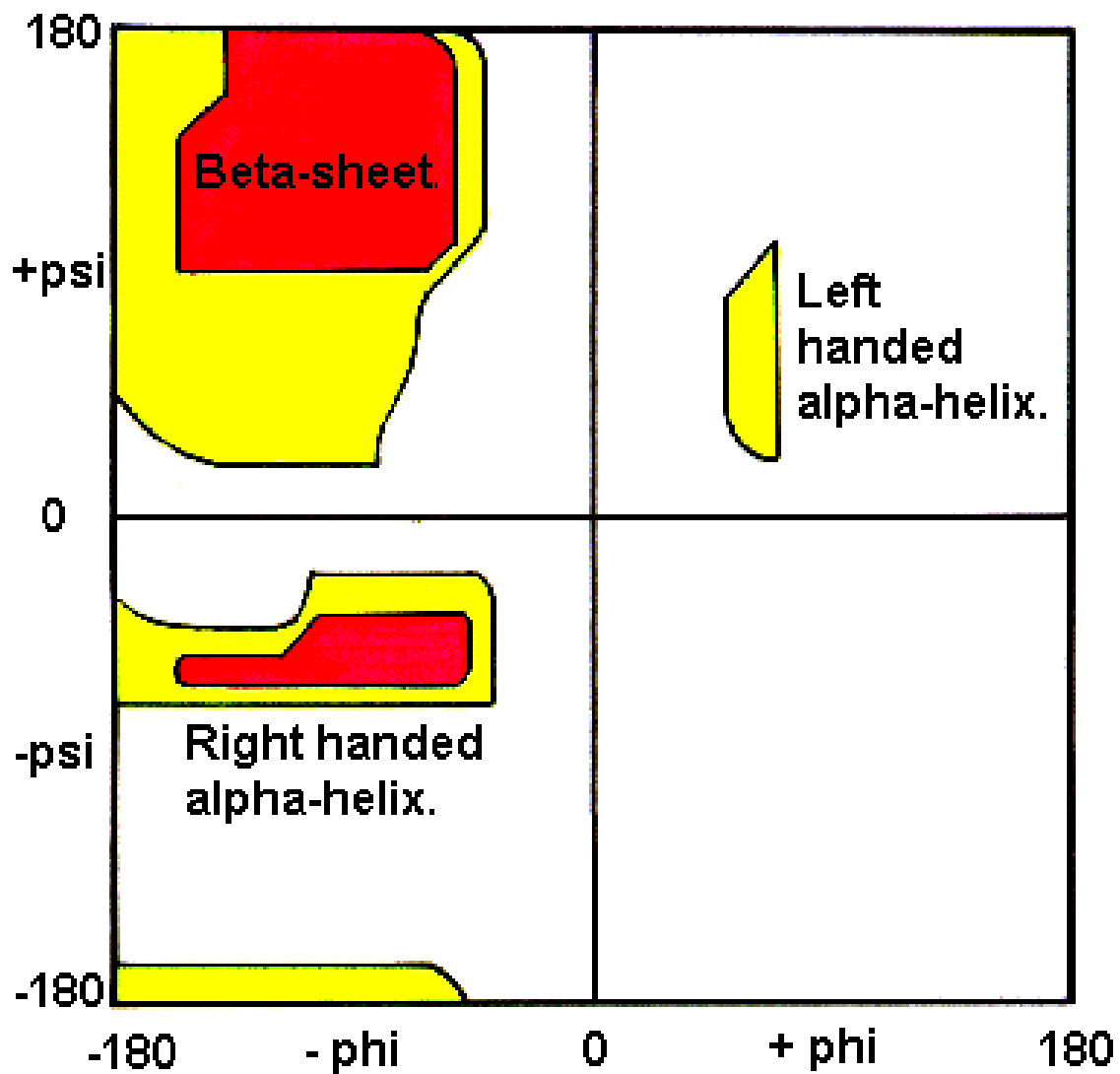


Figure 1-2. Ramachandran Plot describing the phi and psi angle combinations for protein secondary structures.

Reference from <http://swissmodel.expasy.org/course/text/chapter1.htm>.

the sequence. Charged amino acid side chains can form ion pairs to provide electrostatic stabilization interactions, and are also capable of hydrogen bonding. When the charged or hydrophilic residues are on the water-exposed surface of a folded protein, they provide stabilization for the overall tertiary structure and solubility. Disulfide bonds are strong covalent bonds that can form between cysteine residues under oxidizing conditions when they are close in the folded structure, and they can help to maintain the tertiary structure by adding considerably to the folding stability. Protein quaternary structure refers to the number and arrangement of multiple folded protein subunits in a multi-subunit complex. Figure 1-3 gives a brief review of the primary, secondary, tertiary and quaternary structures of proteins.

Many analytical techniques have been developed to study protein structures. X-ray crystallography and nuclear magnetic resonance (NMR) spectroscopy are the two most widely used experimental techniques available that provide detailed three-dimensional structural information of proteins and peptides and can achieve atomic resolution or site-specific resolution. X-ray crystallography can determine the 3D electron density distribution of atoms in the protein (in the crystallized state) and thereby infer the 3D coordinates of all the non-H atoms to a certain resolution.^(6, 7) Currently around 90% of the protein structures available in the Protein Data Bank have been determined by X-ray crystallography. Its strict requirement for crystallization of the protein, which is often difficult to achieve, limits the use of X-ray crystallography.⁽⁸⁾ Roughly 9% of the known protein structures have been obtained by nuclear magnetic resonance (NMR) techniques, which is sensitive to inter nuclear (atomic) distances and

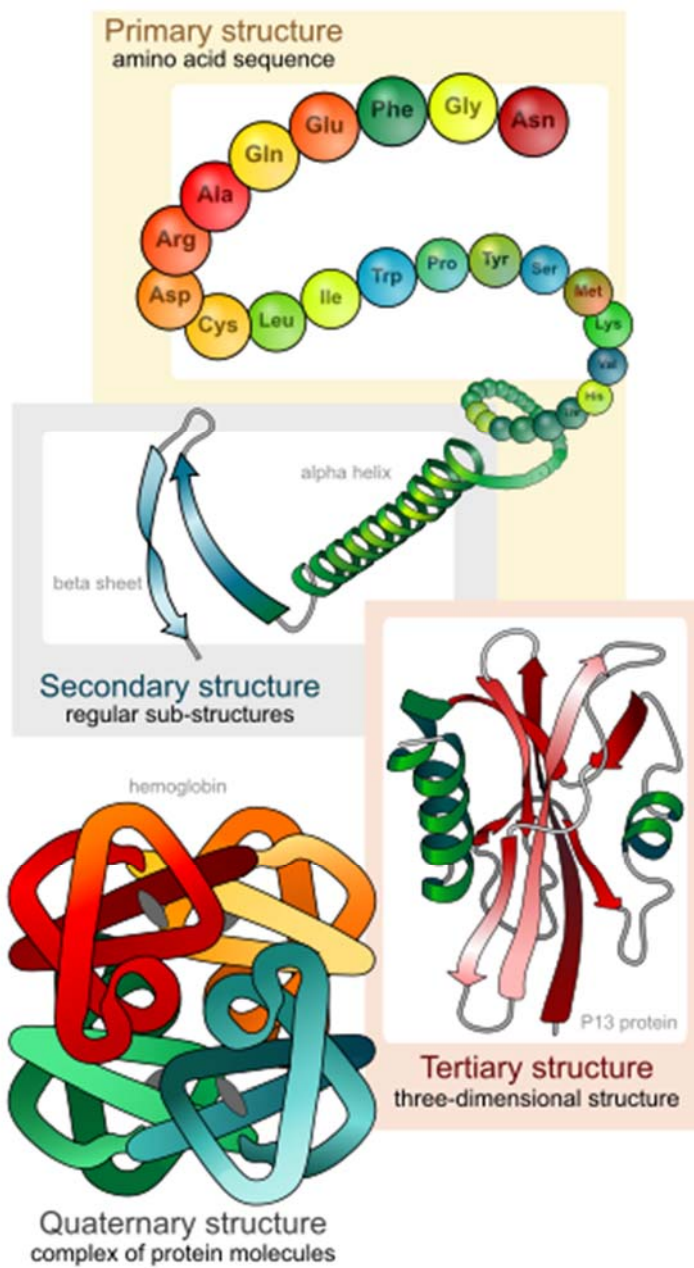


Figure 1-3. Protein Structure: from primary to quaternary structure.

This image is released by its author, LadyofHats.

can also be used to determine secondary structure of specific residues. With rapid experimental and theoretical advances, the ability to use NMR for structure determination of larger proteins has been greatly improved, especially with multi-dimensional experimental techniques.⁽⁹⁻¹¹⁾ However, NMR also has some disadvantages: a concentrated protein solution is required; most NMR studies require isotopic labeling for better spectral resolution; and the analysis requires complicated data acquisition, processing and interpretation.

Optical spectroscopic techniques are often used to determine lower resolution structural characteristics of proteins, i.e. average secondary structures and changes in tertiary structure, as well as inter residue distances in some cases. Optical spectra lack the atomic resolution provided by X-ray crystallography and NMR techniques, but have several advantages. First, there are a variety of optical spectroscopic methods available including ultraviolet-visible (UV-Vis) absorption, fluorescence, circular dichroism, infrared and Raman spectroscopy. Each can provide information about protein or peptide structure and has its own distinct advantages. The combination of them can be used to derive complementary structural information even though none of them can provide a complete picture of protein or peptide structure. Second, sample requirements, such as concentration and states (gas, liquid, or solid), are moderate so that they can be applied to more complicated systems under different conditions. Third, optical spectroscopic techniques have very fast time response so that dynamics of structural changes can be monitored and followed.

1.2 Protein folding

The physical process by which a polypeptide chain in random coil or disordered state folds into its unique and functional three-dimensional structure is called protein folding.^(12, 13) Proteins of a given primary structure often fold into a unique 3-D structure and as a result, the amino acid sequence seems to carry the information necessary to specify the final native 3-D structure of the folded state. Misfolding into a non-native structure usually results in inactive and possibly disease-causing proteins.^(14, 15) Understanding protein folding mechanisms can help us to predict the folding outcomes of a given sequence and thus help develop an understanding of the functions of the protein. Ionic interactions, van der Waals and dipole interactions, hydrogen bonds and disulfide bonds can all contribute to thermodynamic stability of the protein final structure. The entropy contributions to the stability of protein structure can be from the protein folding process, which results in lower entropy, or from the solvent, which gains considerable entropy as a protein folds because of the hydrophobic effect which leads to burying (desolvation of) non-polar residues.

From the thermodynamic point of view, a protein may search out all possible outcomes to find the final native conformation which has the lowest free energy. Each amino acid would have numerous possible favorable or unfavorable conformations and as a result, a typical protein with multiple amino acid residues would have an astronomical number of possible conformations. If even a very small time interval is used for each step in the searching process, this would result in an extremely long overall folding time scale. Such a time is incompatible with experimental protein

folding, which may take microseconds or milliseconds.^(16, 17) This is called the famous Levinthal's paradox,⁽¹⁸⁾ whose solution is that the protein folding process also has kinetic control, in addition to the thermodynamic control in the protein folding process.⁽¹⁹⁾ Protein folding follows particular pathways, not random and time-consuming searches, to seek the lowest free energy state.⁽²⁰⁾ As a result, the protein amino acid sequence must provide not only the information to specify the final 3-D structure of the folded state, but also information to guide the folding process to follow particular pathways and avoid others.⁽²¹⁾ The “framework model” proposes a two-stage folding process, in which local native secondary structure segments are formed first and then these segments subsequently coalesce to form the tertiary structures.^(22, 23) The “hydrophobic collapse model” describes the initial stage of protein folding, during which the protein may form a more compact, so-called “molten globule” state by collapse or condensation of its hydrophobic side chains as driven mainly by hydrophobic effects and subsequent exclusion of the hydrophilic water molecules from the local environment.^(24, 25) The molten globule state usually develops significant secondary structure, which may or may not be similar to the native form, but it does not have a definite tertiary structure.

The energy landscape theory⁽²⁶⁾ uses a three-dimensional “funnel” approach to visualize the correlation between the conformational space of a protein (cross-sectional area of the funnel) and the relative free-energies of the conformations (height in the funnel), as shown in Figure 1-4. It organizes an ensemble of partially folded structures on a free energy surface, which resembles a funnel with a partially rough surface. The

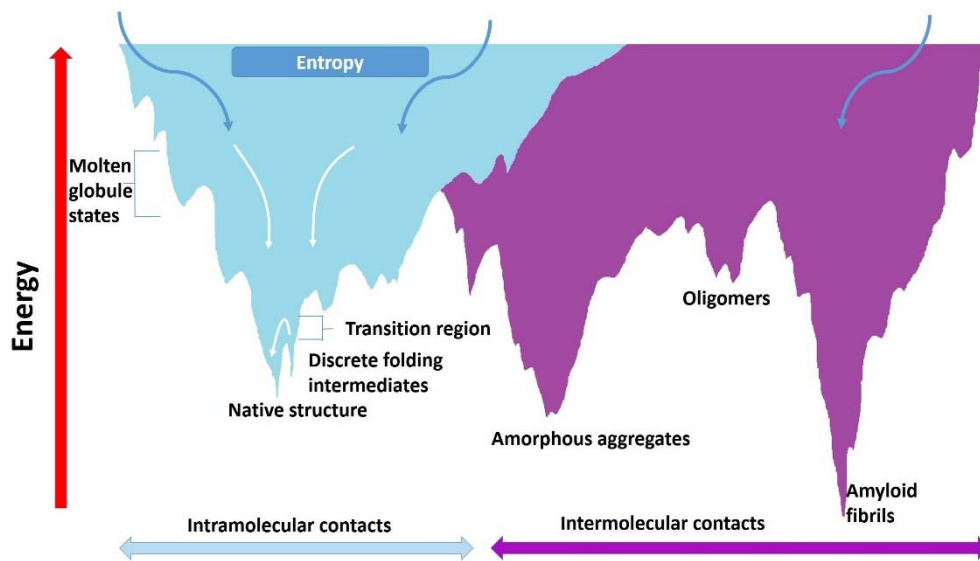


Figure 1-4. The “folding funnel” free energy landscape scheme of protein folding and aggregation.

Drawn based on concepts from Brooks III, Charles L., Onuchic, José N., and Wales, David. J. (2001) *Science* 293, 612–613 and Hartl, F. Ulrich and Hayer-Hartl, Manajit (2009) *Nature Structural & Molecular Biology* 16, 574-581.

native state with the lowest energy lies at the bottom of the funnel and local free energy minima correspond to transient kinetic traps and intermediates at various points on the sides. The folding process is correlated in a way that the search for a minimum in each step is improved in efficiency over the preceding steps, because an energy lowering step also reduces the conformational freedom of the system. Each step not only lowers the energy, but also restricts the possible paths in the search towards the global energy minimum solution along the energy funnel. The energy landscape theory allows multiple folding pathways for a certain protein, which may take the steepest route (fastest), or a slower route that bypasses certain kinetic traps with local minima and transition states with local maxima.

The energy landscape theory also provides an explanation for the protein aggregation mechanism.⁽²⁷⁾ The protein has conformations ‘funneling’ both to the native state via intramolecular contacts and toward amorphous aggregates or amyloid fibrils via intermolecular contacts. In the region of overlap between these energy surfaces (Figure 1-4, blue and purple region contacts), aggregates can be formed from intermediates during the de novo folding or destabilization of native state into partially folded states.

1.3 The role of disulfide bonds on protein folding

Formation of disulfide bonds is an important aspect of protein folding because it is thermodynamically linked to protein folding, and thus affects the folding intermediates and the folding pathways for disulfide-containing proteins. Disulfide bonds are important posttranslational covalent modifications that occur during protein folding. Failure to form the correct disulfide bonds usually results in misfolding into non-native states or protein aggregation. Disulfide bonds are formed by two thiols from cysteine residues facilitated by an oxidizing environment. There is also disulfide reshuffling in which the thiolate of a cysteine attacks an existing disulfide bond and forms a new disulfide bond. The concentration of thiolate anions, the accessibility, proximity and reactivities of the thiol groups and disulfide bonds are the four major factors affecting the disulfide bond formation.

It is generally accepted that correctly formed disulfide bonds can stabilize the native conformation of a protein and destabilize its unfolded state. Disulfide bonds not only stabilize protein structures, but may also be important for proper folding and biological activities. The formation of disulfide bonds is closely linked to the protein folding process and adds an extra dimension of intermediates to the protein folding.⁽²⁸⁾ There are thus two dimensions of equilibria, including thiol disulfide equilibria and protein conformational equilibria, involved in the protein folding process (Figure 1-5). Disulfide bonds can be formed in the unfolded state and thereby limit the conformational space as the protein then folds into its native structure, or the protein can first fold into a native-like state and then the disulfide bonds can form. Disulfide

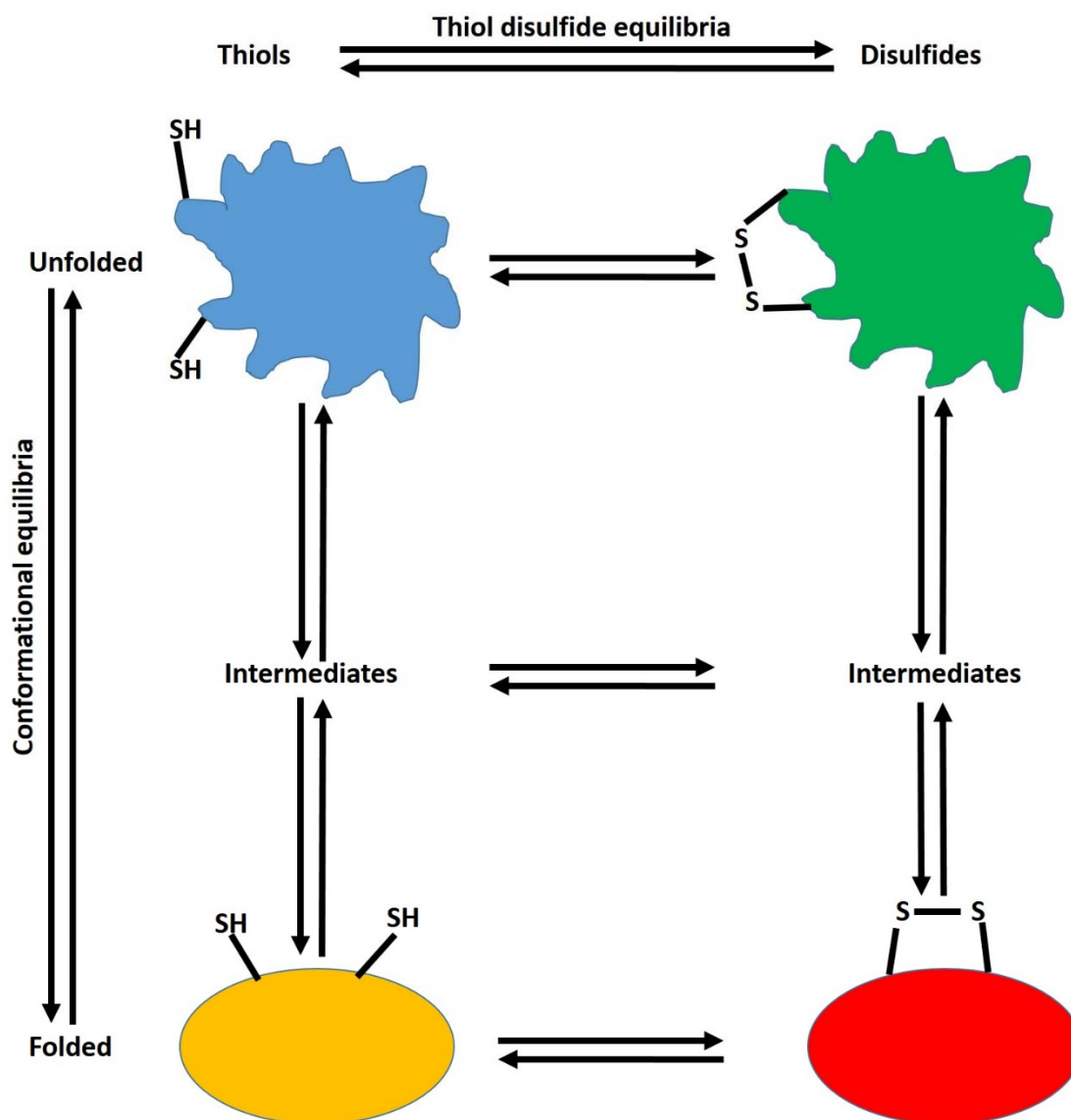


Figure 1-5. Coupling of disulfide bond formation and conformational folding of a protein.

bonds may also be formed during intermediate steps in the folding pathway. The protein folding process can enable or stabilize the formation of disulfide bonds and disulfide bonds can also affect the kinetics of protein folding. Usually, disulfide bonds in or near the folding nucleus can accelerate protein folding while disulfide bonds formed elsewhere may actually slow down protein folding, especially if errors in disulfide bond formation occur.

1.4 Surfactant micelles and lipid vesicles

Surfactants are amphiphilic molecules with both a hydrophilic head group and hydrophobic tail. At low concentrations, surfactant molecules in a solution are in the form of individual molecules or monomers. Increasing the concentration of surfactant in a solution to above a critical concentration, causes surfactant monomers to combine into the form of large aggregates called micelles with hydrophilic head groups facing outward shielding the hydrophobic tails from the aqueous solution (Figure 1-6).⁽²⁹⁾ The concentration above which this occurs is called the critical micelle concentration or CMC of surfactant. At the CMC, some physicochemical parameters such as the equivalence conductivity or the surface tension would experience abrupt changes due to micelle formation. The major factors affecting the CMC are the type of head groups, the length of the hydrophobic tail, ionic strength of solution, pH value⁽³⁰⁾ and temperature. Surfactants can be classified into anionic surfactant, cationic surfactant, zwitterionic surfactant and nonionic surfactant based on the character of head groups.

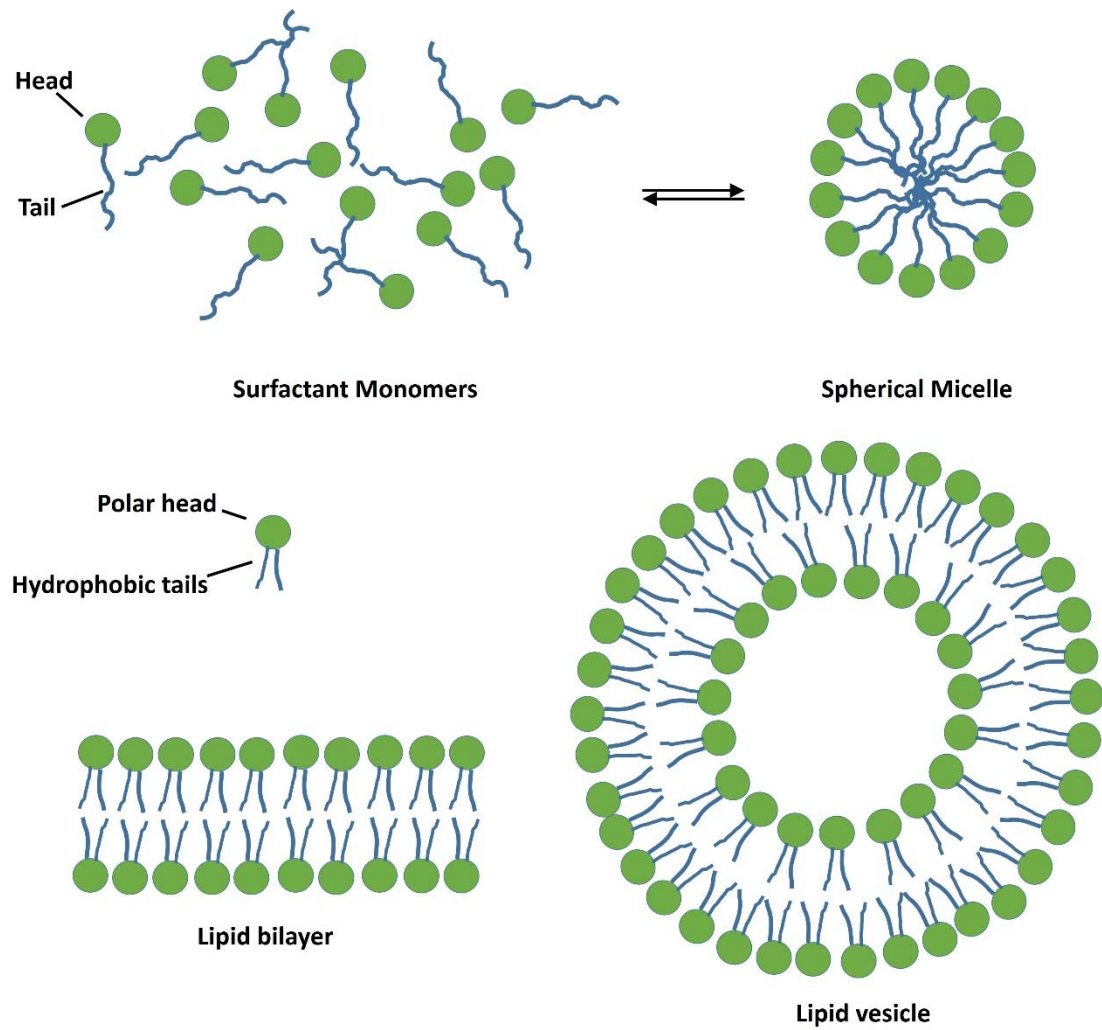


Figure 1-6. Structure of surfactant micelle and lipid vesicle.

Surfactant molecules can bind to proteins and form protein-surfactant complexes which results in changes to the protein secondary and tertiary structures.⁽³¹⁾ There are three major models proposed for the structure of protein-surfactant complexes.⁽³²⁾ The “necklace and bead” model describes the protein-surfactant complex as the string of a necklace represented by the flexible polypeptide chain with the beads formed from the surfactant micelle-like clusters. The “rod-like particle” model claims that the polypeptide chain forms the core of a rod with the surfactant molecules bound along the rod length. In the “flexible helix” model, the surfactant molecules form a flexible cylindrical micelle and the polypeptide chain can then wrap around the cylindrical micelles.

Phospholipids, which are the major components of the lipid bilayer of cellular membranes, contain a head group and one or more acyl hydrophobic chains. Lipids can self-assemble to form a lipid bilayer and form vesicles in an aqueous environment, by which the polar heads of the lipids oriented towards the polar, aqueous environment and the hydrophobic tails minimize their contact with water and tend to align together inside the bilayer (Figure 1-6).⁽²⁹⁾ There is a transition temperature (T_m) for the phospholipid bilayers, at which the structure will undergo a phase change from a gel phase to a liquid crystalline phase. In the gel phase below the transition temperature, phospholipids are tightly packed and ordered, while in their liquid crystalline phase, their packing is loose and they are more fluid. The properties of the lipid acyl chains can affect the transition temperature and the packing of lipid bilayer. For example, introducing a double bond into the acyl chains tends to lower the transition temperature

of the lipid, increase the fluidity of the bilayer and cause the bilayer to not pack well due to the double bond kink.

The lipid bilayer has two chemically distinct regions including the interface region and hydrocarbon core.⁽³³⁾ Proteins can bind to the surface of the bilayer through electrostatic attractions between the charged or polar components of the protein and the charged or polar head groups from the lipids. Proteins can also insert into the hydrocarbon core of lipid bilayer where hydrophobic effects are the main driving forces.

1.5 Thesis structure

This thesis consists of five chapters. Chapter 1 introduces background knowledge for the related research work described in the following chapters. Chapter 2 summarizes the general sample preparation and spectroscopic methods used. Chapters 3 and 4 present the results for the refolding of reduced lysozyme and mutants with micelles and lipid vesicles, respectively. Chapter 5 represents my contribution to a collaborative project studying the collagen-collagen interactions mediated by plant-derived proanthocyanidins using spectroscopic methods.

2. Material preparations and spectroscopic methods

2.1 Electronic Circular Dichroism (ECD)

2.1.1 Theory for Electronic Circular Dichroism

Electronic circular dichroism (ECD) is a widely used technique for the study of protein and peptide conformation with high sensitivity. ECD measures the difference of absorbance between left-circularly polarized (LCP) light and right-circularly polarized (RCP) light by a sample which arises due to structural asymmetry, typically evidenced as molecular chirality. All proteins and peptides give rise to measurable ECD spectra because they are chiral molecules (assuming the peptides are based on L- or D-amino acids).

According to the Beer-Lambert law, at a given wavelength,

$$\Delta A = A_L - A_R = -\log\left(\frac{I_L}{I_{L0}}\right) - \left(-\log\left(\frac{I_R}{I_{R0}}\right)\right) = (\varepsilon_L - \varepsilon_R)Cl = \Delta\varepsilon Cl \quad (\text{eq.2-1})$$

where ΔA is the difference between absorbance of left and right circularly polarized light (A_L and A_R), I_{L0} and I_{R0} are the intensities of LCP and RCP light before passing through the sample and I_{L0} is assumed to be equal to I_{R0} (this is a component of instrument design), I_L and I_R are the intensities of LCP and RCP light after passing through the sample and they may be different due to LCP and RCP interacting with chiral molecules differently, ε_L and ε_R are the molecular absorptivities for LCP and RCP light, l represents the path length in centimeters, C is the molar concentration and $\Delta\varepsilon$ is the molar circular dichroism. CD is actually measured as ΔA but most data is usually reported as degrees of ellipticity (θ) or molar ellipticity $[\theta]$ for historical

reasons.⁽³⁴⁾ Degree of ellipticity (θ) and molar ellipticity $[\theta]$ are readily interconverted from ΔA or $\Delta\epsilon$, respectively, by the equations:

$$\theta(\text{deg}) = \Delta A \left(\frac{\ln 10}{4} \right) \left(\frac{180}{\pi} \right) = 32.98 \Delta A \quad (\text{eq.2-2})$$

$$[\theta] = \frac{100\theta}{Cl} = 100\Delta\epsilon \left(\frac{\ln 10}{4} \right) \left(\frac{180}{\pi} \right) = 3298.2 \Delta\epsilon \quad (\text{eq.2-3})$$

Expressing the CD in terms of molar ellipticity $[\theta]$ removes the linear dependence of solute concentration and pathlength and has unusual units of $\text{deg}\cdot\text{cm}^2/\text{dmol}$, again for historical reasons.

2.1.2 ECD of Proteins and Peptides

ECD analyses can provide rapid determination of the average secondary structure for proteins and peptides in the "far-UV" spectral region (190-250 nm). For peptides and proteins, the most important CD chromophore in the far-UV region is the peptide bond, and different protein and peptide conformations (α -helix, β -sheet and random-coil) show distinct characteristic band shapes and magnitudes of ECD spectra.⁽³⁵⁾ Figure 2-1 shows the CD spectra for representative protein and peptide conformations. In the far UV region, the amide chromophore has one $n\text{-}\pi^*$ transition (~ 220 nm), and two $\pi\text{-}\pi^*$ transitions (~ 190 and ~ 140 nm).⁽³⁶⁾

CD spectra for α -helices have one positive band ($\pi\text{-}\pi^*$ transition) at around 190~195 nm with a high intensity, 60,000 to 80,000 $\text{deg}\cdot\text{cm}^2/\text{dmol}$, one negative band at ~ 208 nm ($\pi\text{-}\pi^*$ transition) and a second negative band at ~ 222 nm ($n\text{-}\pi^*$ transition) both with intensities of -33,000 to -39,000 $\text{deg}\cdot\text{cm}^2/\text{dmol}$.

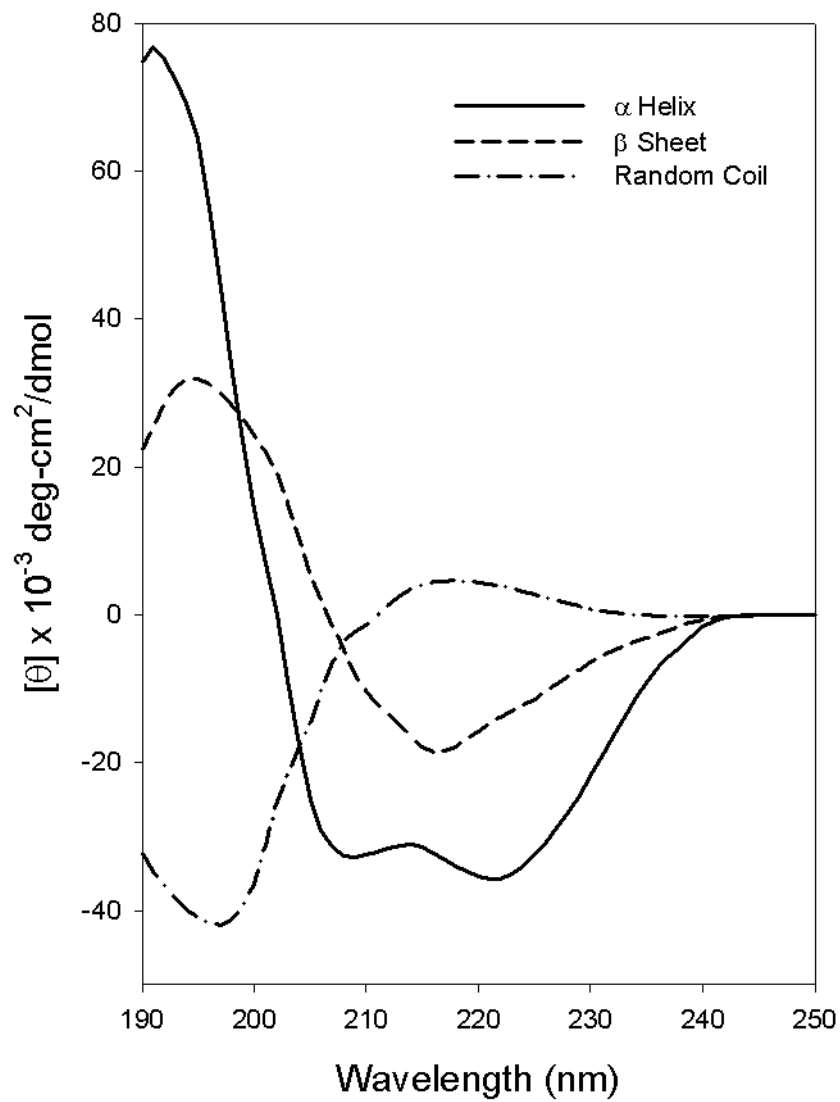


Figure 2-1. CD spectra for representative protein secondary structures: poly-L-lysine in α -helical, β -sheet and random-coil conformations.

Adapted from Greenfield, N. J. and Fasman, G. D. (1969) *Biochemistry* 8, 4108 with permission.

CD spectra for β -sheets have one positive band at around 195~200 nm (π - π^* transition) with an intensity of 30,000 to 50,000 deg·cm²/dmol and one negative band at around 215~200 nm (n - π^* transition) with an intensity of -10,000 to -20,000 deg·cm²/dmol.

Random-coils have one strong negative band at 200 nm (π - π^* transition) with an intensity around -20,000 deg·cm²/dmol and a very weak positive band at 220 nm (n - π^* transition). It is important to note that "random coils" have the same shape ECD as poly-L-proline II structures, which are left-handed helices.

CD spectra in the near-UV region (250-350 nm) for proteins and polypeptides can provide important structural information about (or a means of detection for change in) tertiary structure, typically used to detect loss of tertiary structure on unfolding.⁽³⁷⁾ Aromatic amino acid side chains, such as tryptophan (250-270 nm), phenylalanine (280-300 nm) and tyrosine (270-290 nm), and disulfide bonds (broad weak bands throughout the near-UV region) provide chromophores contributing to the CD signal in the near-UV region. Near-UV CD spectra can be used to monitor small tertiary structure changes due to the changes of the environment surrounding aromatic side chains. Such near-UV CD is usually much weaker than the far-UV CD, first, because there are fewer chromophores contributing to the near-UV region than in the far-UV region. But more importantly, the near-UV CD is weaker because they gain most of their chirality through coupling which is inversely dependent on distance and the separations of the same type chromophores. Since the separations in a protein can be large, this leads to weaker coupling. The local protein environment also provides a chiral perturbation but that

source of CD is weaker, thus near-UV CD spectra require longer path length and/or higher protein or peptide concentration than do far-UV CD spectra.

2.1.3 ECD Instrument and Measurements

Far-UV CD spectra were measured from 185 nm to 250 nm with a 50 nm/min scanning rate, 2 s response time, 1 nm bandwidth and as the average of 8 scans on a Jasco 810 spectrometer (JASCO, Inc.). For equilibrium measurements, the protein solutions were measured in a 1-mm path length quartz cuvette (Starna, Inc). The concentration required for CD measurement of protein solutions is determined by considering the balance between good CD signal and the necessity of avoiding too high of a HT (voltage) level applied to the PMT detector. This HT voltage level is determined by an automatic gain control in the instrument which makes the PMT average signal (current) a constant thus effectively a normalization of the differential (raw CD) signal, which then scales as ΔA . All sample spectra were corrected by subtraction of the corresponding spectrum of the buffer. The fractional secondary structures were calculated with the CDPro suite of programs (lamar.colostate.edu/~sreeram/CDPro/main.html) using CD spectra for the 195 nm to 250 nm range. Near-UV CD spectra were measured from 250 to 350 nm with the same instrument parameters except for using a higher concentration and a 1-cm path length quartz curvette to improve S/N ratio. A temperature controller (Model CDF-426S, JASCO, Inc.) is used to control the temperature of the sample holder for temperature variation CD measurements.

2.2 Stopped-flow measurements

For stopped-flow mixing dynamics, a SFM-400 accessory (Bio-logic) and MPS-52 control console were connected to the Jasco-810 spectrometer. Figure 2-2 shows a simple scheme for the setup. The Xe lamp in the CD spectrometer was changed to a Xe-Hg lamp to enhance far-UV intensity. The mixing dead time under our measurement conditions was ~ 10 ms, but instrument response was much faster and the signal change large enough to allow determination of kinetics in the ms and longer time range. The CD signal channel was recorded for 5 s with 1 kHz sampling of the signal at 222 nm using a 4 nm bandwidth by means of standard JASCO kinetics methods with a fixed PMT HT and normalization to the detector current (in the software) to determine ΔA with a faster response. The total fluorescence signal was simultaneously collected on the same sample for all emission above 320 nm using a cut-off filter in front of a separate fluorescence detector which was located at right angles to the CD and excitation beam. The results for both CD and fluorescence were fit with multiple exponential functions using the Bio-Kin32 software.

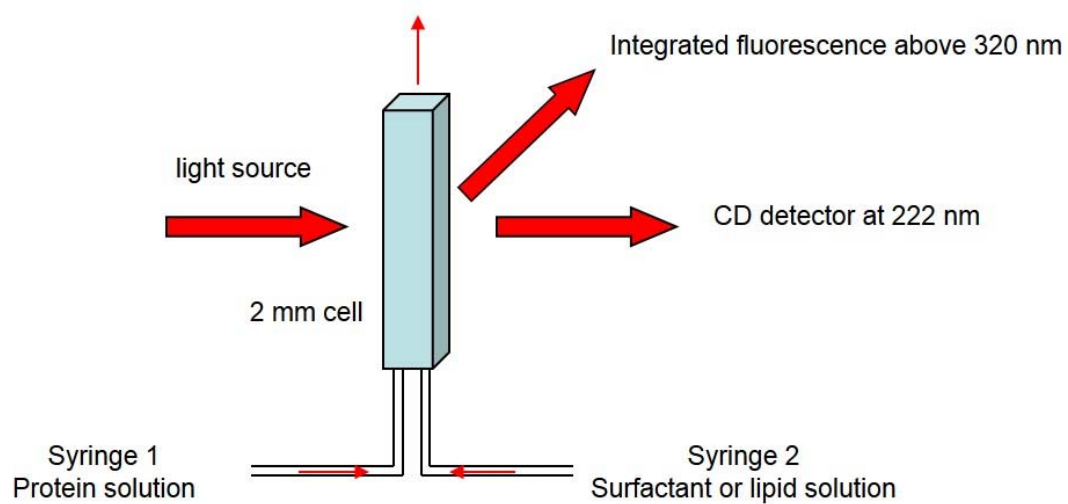


Figure 2-2. A simple scheme for stopped-flow system setup: collecting CD and fluorescence measurements simultaneously. Small red arrows indicate fluid flow.

2.3 Fluorescence Spectroscopy

Intrinsic fluorescent probes such as tryptophan, phenylalanine and tyrosine in proteins are sensitive to the microenvironment surrounding the probes. The fluorescence emission spectrum of intrinsic fluorescent probes will have intensity change or peak position shift when the environment around the probes is changed due to structure changes or solvent changes.⁽³⁸⁾ Thus fluorescence spectroscopy can provide information about tertiary structure of proteins and polypeptides. In this thesis we used excitation wavelength at 295 nm to monitor the fluorescence from tryptophan which dominates tyrosine and phenylalanine fluorescence. Fluorescence spectra were measured on a Fluoromax-3 spectrofluorometer (Horiba Jobin Yvon Inc.) with the samples in a 1 mm×1 cm quartz cell. Both excitation and emission slits are 5 nm and the scan speed is 1 nm/s. The emission spectra were collected from 300 nm to 500 nm. All the spectra were corrected by subtraction of the buffer spectrum.

2.4 UV-Vis Spectroscopy

UV-Vis absorbance at 280 nm was used to determine protein concentration. In this thesis UV-Vis spectra were also used to carry out a lysozyme activity assay and measure the CMC for surfactants, for which detailed protocols will be presented in corresponding chapters. All the UV-Vis absorbance spectra were collected on a CARY 300 Bio UV/Vis (Varian) spectrometer.

2.5 Attenuated Total Reflectance Fourier Transform Infrared (ATR-FTIR)

FTIR spectra are widely used to identify secondary structures of proteins. Amide I, amide II and amide III bands are usually used for secondary structure identification.^(39, 40) The Amide I band (1600 to 1700 cm^{-1}) arises from the C=O stretching vibrational mode coupled with N-H bending mode. The Amide II band (1480 to 1580 cm^{-1}) is from an out-of-phase combination of N-H bending and C-N stretching modes. The Amide III band (1229 to 1300 cm^{-1}) is primarily an in-phase combination of N-H bending and C-N stretching modes with some contributions from the $\text{C}\alpha$ '-H deformation. FTIR usually requires relatively high concentration for proteins, especially in comparison to ECD measurement, and typically deuterated samples are used due to the overlap of the H_2O bending mode with the amide I band.

Attenuated total reflectance Fourier transform infrared (ATR-FTIR) is a sampling technique which can examine solid or liquid samples directly without further preparation like lyophilization, deuteration and IR cell preparation.⁽⁴¹⁾ The light path length for ATR measurement is about 1 micrometer so there is no requirement to replace H_2O with D_2O for aqueous samples, and it can be used to study low concentration protein systems (if they are evaporated to a film or if a design incorporating a large number of reflections is used). The FTIR spectrometer (Bruker Vertex 80) was used with an ATR accessory fitted with a diamond/ZnSe crystal (PIKE MIRacle single/three reflection ATR). Solution samples were dried on the crystal surface to form a uniform thin film on the crystal surface and solid samples were flattened onto the crystal surface using a pressure clamp to better cover the active area. Sample absorbance spectra over

the range 4500 cm^{-1} to 600 cm^{-1} were collected as an average of 512 scans (10 kHz scan speed with a DTGS detector) and processed with 3-term Blackman-Harris apodization and zero filling of 2. Background transmission spectra collected with same measurement parameters but without sample on the ATR crystal surface were subtracted as a baseline correction. Polarized ATR of lipid vesicles collapsed on the surface can provide information about the relative orientation of protein secondary structures to the lipid membrane surface.⁽⁴²⁾ Polarized ATR spectra were collected with a wire grid polarizer placed in front of the sample for 0° and 90° polarizations of the incident light beam. The dichroic spectra were obtained by subtracting the spectrum recorded at 0° from that recorded at 90° using a weight coefficient ratio, R_{iso} . R_{iso} is obtained by calculating the ratio of integrated absorbance of the lipid carbonyl band (1699 cm^{-1} to 1770 cm^{-1}) in spectra measured at 90° to the integrated absorbance of the spectra measured at 0° .⁽⁴²⁾

3. Interaction of reduced lysozyme with surfactants: Disulfide effects on reformed protein structure in micelles

This chapter represents work already published in Biochimica et Biophysica Acta 1834, p593–600 (2013) by Weiyang Zhu and T.A. Keiderling

3.1 Introduction

Protein folding remains a vital area of biophysical research. Many proteins fold spontaneously in a manner that seems based solely on their sequence, while others misfold or require external conditions or chaperones to aid in folding. Sequence dependence of folding has dominated many studies over the past few decades, and remains a fundamental issue. One special aspect arising from the sequence is the role of Cys and the presence or absence of disulfide bonds in the folding sequence. Forming the correct disulfide bonds before the polymer folds to a stable secondary and tertiary structure would greatly limit the conformational entropy, and thus facilitate the search for a global minimum structure. Conversely forming the wrong disulfide bond will insert a misfolding step into the mechanism and dramatically slow progress toward the minimum energy structure.

Previous studies have shown that reduction of disulfide bonds decreases the stability of the native protein.⁽⁴³⁻⁴⁷⁾ Some studies have maintained that disulfides have a stabilizing effect on the native state but do not determine either the folding pathway or the final three-dimensional structure of the protein, so that in such cases disulfide links can be formed at late stages of the folding process.⁽⁴⁸⁾ Other studies contradict this point of view and show that native disulfide bonds can greatly accelerate secondary

structure formation at early stages of the folding process when the protein has no defined tertiary structure.⁽⁴⁹⁾ The effects of disulfide bond formation in the folding process remain unclear: does correct disulfide bond formation determine the folding pathway or just stabilize the elements of secondary structures formed and contribute to the formation of tertiary structure? Sorting these out for proteins in only buffer conditions is challenging because many reduced proteins do not fold, so no sensible comparison of structure or stability is possible with the oxidized form.

Ionic surfactants can interact strongly with oppositely charged globular proteins, often resulting in denaturation.⁽⁵⁰⁾ Such studies have been long pursued; however, the mechanism by which the surfactants influence protein structure is still not well defined. Bovine serum albumin (BSA) has been most frequently studied with sodium dodecyl sulfate (SDS), a representative anionic surfactant.⁽⁵¹⁻⁵⁴⁾ Even millimolar levels of SDS are known to be a strong denaturant for many proteins,^(52, 55) yet SDS can also counteract the effect of other denaturants.^(56, 57) SDS has been shown to lead to compact, highly helical (molten globular) structures for acid denatured cytochrome c^(58, 59) and to induce sheet-to-helix transformations in β -lactoglobulin.⁽⁶⁰⁻⁶²⁾ These effects can be strongly concentration sensitive, with the latter results being seen for proteins in micellar environments. Such surfactants may provide a simple model for study of protein-membrane like interactions (since both offer an interfacial interaction where charge and hydrophobic elements are separated or organized at some level). These can have some advantages for biophysical studies due to the higher solubility and smaller size of surfactants as micellar forms. Membrane interaction (and by extension, surfactants) can

also offer an alternative folding pathway which may illustrate the relative role of disulfide bond formation in a consistent medium. Such environments do allow both reduced and oxidized forms to fold to some structure which can then be compared and may or may not be related to the native state structure. Kinetic studies of SDS interaction with proteins are less common than are equilibrium evaluations, but several studies have been undertaken that monitored heme absorbance changes and near UV CD,⁽⁶³⁾ fluorescence changes,⁽⁶⁴⁾ and include previous CD and fluorescence studies of acid denatured Cyt c from our group.⁽⁵⁸⁾

This study is focused on hen egg white lysozyme (HEWL), which has four disulfide bonds in its native state (indicated schematically in Figure 3-1), and compares surfactant effects on folding, or regaining structure to a new state, by study of the reduced form of the protein as induced by interaction with various surfactants which provide a model system for study of charge and hydrophobic interactions. These systems may mimic protein-membrane interactions although the structures and presumably the detailed interaction mechanisms are admittedly different. It is interesting to note that, for some gram-negative bacteria, native lysozyme or partially unfolded forms of lysozyme can penetrate the outer membrane and acquire bactericidal capacity.⁽⁶⁵⁻⁶⁷⁾ The mechanism of the antimicrobial properties of lysozyme on gram-negative bacteria is still unclear, and the driving forces behind such interactions of membrane surfaces and the HEWL structure under such conditions remain an interesting problem.

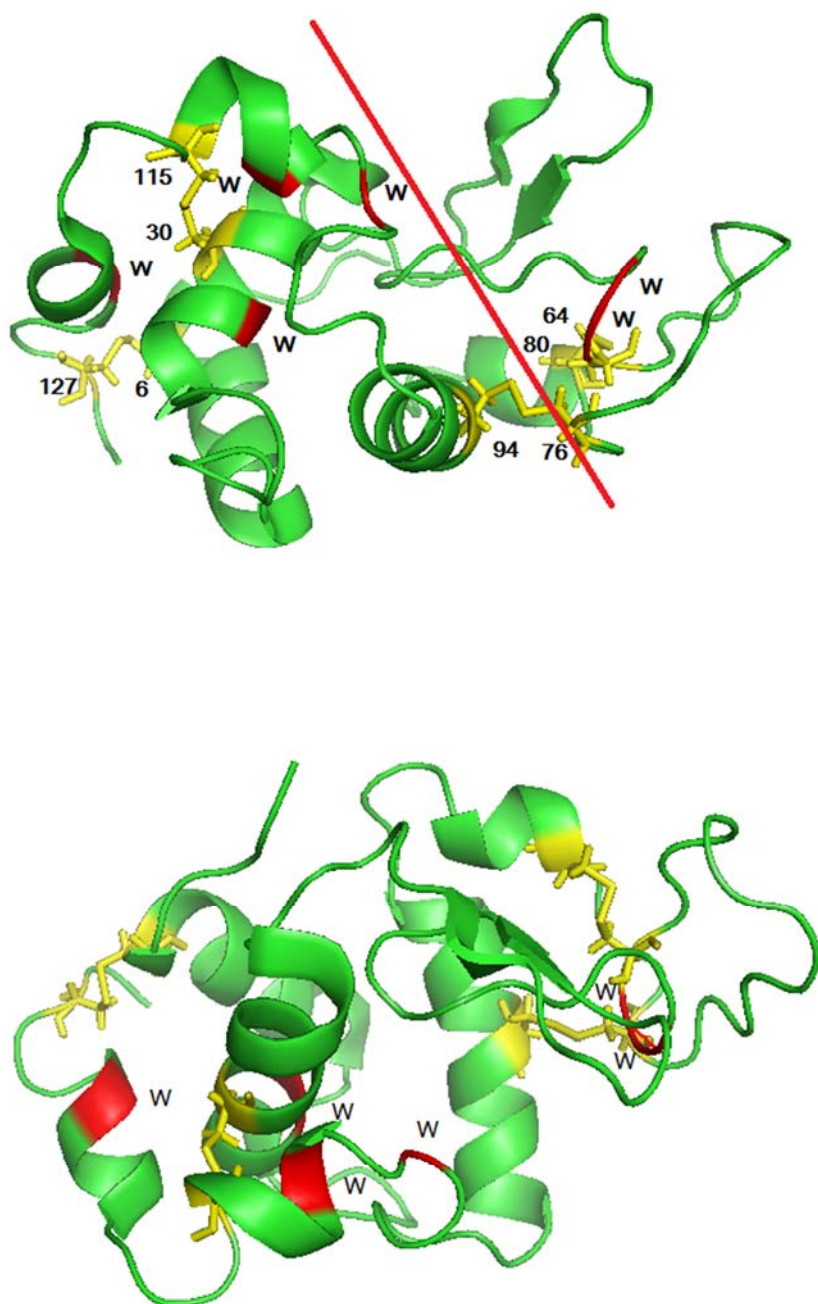


Figure 3-1. The structure of native HEWL with four disulfide bonds shown in yellow and six tryptophans shown in red and labeled as “W”. In the top figure, the region above the red line is the β -domain and the region below the red line is the α -domain. The bottom figure is the rotated view along the horizontal axis.

3.2 Experimental

3.2.1 Materials

Lysozyme from hen egg white (HEWL) and lyophilized *Micrococcus lysodeikticus* cell were purchased from Sigma. A comparative test experiment was carried out on a mutant lysozyme in which all the cysteines are replaced by alanines which was kindly provided by Prof. Harald Schwalbe and Dr. Robert Silvers, University of Frankfurt. The surfactants used (compared in Figure 3-2): sodium dodecyl sulfate (SDS), sodium 1-dodecanesulfonate ($C_{12}SO_3$), sodium 1-decanesulfonate ($C_{10}SO_3$) and sulfobetaine (SB3-10) were purchased from Sigma except for dodecyltrimethylammonium chloride (DTAC) which was from Fluka. The reducing agent 1,4-dithio-DL-threitol (DTT) was purchased from Fluka. Solution pH was measured with a HANNA HI 98180 pH meter. All the materials were used without further purification. To prepare reduced lysozyme solution, the protein was dissolved (0.4 mg/mL) in 20 mM phosphate buffer at pH 4.6 and incubated with 5 mM DTT for 24 hours at 65 °C. The reduction of the sample was quenched by rapid cooling at -20 °C for 20 minutes and then stored at 5 °C. This procedure is a modification of previously published methods.⁽⁶⁸⁾ All samples were studied at pH 4.6 to enhance solubility of the reduced form with DTT reductant.

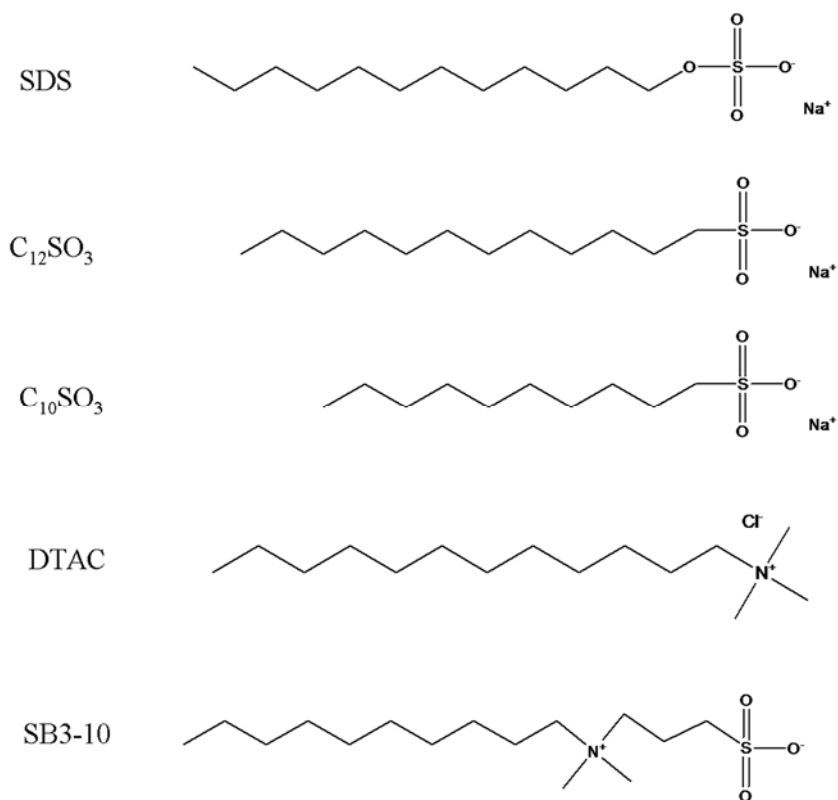


Figure 3-2. Schematic representations of the structures of surfactants used in this study.

3.2.2 CMC measurement of surfactants

CMC (critical micelle concentration) for the various surfactants under the experimental conditions, which include buffer, lowered pH and reductant, were determined by a UV-absorption spectroscopy method detecting absorbance change of BZA (benzoylacetone or 1-phenyl-1,3-butadione) using literature methods as summarized here.⁽⁶⁹⁾ BZA has two tautomeric forms: the ketonic and the enolic forms. This keto-enol equilibrium of BZA is solvent sensitive and there will be more enolic form in nonpolar solvents and more ketonic form in polar solvents. When a surfactant is added to an aqueous solution of BZA, there is no change to the keto-enol equilibrium when surfactant concentration is below the CMC and there are only surfactant monomers. When surfactant concentration is above the CMC, the micelles of surfactant will form and provide a less polar solvent and the amount of enolic form will increase abruptly and the amount of ketonic form will decrease. The enolic form and ketonic form have separate UV absorbance peaks at 312 nm and 250 nm respectively so monitoring the changes in the absorbance measurements at these two wavelengths with varying concentration of surfactant in aqueous solutions can determine the CMC of surfactants.

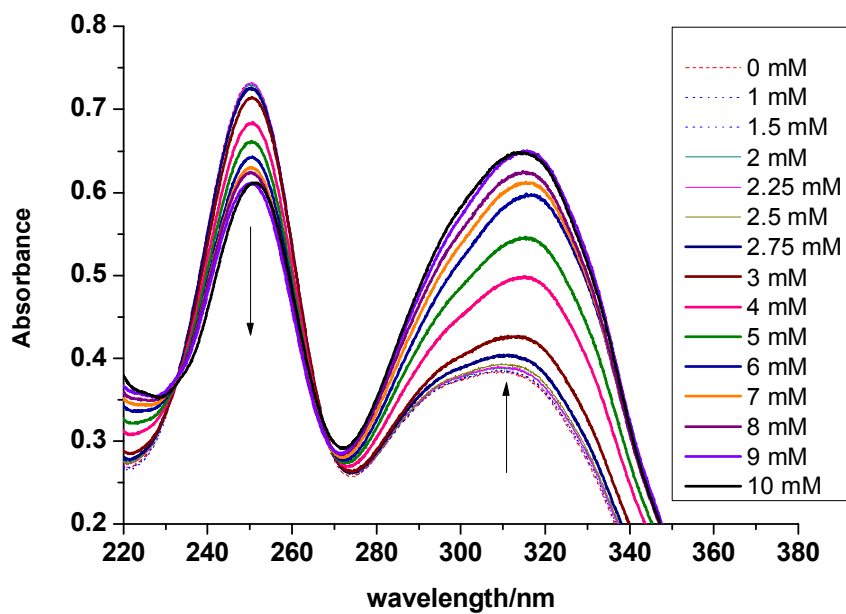
The stock BZA solution was prepared with high concentration at 5 mg/mL in dioxane. The stock BZA solution in dioxane was then diluted with buffer to 0.08 mg/mL. For each sample, 0.4 mL of the aqueous BZA solution was mixed with the appropriate amount of surfactant, the additive such as DTT and HEWL, and buffer to 3 mL of total volume of solution with constant BZA concentration in all samples. The spectra of BZA

samples with varying surfactant concentrations were measured on a CARY 300 Bio UV/Vis (Varian) spectrometer. The results of CMCs of different surfactants under the experimental conditions are shown in table 3-1. Figure 3-3 shows one example of the absorbance changes and the determination of the surfactant CMC.

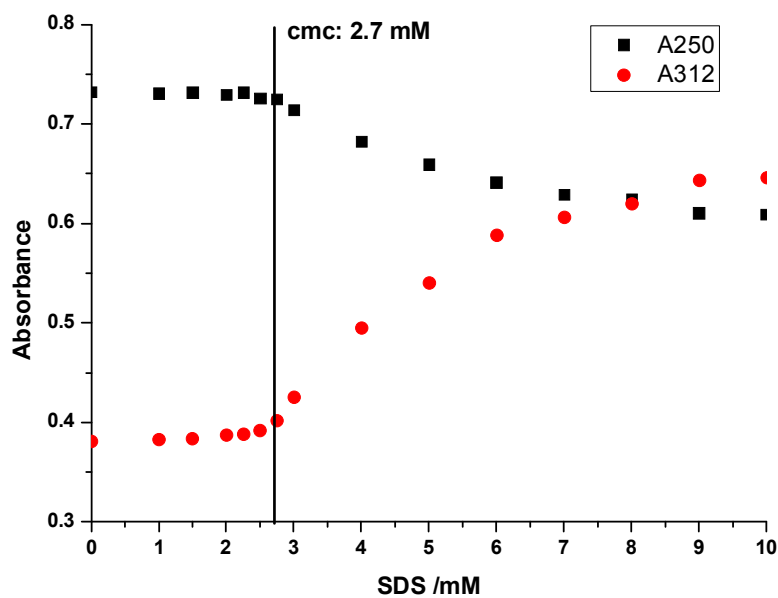
Table 3-1. Measured cmc of surfactants in 20 mM phosphate buffer at pH 4.6 at 25 °C

Surfactant samples	cmc measured
SDS	2.7 mM
DTAC	17 mM
C ₁₂ SO ₃	6.5 mM
C ₁₀ SO ₃	35 mM

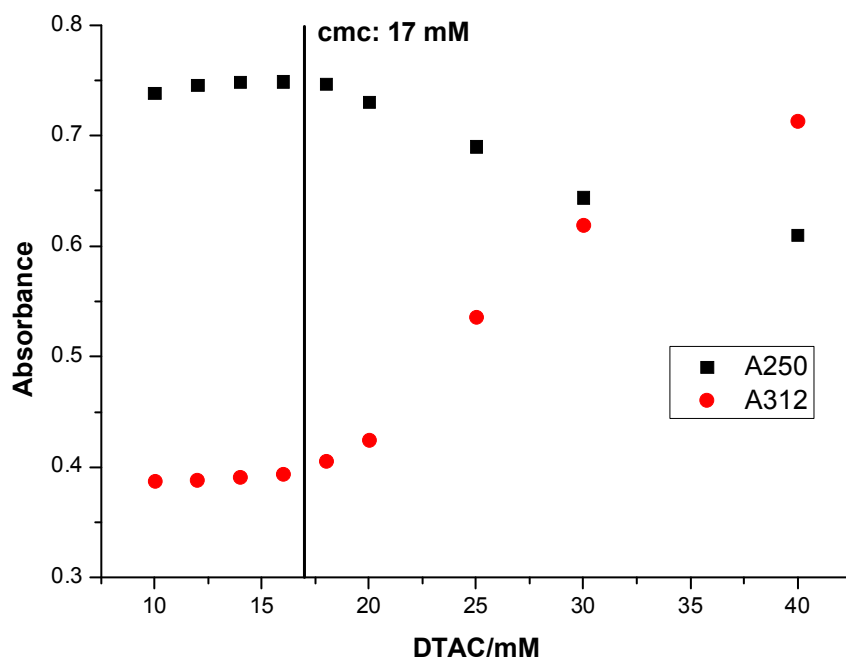
(a)



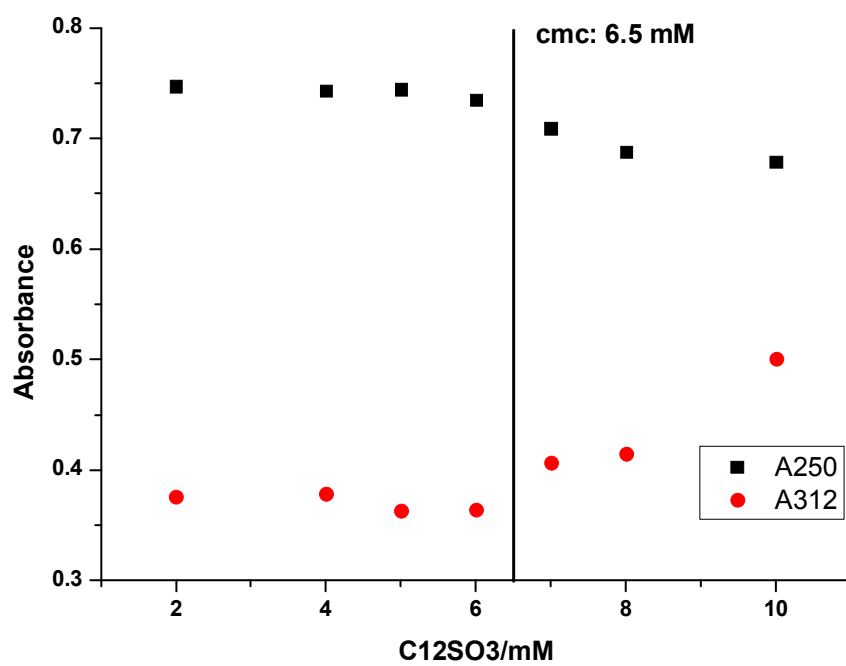
(b)



(c)



(d)



(e)

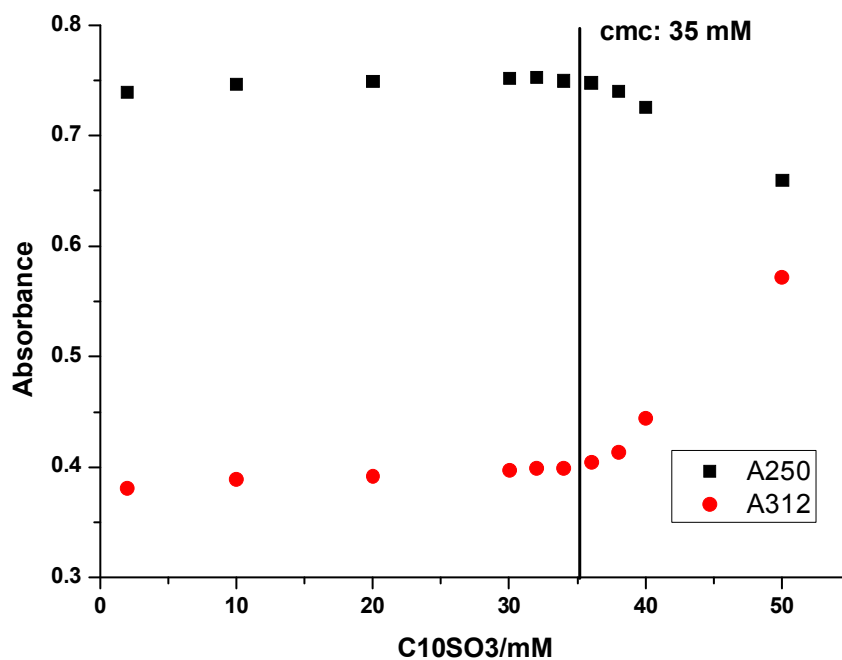


Figure 3-3. Absorbance spectra of BZA in various SDS concentration solutions (a) and absorbance of BZA as a function of concentration of SDS (b), DTAC (c), C12SO3 (d) and C10SO3 (e) at 312 nm and at 250 nm. The CMC is obtained by drawing two tangent lines in the region of absorbance changes and the intercept of those two tangent line is at the CMC.

3.2.3 CD measurements

CD spectra were measured from 185 nm to 250 nm with a 50 nm/min scanning rate, 2 s response time, 1 nm bandwidth and as the average of 8 scans on a JASCO 810 spectrometer (Jasco, Inc.). For equilibrium measurements, the protein solutions were prepared at 0.2 mg/mL in 20 mM pH 4.6 phosphate buffer and measured in a 1 mm pathlength quartz cuvette (Starna, Inc) at room temperature. All sample spectra were corrected by subtraction of the corresponding spectrum of the buffer. The fractional secondary structures were calculated with the CDPro programs (accessible at: lamar.colostate.edu/~sreeram/CDPro/main.html) using data for 195 nm to 250 nm.⁽⁷⁰⁾

3.2.4 Fluorescence

Fluorescence spectra were measured on a Fluoromax-3 spectrofluorometer (Horiba Jobin Yvon Inc.) with the samples in a 1 mm × 1 cm quartz cell. The excitation wavelength was 295 nm and the emission spectra were collected from 300 nm to 500 nm. All the spectra were corrected by subtraction of the buffer spectrum.

3.2.5 Stopped-flow measurements

For stopped-flow mixing dynamics, an SFM-400 accessory (Bio-logic) and MPS-52 control console were connected to the Jasco-810 spectrometer. The Xe lamp in the CD spectrometer was changed to a Xe-Hg lamp to enhance far-UV intensity. The mixing deadtime under our measurement conditions was ~10 ms, but instrument response was much faster and the signal change large enough to allow determination of

kinetics in the ms and longer time range. The CD signal channel was recorded with 1 KHz sampling for 5 s of the signal at 222 nm using a 4 nm bandwidth by means of standard JASCO kinetics methods. The HV was fixed and the CD signal was normalized to the detector current (in the software) to enable determination of the ΔA with a faster response. The total fluorescence signal was simultaneously collected on the same sample by collecting emission at all wavelengths above 320 nm using a cut-off filter in front of a separate fluorescence detector which was located at right angles to the CD and excitation beam. The results were fitted with multiple exponential functions using the Bio-Kin32 software.

3.2.6 Lysozyme activity assay

The enzymatic activity of lysozyme was measured by monitoring the rate of decrease in the turbidity of a *Micrococcuslysodeikticus* cell suspension. For this assay, 0.02 ml of lysozyme sample (0.1 mg/ml) was added to a 1 cm cuvette with 0.98 ml cell suspension (0.3 mg/ml), which was then was agitated via a pipette action for 10 s. The absorbance was recorded at 450 nm on a CARY 300 Bio UV/Vis (Varian) spectrometer every 10 s for 10 minutes. One unit of activity corresponds to an absorbance decrease of 0.0026/min.

3.3 Results and discussion

3.3.1 The refolding of reduced HEWL with anionic surfactant micelles

After reduction HEWL loses all four S-S bonds as demonstrated by mass spectra which show the molecular weight to increase from the native state value by eight mass units (Figure 3-4). CD spectra (Figure 3-5, truncated at 200 nm because spectra became prohibitively noisy at <200 nm due to absorbance of the reductant and SDS) show that the reduced/unfolded HEWL (blue dotted trace) has a higher fraction of unordered structure and much less helical structure than the native state (red dash line). The fluorescence spectra (Figure 3-6) of the reduced HEWL (red solid line) has 50% more intensity than that of the native state (black solid line), and a red shift of the peak position from 344 to 354 nm is observed, which is consistent with the tryptophans being more exposed to solvent after reduction. (The lower pH of 4.6 is needed for solubility of the protein in reductant, but has little effect on native HEWL.) Low concentrations of negatively charged surfactants (e.g. SDS) cause HEWL to aggregate and precipitate, limiting the range of concentrations for which we can study HEWL-surfactant interaction. Reduced HEWL is somewhat more soluble in SDS, but concentrations below 1 mM remain problematic, since dilute SDS will precipitate the protein due to charge neutralization.

The far-UV CD spectra of reduced HEWL in the presence and in the absence of anionic surfactant SDS as compared to that of native HEWL are shown in Figure 3-5a, and the average fractional secondary structure derived from these spectra (using CDPro) are shown in Figure 3-5b. The CD spectra show that with the addition of anionic

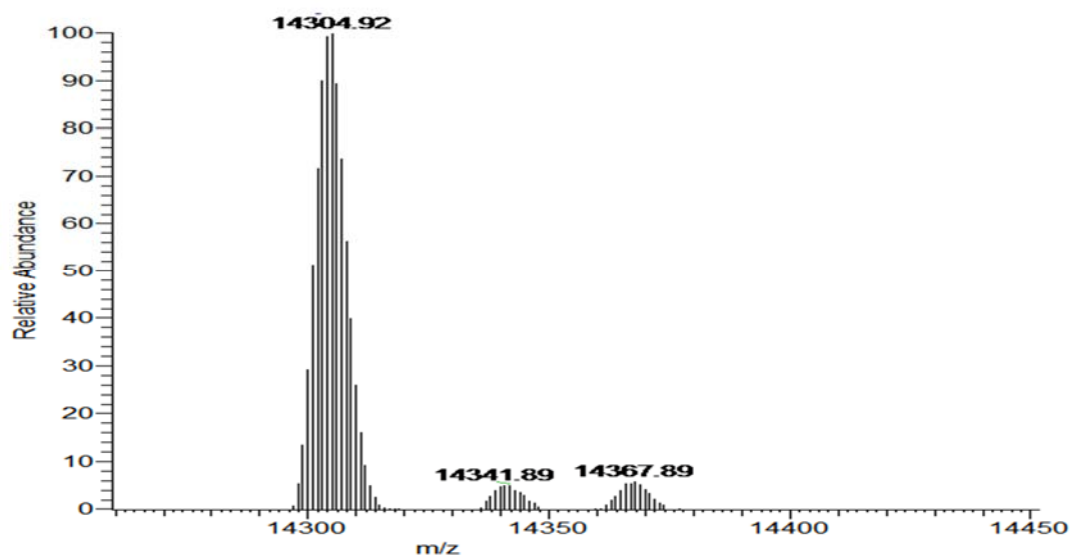
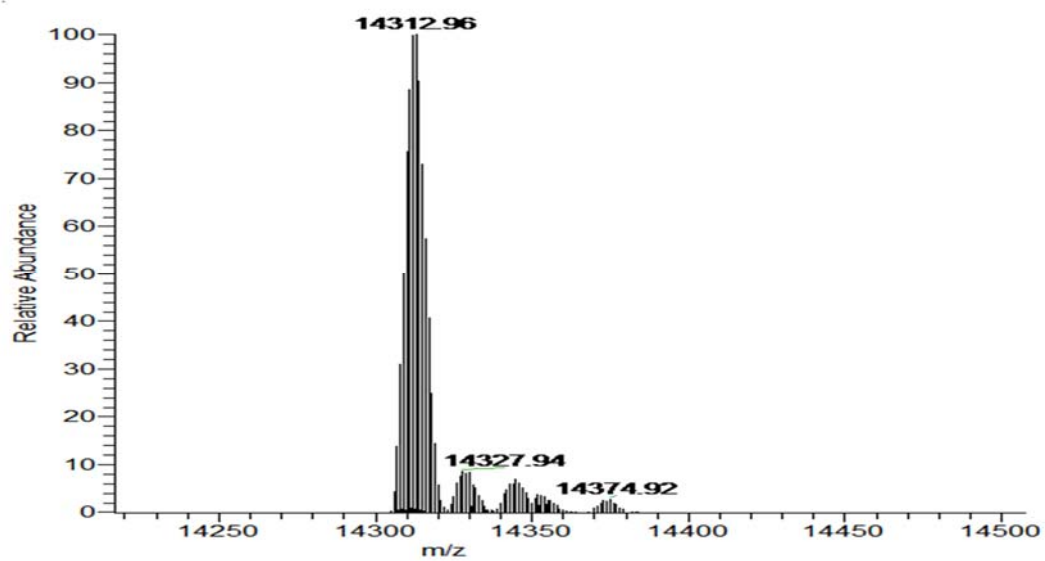
(a)**(b)**

Figure 3-4. The mass spectra of **(a)** oxidized and **(b)** reduced lysozyme.

[Provided by UIC-RRC MassSpec service]

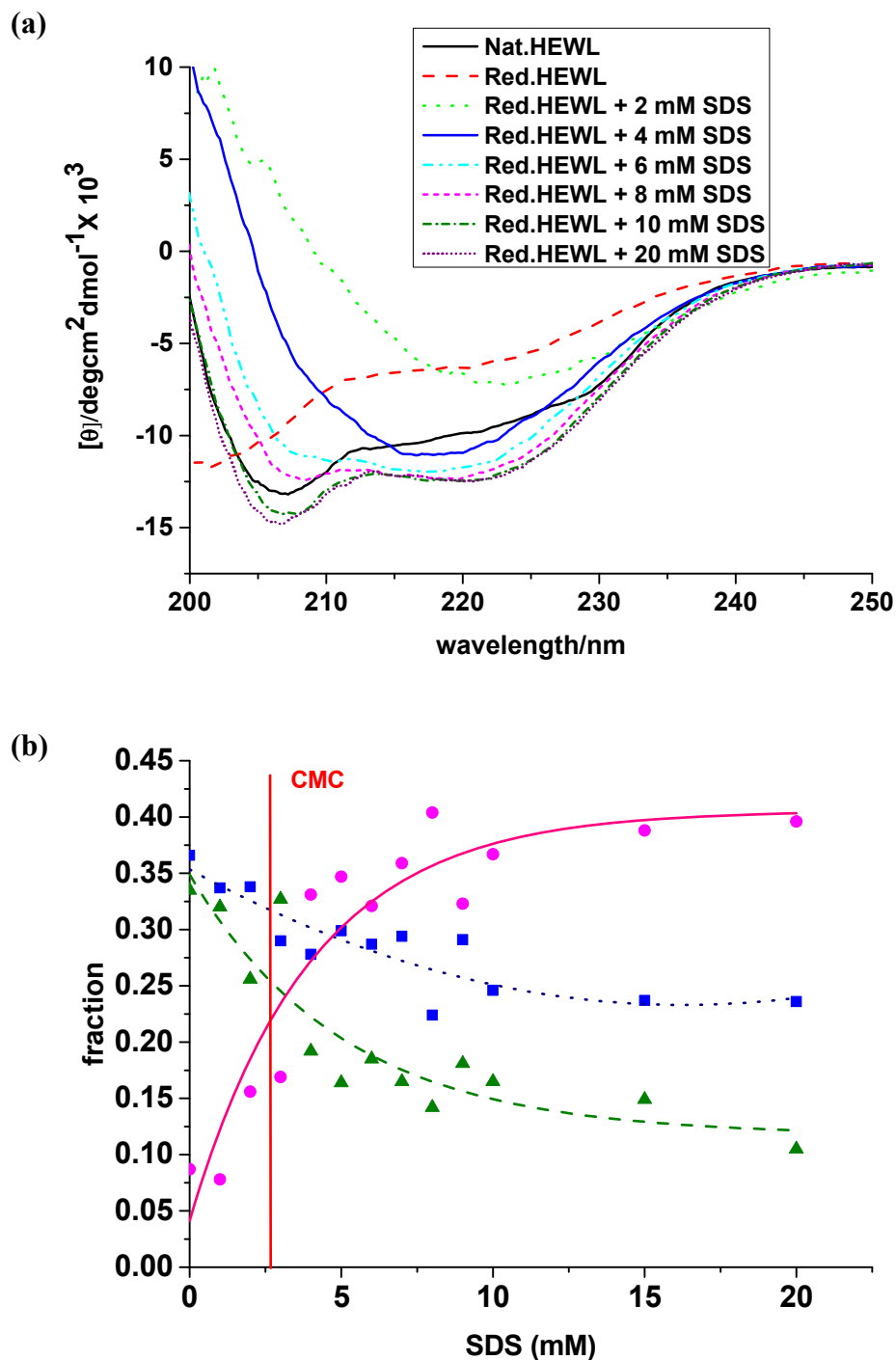


Figure 3-5. (a) Far-UV CD spectra of native HEWL and reduced HEWL, and with addition of different concentrations of SDS at pH 4.6. (b) Calculated secondary structure fractions: helix (pink circles, pink solid line), sheet (green triangles, green dash line) and unordered structures (blue squares, blue dot line). CDPro outputs fractions for regular and distorted helices, regular and distorted sheet strands, unordered structure and turns. The fractions of turns are not plotted.

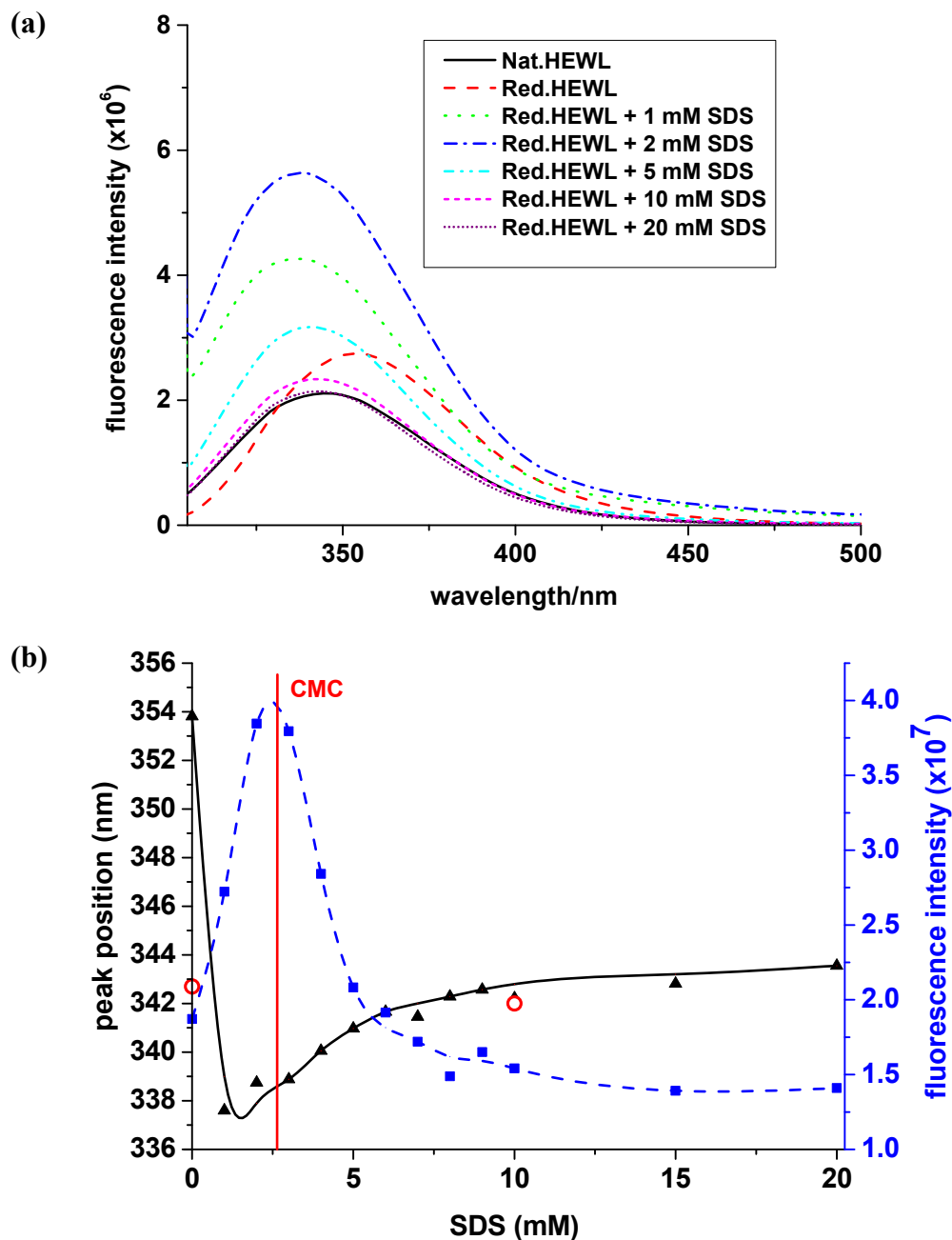


Figure 3-6. (a) Fluorescence spectra of native HEWL and reduced HEWL, and with addition of different concentrations of SDS at pH 4.6. (b) Variation of the integrated fluorescence intensity (squares, dash line) and peak position (triangles, solid line) with addition of anionic surfactant SDS (red circles show the peak positions of oxidized HEWL and oxidized HEWL in 10 mM SDS).

surfactant, SDS, the reduced HEWL structure becomes increasingly helical, coming to a saturated value well above the critical micelle concentration (CMC) in this environment (2.7 mM as corrected for buffer, reduced pH, protein and reductant, Table 3-1). Reduced HEWL with SDS above the CMC has even more helical structure than does the native state. However, adding SDS to native HEWL also increases its helicity (Figure 3-7a and Figure 3-8), so that both reduced and oxidized HEWL in SDS above its CMC have similar fractional helical compositions. While native HEWL has ~32% helix, it increases to ~37% for the oxidized form in micellar SDS. The CMC is buffer and pH sensitive, such that the altered conditions of our experiment yield lower values than often quoted in the literature, as we have determined by absorbance change of BZA (benzoylacetone or 1-phenyl-1,3-butadione). The relevant values for our experiments are indicated on the figures (and summarized in Table 3-1). These plots show that the maximal gain of helical structure occurs well after the CMC has been reached, indicating monomer surfactant-protein interaction is insufficient for saturation and that micelles have a role in the final state.

The intrinsic fluorescence emission from the six tryptophan residues undergoes a two-step change upon interaction with SDS. The fluorescence intensity first increased at low SDS concentration and then decreased back to the level of native HEWL upon further addition of SDS to higher concentration (10 mM, Figure 3-6b). The fluorescence peak position for reduced HEWL in SDS also changed in a similar manner: first becoming blue shifted and then red shifted back to nearly the native (oxidized) HEWL value (342 nm). At low concentrations of SDS, surfactant monomers with negative

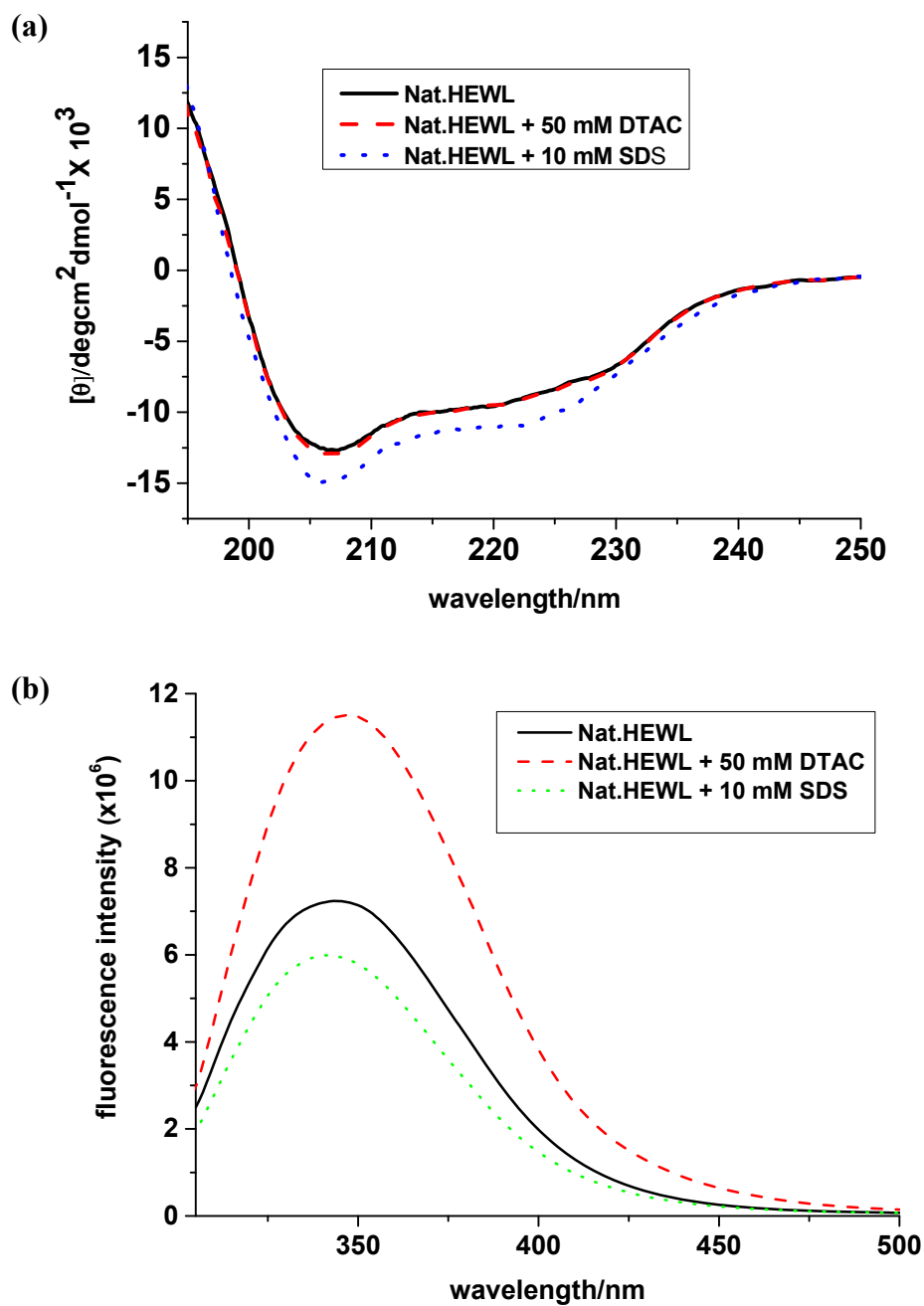


Figure 3-7. Comparison of surfactant effects on native HEWL, **(a)** ECD and **(b)** fluorescence spectra of native HEWL (black solid line) and HEWL with addition of SDS (red dash line) and DTAC (blue dot line) above their CMC.

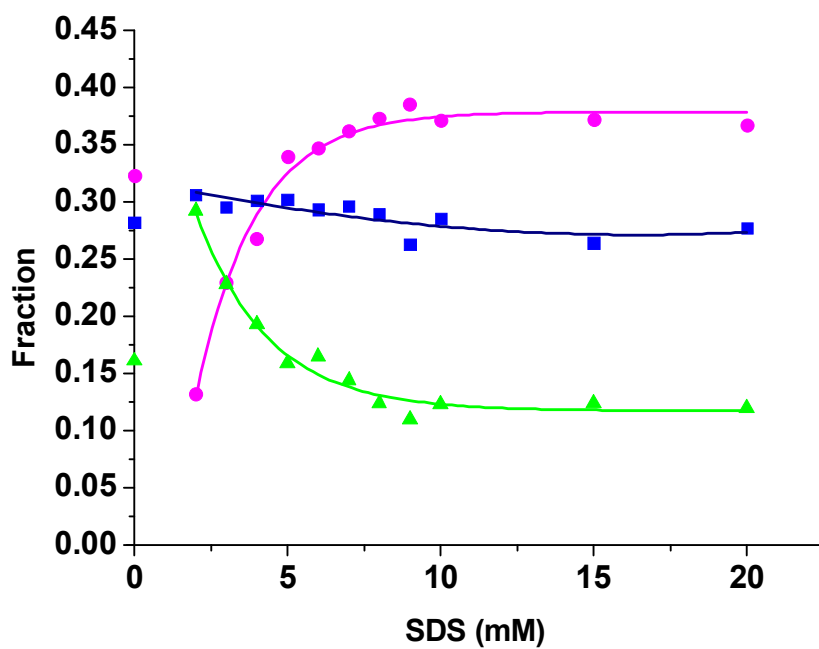


Figure 3-8. Variation of fractional secondary structure for oxidized HEWL on addition of anionic surfactant SDS, from fitting CD: helix (pink circles), sheet (green triangles) and unordered structures (blue squares) as in figure 3-5.

charges can bind specifically to the positively charged sites and neutralize the protein, which leads to some helical formation and considerable increase in fluorescence intensity and blue shift.⁽⁷¹⁾ Increasing the SDS concentration increases hydrophobic interaction between the reduced HEWL and SDS, which steadily increases the initially reduced HEWL fluorescence until the CMC is reached, whereupon the hydrophobic interaction with the protein appears to become limited by micelle formation. Above the CMC the helicity continues to grow but the fluorescence characteristics reverse, quenching intensity and red-shifting the maximum frequency, indicating an altered interaction with micelles having increased exposure to solvent and charge. For the micellar saturated reduced HEWL state, which has similar average secondary structure content to the oxidized micellar state (i.e. for oxidized HEWL with SDS above CMC), the reduced HEWL in SDS fluorescence also has similar frequency to the native state with and without SDS (see open red circles, Figure 3-6b). (None-the-less, despite the fluorescence recovery, both oxidized and reduced HEWL have non-native tertiary structure in SDS micelles, see below.)

Near-UV CD can monitor changes in Trp environments and by extension changes in tertiary structure. In Figure 3-9, the near-UV CD spectra for native and reduced HEWL with and without SDS addition are compared. The spectra vary and the CD intensity at 290 nm, which indicates Trp structure for oxidized HEWL, is lost in the SDS interacting species. Reduced HEWL tertiary structure does change with addition of SDS, but the native form is not recovered. By comparison, the form of the near-UV CD for oxidized HEWL in SDS is also different, indicating a loss of tertiary structure

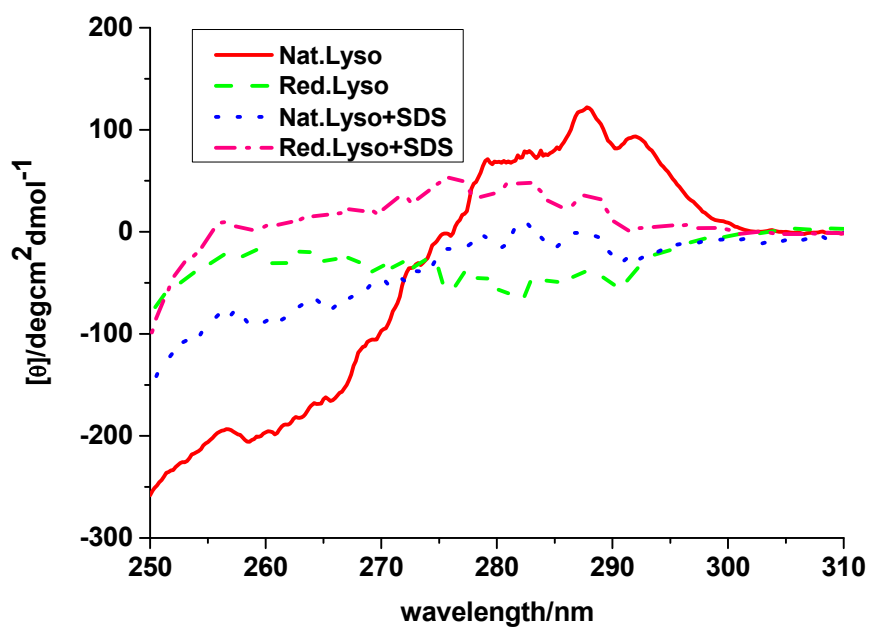


Figure 3-9. Near-UV CD spectra of native HEWL (red solid line), reduced HEWL (green dash line), native HEWL in 50 mM SDS (blue dot line) and reduced HEWL in 50 mM SDS (pink dash dot line). [Note these CD, as measured, are very weak with approximate value of 4 millidegrees due to a need to use shorter paths for the reduced samples.]

in both forms that is not recovered in the surfactant medium.

The balance of the electrostatic interactions and hydrophobic interactions between protein and surfactants is an important aspect in this process of reforming helical structure. Two more surfactants were studied that alter the relative distribution of negative charge and hydrophobicity. $C_{12}SO_3$ has the same length hydrophobic tail as SDS but contains a different head group with less partial negative charge distribution.⁽⁷²⁾ Interaction with reduced HEWL results in the same effects on the spectra, and by extension on the structure, as found with SDS, but requires a higher concentration of $C_{12}SO_3$ to restore secondary structure for the reduced HEWL (Figure 3-10). More helical structure can be obtained for reduced HEWL under conditions above the $C_{12}SO_3$ CMC than for native state HEWL, suggesting that disulfides restrict the ultimate helical structure that can be formed with the HEWL polymeric sequence, in the presence of negatively charged surfactant micelles. Paralleling the SDS result, the fluorescence intensity first increased and then decreased back to a level characteristic of native HEWL upon addition of $C_{12}SO_3$, and the fluorescence peak position first blue shifted and then red shifted back to the native HEWL position, but this fluorescence change is not strictly correlated to the CMC.

By contrast $C_{10}SO_3$ has the same head group, and thus charge, as $C_{12}SO_3$ but has a shorter hydrophobic tail and higher CMC, and thus paralleling the overall CMC dependent pattern, it requires even higher concentration to induce full recovery of the helical fraction in reduced HEWL (Figure 3-11). This contrast in behavior for different length surfactants reinforces the importance of the micellar formation to induce the

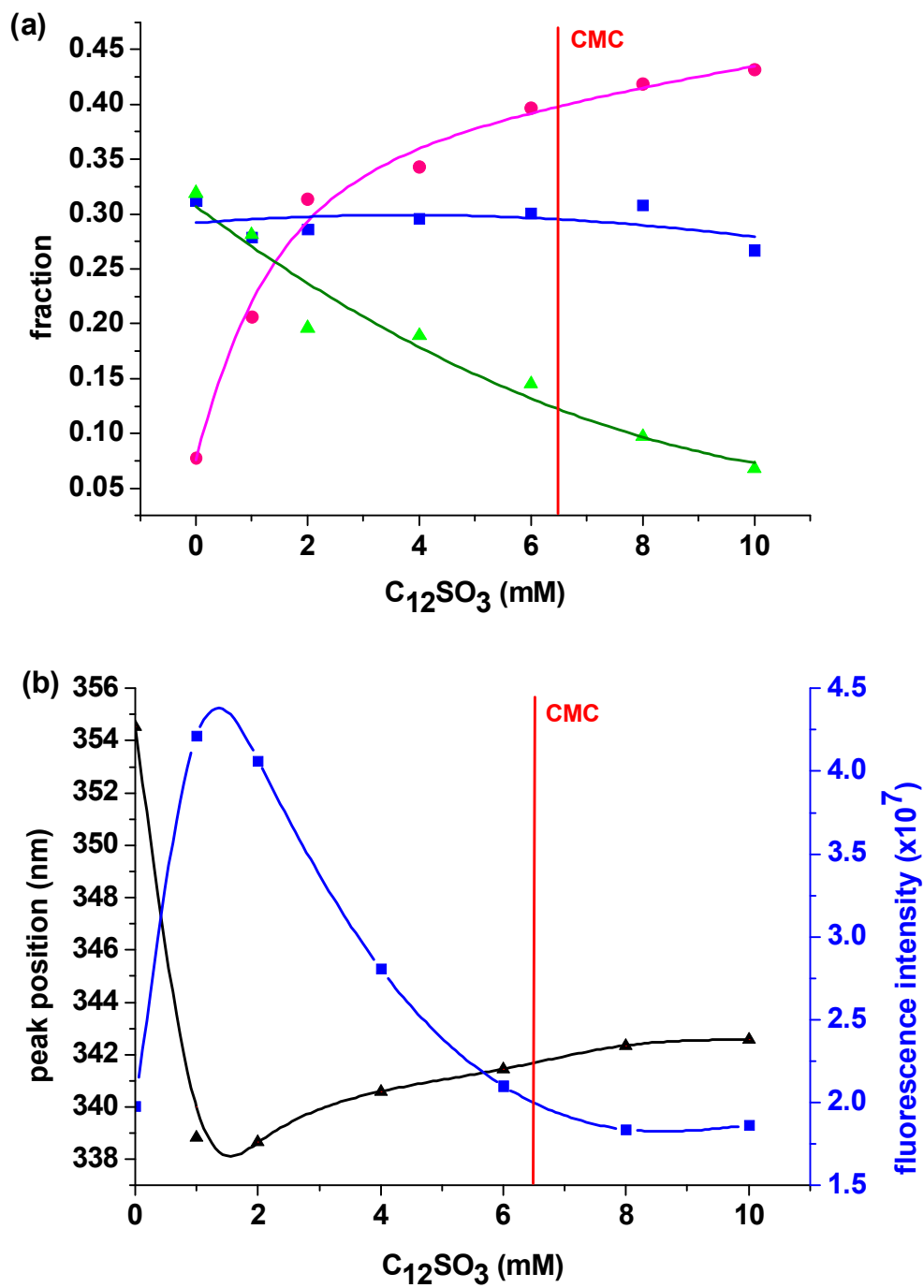


Figure 3-10. (a) Variation of fractional secondary structure for reduced HEWL on addition of anionic surfactant $C_{12}SO_3$, from fitting CD: helix (pink circles), sheet (green triangles) and unordered structures (blue squares) as in figure 3-5. (b) Integrated fluorescence intensity (blue squares) and peak position (black triangles).

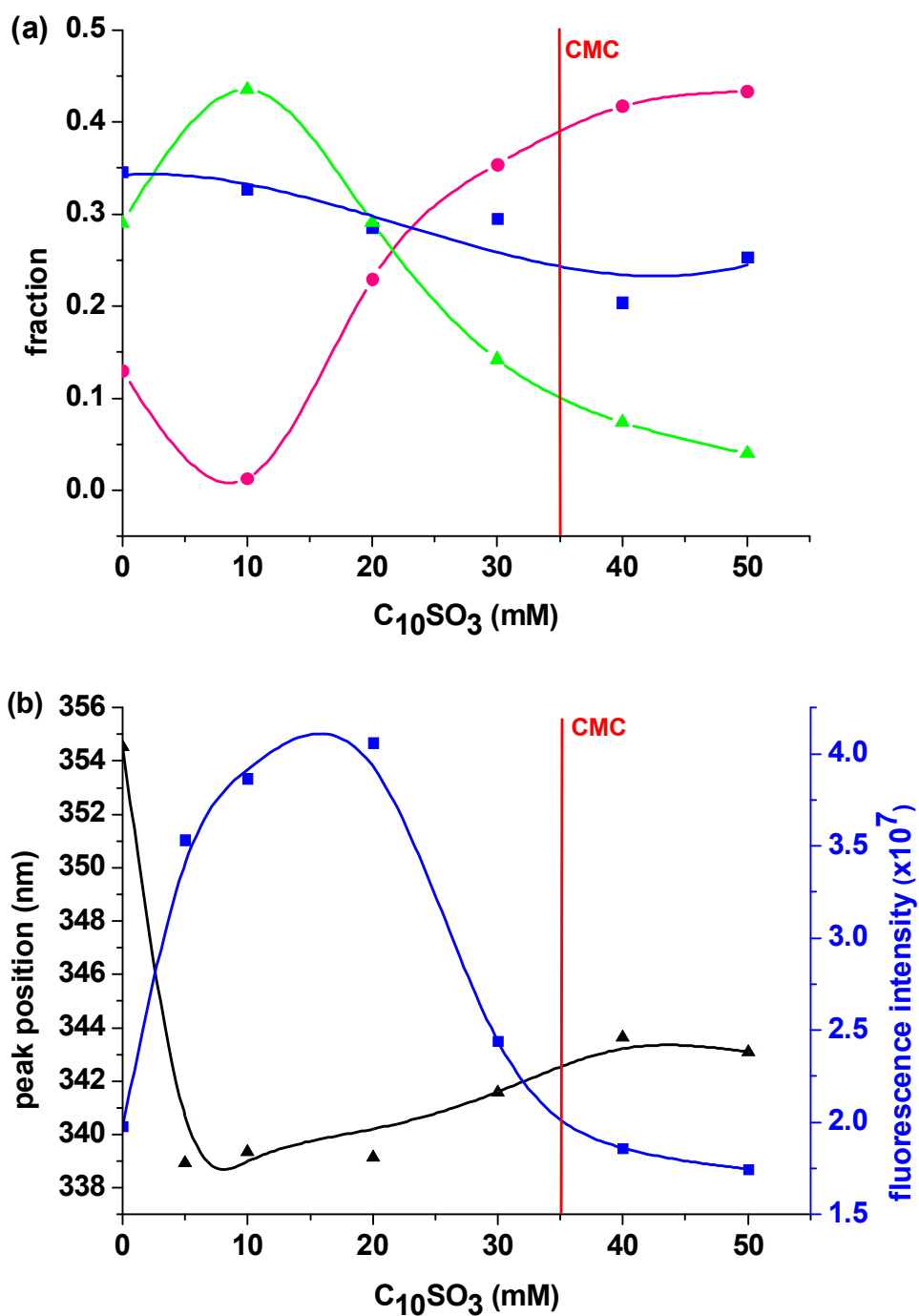


Figure 3-11. (a) Variation of fractional secondary structure for reduced HEWL on addition of anionic surfactant $C_{10}SO_3$, from fitting CD: helix (pink circles), sheet (green triangles) and unordered structures (blue squares) as in figure 3-5. (b) Integrated fluorescence intensity (blue squares) and peak position (black triangles). [values for low surfactant concentrations may have high error due to possible precipitation]

maximum helicity for each surfactant with this protein. In the same way as seen with SDS, both $C_{12}SO_3$ and $C_{10}SO_3$ can restore helical content for reduced HEWL when the surfactants interact with the protein above their CMC, but these two $-SO_3$ based surfactants require higher concentrations, which appears to be due to their having less charge on their head groups and, for $C_{10}SO_3$, less hydrophobic interaction. The difference in hydrophobicity between $C_{10}SO_3$ and $C_{12}SO_3$ alters the CMC and that may be the critical parameter for achieving ultimate structural change in reduced HEWL. These comparisons lead to the added conclusion that more negative charge and more hydrophobicity on the anionic surfactant will favor the process of regaining secondary structure and altering Trp exposure in reduced HEWL.

3.3.2 The interaction of reduced HEWL with cationic and zwitterionic surfactant micelles

While anionic surfactant micelles should have coulomb attraction to the positively charged reduced HEWL protein at these reduced pH 4.6 values (since the HEWL isoelectric point is 10.7), for cationic surfactant micelles we might expect different behavior, even though both offer hydrophobic interactions. In contrast to its behavior in anionic surfactants, the reduced HEWL can only partially recover helical structure by addition of the cationic surfactant, DTAC, even for concentrations above the DTAC CMC (Figure 3-12). The helical fraction for reduced HEWL in DTAC above the CMC is only ~25% which remains below the ~33% helix in native HEWL structures. Figure 3-12b shows the fluorescence intensity and peak position values upon adding

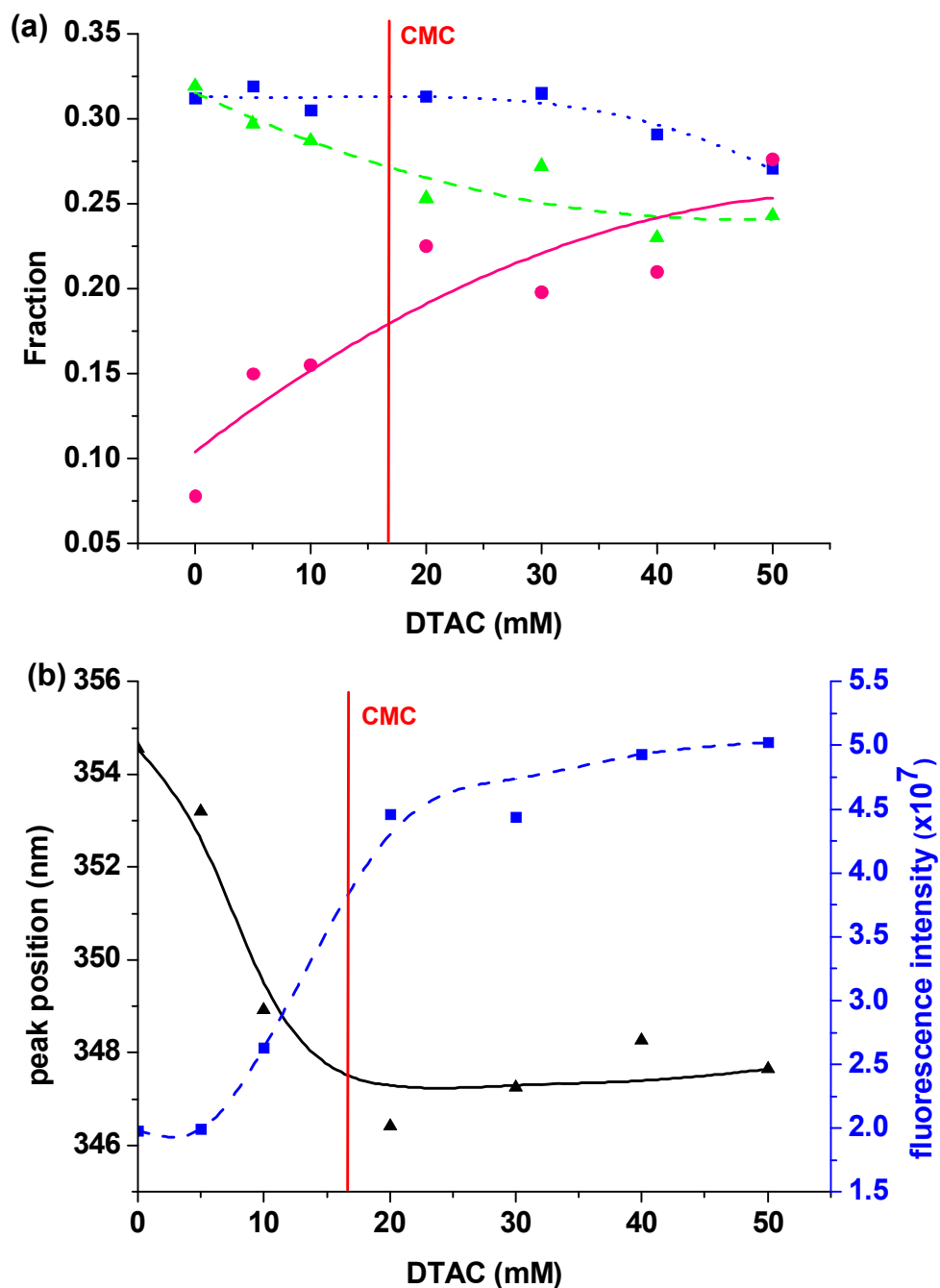


Figure 3-12. (a) Variation of fractional secondary structure for reduced HEWL on addition of cationic surfactant DTAC, from fitting CD: helix (pink circles, pink solid line), sheet (green triangles, green dash line) and unordered structures (blue squares, blue dot line) as in figure 3-5. (b) Variation of fluorescence integrated intensity (blue squares, blue dash line) and peak position (black triangles, black solid line) under similar conditions.

DTAC, which undergo a simpler change than with the anionic surfactants, showing only further intensity increase and blue shift from native HEWL, both aspects stabilizing above the CMC. For the zwitterionic surfactant, sulfobetaine (SB3-10), similar effects on the structures of reduced HEWL were seen as for DTAC (Figure 3-13), implying that the hydrophobic interaction is primarily operative for both of these with HEWL.

Comparison of the effects of different surfactants on the refolding of reduced HEWL suggests that negative charge on surfactants is required to specifically bind to the positively charged protein and to refold and increase the helical fraction of secondary structure for the reduced HEWL. Hydrophobic interactions then dominate higher, micelle forming, concentrations and develop maximal helix fraction. Native HEWL also increases helicity and loses tertiary structure when interacting with negative surfactant micelles, showing a parallel behavior with and without disulfides that is not obvious in only buffer environments. However, with positive micelles, DTAC, there is little change in secondary structure (Figure 3-7a), although the fluorescence changes (Figure 3-7b) indicate an interaction with surface Trp residues. Analogous experiments with a mutant HEWL where all cysteins were converted to alanines gave similar variations with SDS and DTAC (shown below) further supporting the role of disulfides in this difference.

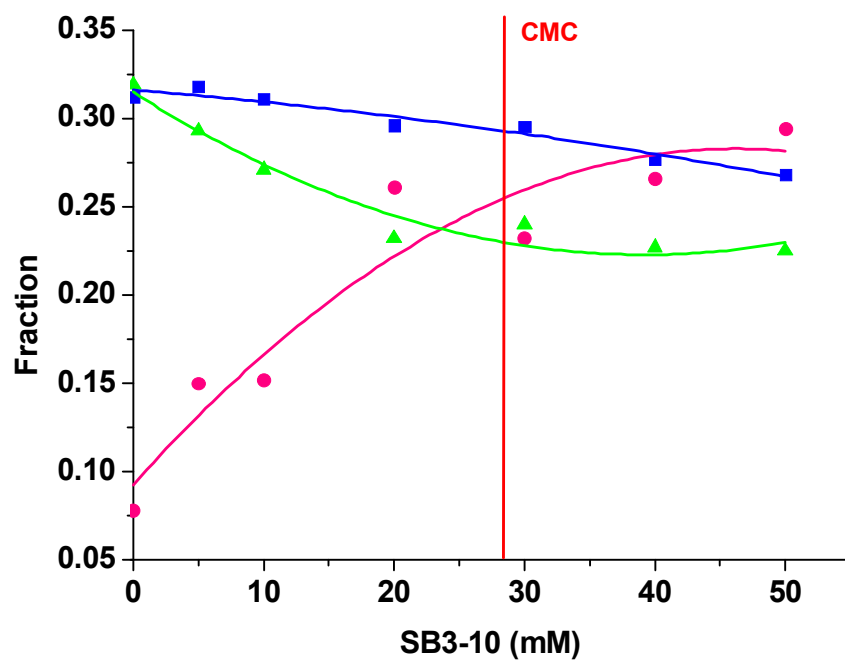


Figure 3-13. Variation of fractional secondary structure for reduced HEWL on addition of zwitterionic surfactant SB3-10, from fitting CD: helix (pink circles), sheet (green triangles) and unordered structures (blue squares) as in figure 3-5.

3.3.3 The folding of OSS mutant HEWL with anionic and cationic surfactant micelles

The OSS mutant HEWL was prepared by replacing all the eight cysteines by alanines so there can be no disulfide bonds and was graciously provided to us by Prof. Harald Schwalbe and Dr. Robert Silvers, University of Frankfurt. It can also be refolded to a non-native highly helical state with addition of anionic surfactant micelles (Figure 3-14) and can be only partially refolded with cationic surfactant micelles (Figure 3-15). This indicates that the reduced HEWL and the mutant HEWL have the same structures and structure reforming processes. Despite both species having a total loss of S-S bonds, they differ in that reduced HEWL has cysteine and OSS has alanine in the eight mutated positions. As a result, the initial CD change is bigger and occurs faster and steeper for OSS than reduced HEWL, and occurs at lower SDS concentrations, with gradual further increase in helicity up to the CMC. On the other hand, the fluorescence in the OSS mutant changes directly parallel those seen with reduced HEWL.

3.3.4 The refolding of helical structure in reduced HEWL induced with trifluoroethanol (TFE)

TFE is known to induce helical structures in proteins, not only by disturbing native hydrophobic interactions, binding to the protein backbone via hydrogen bonds, but also providing hydrophobic surface areas to mimic interaction of the polypeptide chain with membranes. The CD spectra (Figure 3-16a) show that increasing TFE

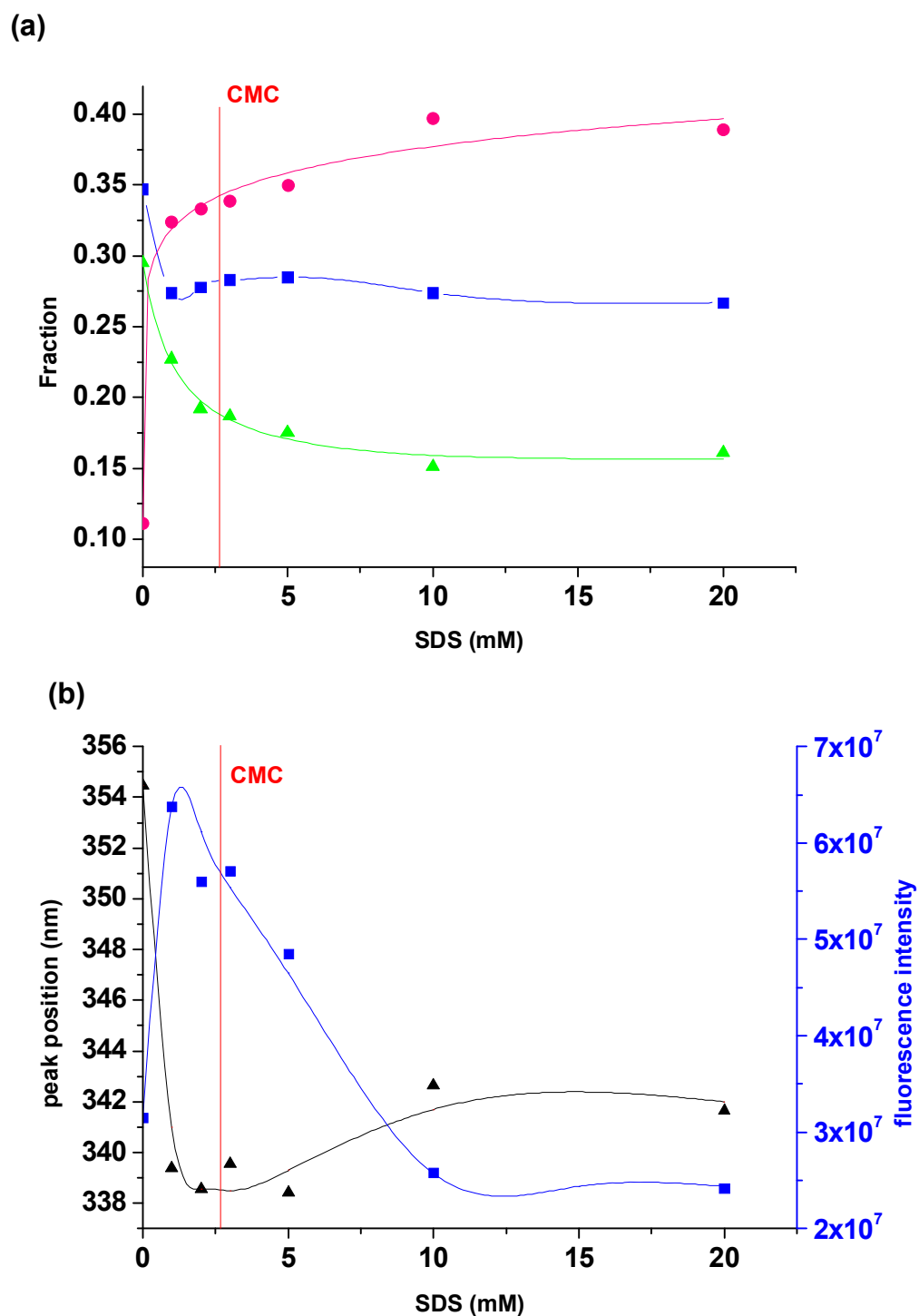


Figure 3-14. (a) Calculated fractions of secondary structures: helix (pink circles), sheet (green triangles) and unordered structures (blue squares) as in figure 3-5. (b) Fluorescence peak intensity (squares) and peak position (triangles) variation with addition of anionic surfactant SDS to OSS mutant HEWL.

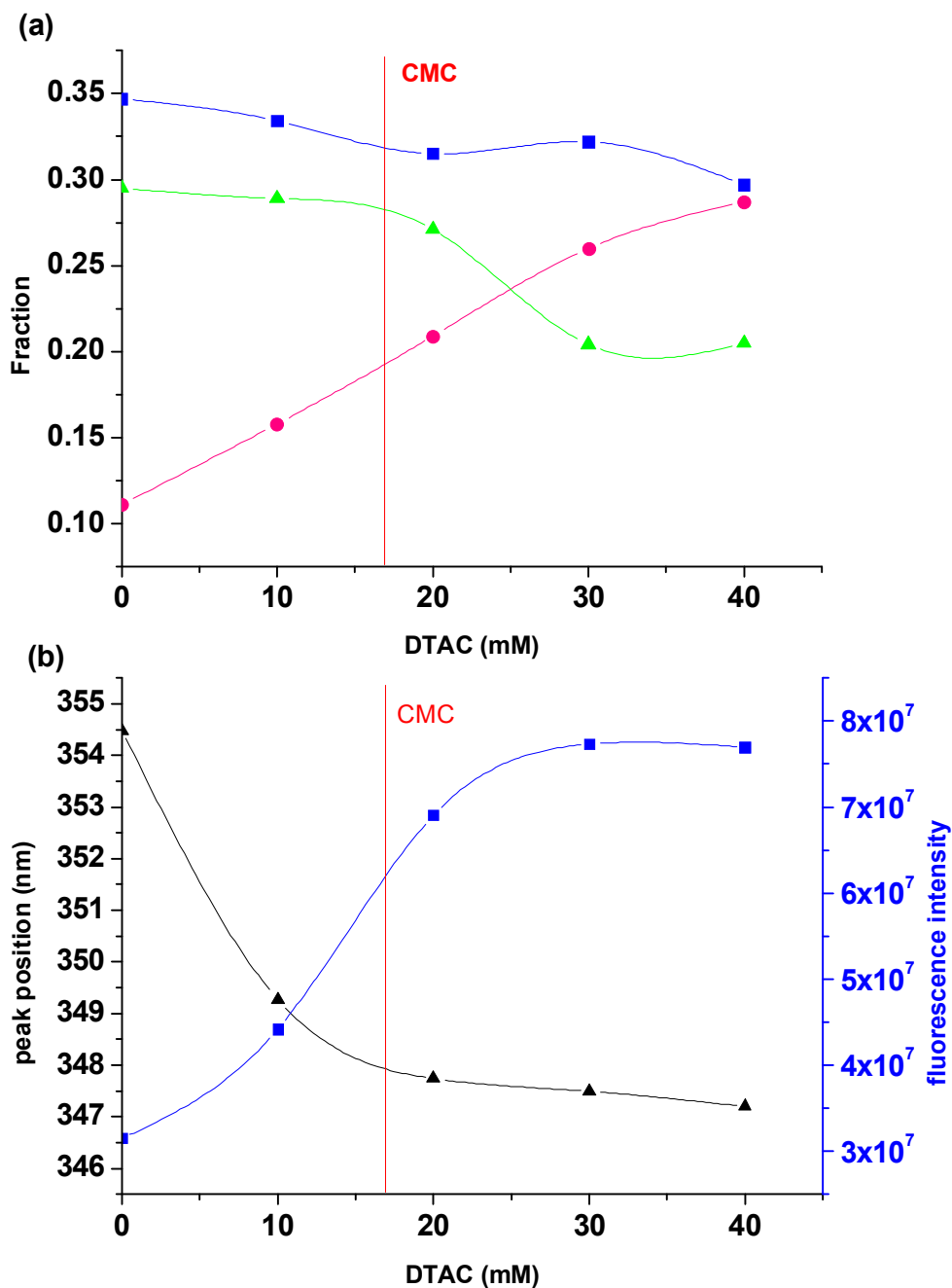


Figure 3-15. (a) Calculated fractions of secondary structures: helix (pink circles), sheet (green triangles) and unordered structures (blue squares) as in figure 3-5. (b) Fluorescence peak intensity (squares) and peak position (triangles) variation with addition of cationic surfactant DTAC to OSS mutant HEWL.

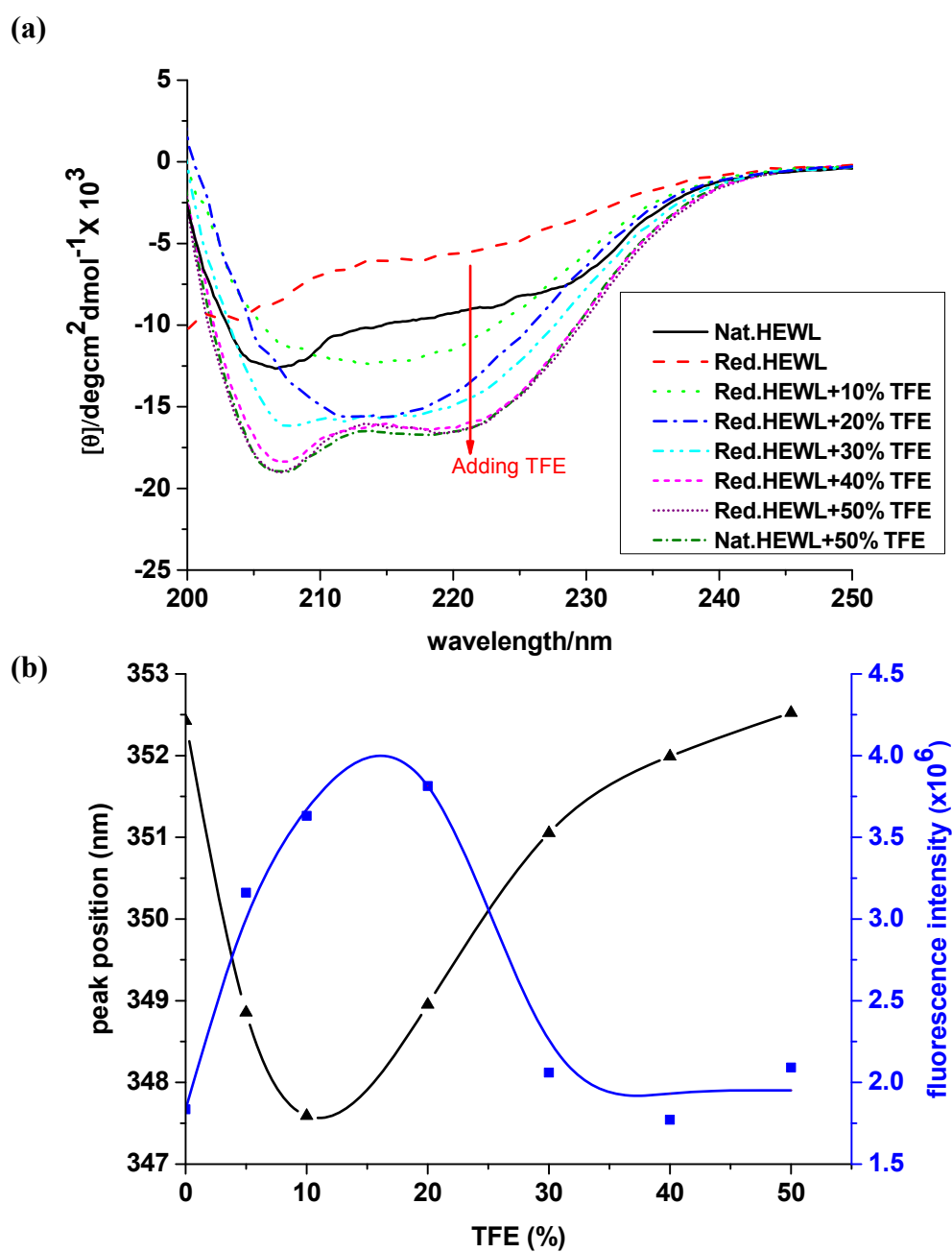


Figure 3-16. Variation of reduced HEWL with different concentrations of TFE (a) CD spectra of reduced HEWL with added TFE. (b) Change in fluorescence peak intensity (blue squares) and peak position (black triangles).

concentration can steadily induce formation of more helical structure in HEWL. At 50% TFE, both reduced and oxidized HEWL have increased ellipticity, more than twice that of native HEWL in aqueous buffer. At low concentration of TFE (15%) there is no significant effect on the oxidized HEWL secondary structure, but reduced HEWL gains helical structure at even lower concentrations of TFE. This may be due to the reduced HEWL not being as compact as native HEWL resulting in its hydrophobic sites being more exposed to the solvent, and thus the TFE having more relative impact on structure. However, the conformational transition is virtually complete at 50% TFE for both reduced HEWL and oxidized HEWL suggesting that the binding of TFE to surface sites is saturated, forming a direct parallel to the above (negative) surfactant results. It is interesting that with stepwise addition of TFE, reduced HEWL does not pass through an intermediate state that matches the secondary structure of the oxidized state HEWL at some specific concentration of TFE. Presumably this is because the original hydrophobic interactions of the protein are disrupted once TFE is added, and the refolding is taking place on a different path to another, partially helical but non-native structure.

With increasing TFE concentration, the fluorescence intensity first increases then decreases back and the peak position blue-shifts then red-shifts back, much as seen with the anionic surfactants (Figure 3-16b). At low concentration, TFE binds to sites on the protein to form hydrogen bonds and make the tryptophans less exposed to solvent.⁽⁷³⁻⁷⁶⁾ When TFE binds to more hydrophobic surface sites at higher concentrations and disrupts hydrophobic interactions between helical segments, the

tryptophans will most likely be more solvent exposed.

3.3.5 Thermal stability studies on the refolded state of reduced HEWL in surfactant micelles

The thermal stability studies shown in Figure 3-17 show a nearly linear decrease in the (negative) ellipticity magnitude in the far-UV CD on heating the highly helical state of reduced HEWL in surfactant micelles. This can be contrasted with the clearly cooperative thermal denaturation of native HEWL (filled squares, Figure 3-17), which means the cooperativity of structural stabilization is lost for the helical states of reduced HEWL in surfactant micelles. This would be consistent with formation of a conformation, often termed a molten globule,⁽⁷⁷⁾ in the presence of micelles that has substantial secondary structure (helix) but little tertiary structure. This may represent a dynamic equilibrium of related conformational substates resulting in the loss in cooperativity in the structural transition. It is important to see that addition of anionic or cationic surfactant to native HEWL also resulted in a loss of cooperative unfolding (Figure 3-17), indicating the surfactant had a similar effect on oxidized state tertiary structure. In other words, inclusion of disulfides does not change the surfactant effect on cooperativity.

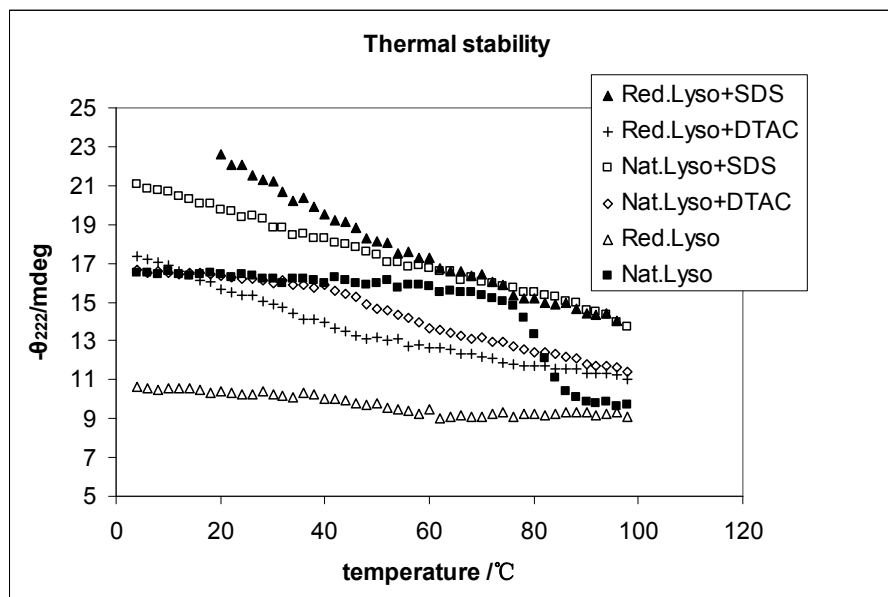


Figure 3-17. Thermal denaturation of native HEWL in buffer (filled squares), and with DTAC (diamonds) and SDS (unfilled squares), and reduced HEWL in buffer (unfilled triangles), and with DTAC (crosses) and SDS (filled triangles)

3.3.6 Stopped-flow kinetic study of the refolding of reduced HEWL with surfactant micelles

The kinetics of the structural changes induced in reduced HEWL by interaction with surfactant micelles were monitored by measuring both CD ellipticity change at 222 nm and total fluorescence intensity above 320 nm under stopped-flow mixing conditions. The CD (summarized as fits only, since the data have a large noise level as shown by the example trace in Figure 3-18) and fluorescence kinetic traces for reduced HEWL refolding with anionic (SDS) and cationic (DTAC) surfactant micelles are shown in Figure 3-19 and Figure 3-20, respectively. The stopped-flow curves, $\phi(t)$, are fit with a multiple exponential function to determine rate constants in the structure reforming process using the following relationships:

$$\phi(t) = at + b + \sum c_i \cdot e^{-k_i t} \quad (\text{eq.3-1})$$

where k_i and c_i are the rate constant and amplitude of the i th phase and a and b represent linear baseline corrections.

The stopped-flow kinetics of the reduced HEWL structure change with SDS micelles show a biexponential behavior for the ellipticity change at 222 nm. The rate constants obtained from the stopped-flow data analysis at various concentrations are listed in Table 3-2. The faster rate constant, $k_1 \sim 250 \text{ s}^{-1}$, corresponds to a fast phase which results in a large gain in helical secondary structure. This fast phase is followed by a slower kinetic phase with a rate constant, $k_2 \sim 10 \text{ s}^{-1}$, which indicates relatively small structural change after further interaction with SDS micelles. The fluorescence curves also show an initial fast decrease with a rate constant, $k_1 \sim 150 \text{ s}^{-1}$, which is followed by

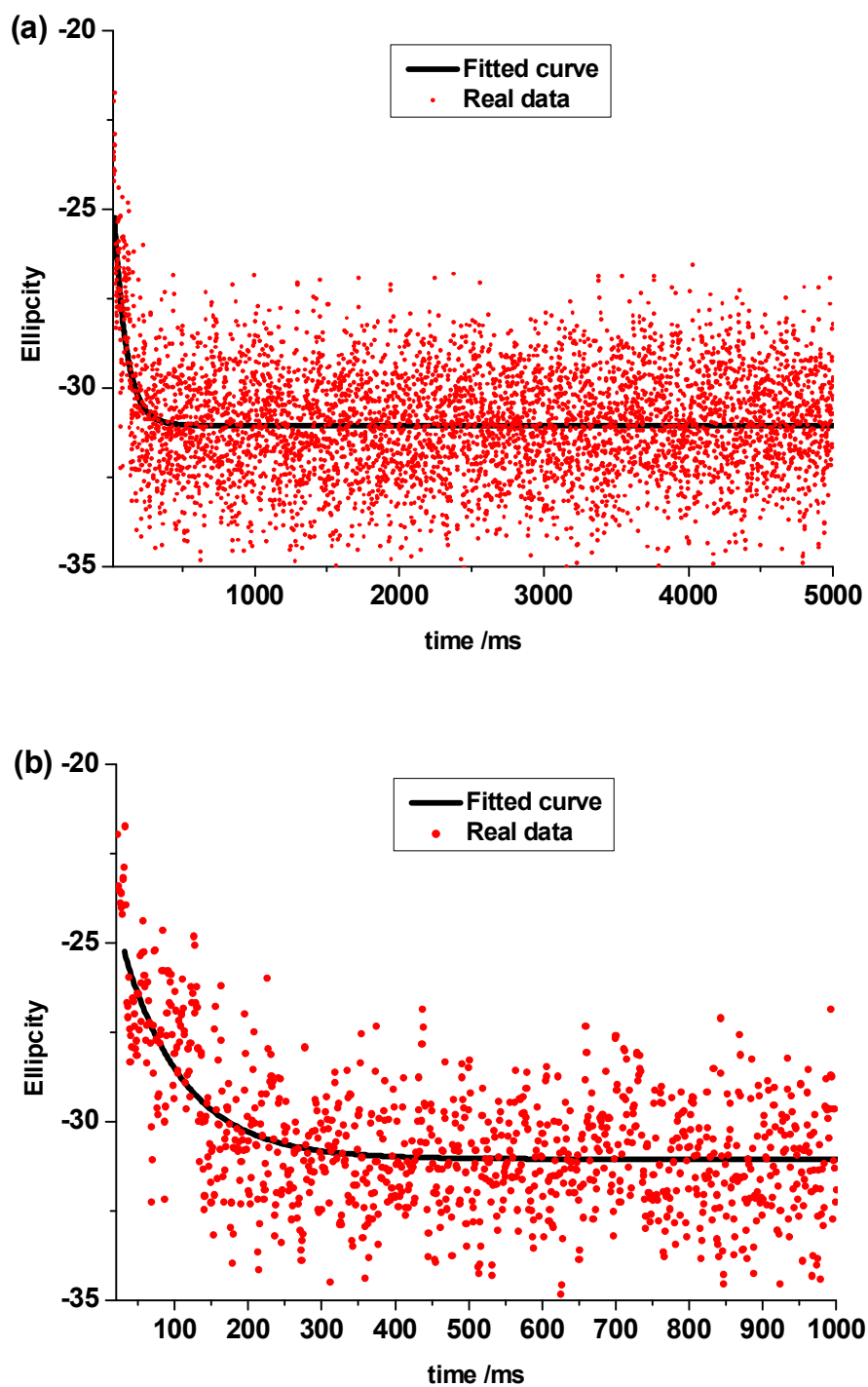


Figure 3-18. (a) An example of stopped-flow kinetic ECD actual measured data (shown in red dots) and fitted curve (shown in black solid line). (b) Expanded view of the short time component of (a).

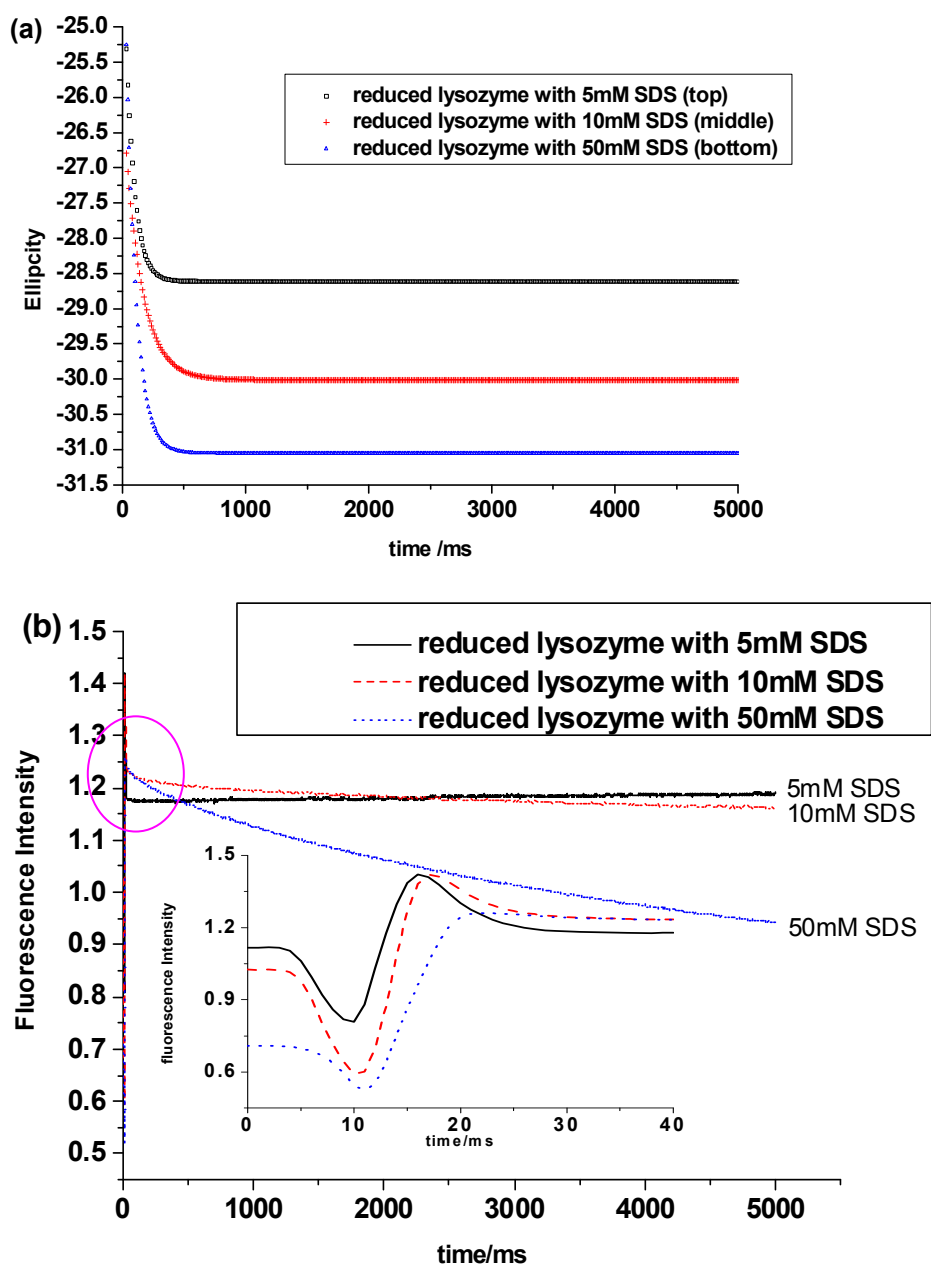


Figure 3-19. Kinetic variation of reduced HEWL spectral response on mixing with SDS. **(a)** Fitted curves for the CD signal at 222 nm (example of actual data available in Figure 3-17) and **(b)** Curves for the fluorescence intensity, where inset shows early time behavior. [The first 10 ms is the dead time of mixing turbulence and not fit. The fast increase step from 10 ms to 17 ms is fit separately from the slow steps beyond 17 ms due to overshoot.]

Table 3-2. Stopped-flow kinetic parameters from ECD and fluorescence for reduced HEWL mixing with SDS and DTAC^a

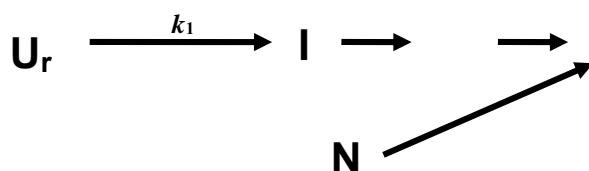
	stopped-flow ECD		stopped-flow fluorescence	
	k_1 / s^{-1}	k_2 / s^{-1}	k_1 / s^{-1}	k_2 / s^{-1}
5 mM SDS	231.5± 7.1	12.3± 1.4	230.2± 14.1	-
10 mM SDS	271.1± 4.6	8.7± 1.7	169.3± 8.2	1.8±0.6
50 mM SDS	336.3± 16.6	10.2± 1.9	129.9± 5.1	0.7± 0.3
10 mM DTAC	209.4± 5.6	10.6± 1.4	193.9±16.1	0.6± 0.3 ^b
25mM DTAC	250.9± 6.4	11.5±0.8	199.2± 21.1	8.0± 1.3
35 mM DTAC	260.1± 5.9	12.3± 2.5	202.3± 23.9	7.6± 0.6
native HEWL with SDS	9.61	-	127.9	8.2

^a the errors are calculated with the results of three trials

^b concentration 10 mM is below the CMC of DTAC

a slow decrease with a rate constant, $k_2 \sim 0.7-1.8 s^{-1}$. This indicates that there is a collapse of the polypeptide chain accompanying the major secondary structure change at the very early stages of folding in the fast phase, in other words, these fast CD and fluorescence spectral changes may result from the same process or kinetic step. It is important to note that the CD kinetic data is quite noisy and the fast steps are close to our mixing time limits, so there may be additional, undetected fast steps or added error in the fast step kinetic constant determinations, which would make discrimination between CD and fluorescence results tentative. However the slower components (k_2)

appear to be different processes which may result from one or multiple sequential mechanistic steps. We propose that these steps correspond to a kinetic mechanism for the refolding of reduced/unfolded HEWL with surfactant micelles as follows:



Scheme 3-1. Proposed mechanism for refolding of reduced HEWL, showing the possibility of multiple intermediates.

In scheme 3-1, U_r represents the unfolded state after reduction; N denotes the native state; I is an intermediate state and F_m is the highly helical, compact state for HEWL in surfactant micelles. I is formed in the fast kinetic phase corresponding to refolding of much of the secondary structure. The I state will further fold to the F_m state, possibly through added intermediate steps, implied by ? in Scheme 3-1, which has even more helical structure than the native state (N). This can occur in the second kinetic phase as induced by further interaction with SDS micelles. As noted above, this latter process may be multistate, given the differences in the CD and fluorescence k_2 values.

The state of reduced HEWL in SDS micelles (F_m) has almost the same fractional secondary structure and similar tertiary structure as does oxidized HEWL in SDS micelles, which is supported by CD (both near and far-UV) and fluorescence measurements. We also measured the unfolding kinetics of native state HEWL to the F_m state, and with CD detection a single exponential was determined yielding a rate constant, $k' \sim 10 \text{ s}^{-1}$, which is close to the CD determined k_2 for the reduced HEWL interacting with micelles. The interaction between the partially folded intermediate state

I or the native state N and SDS micelles thus appears to undergo a kinetic phase with rate constant $\sim 10 \text{ s}^{-1}$ that induces formation of more helical structure as well as loss of tertiary structure, but results in shielding of the Trps by the micelle.

The refolding kinetics of reduced HEWL in cationic micelles DTAC (Figure 3-20) also show biexponential behavior as is seen with SDS, but the amplitude of the CD ellipticity change at 222 nm is smaller, which is consistent with the equilibrium result that the helical fraction for reduced HEWL can not be as fully recovered in cationic as in anionic surfactant micelles. The fluorescence intensity increases biexponentially on mixing with DTAC, instead of decreasing as was seen in anionic surfactant micelles, such as SDS. The stopped-flow experiments measure the kinetics both below and above the CMC of DTAC and the fit kinetic parameters are comparable except for the k_1 from CD measurement and k_2 from fluorescence measurement (see Table 3-2).

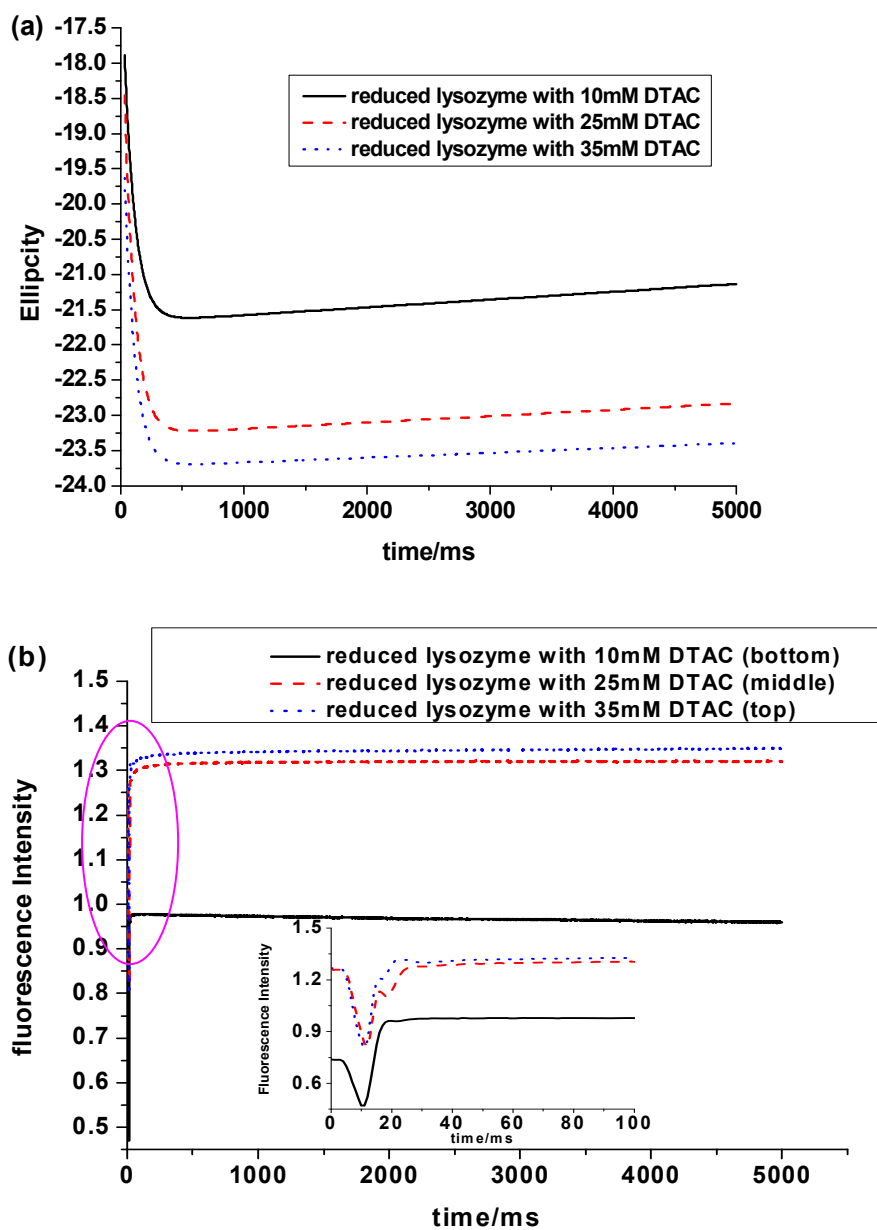


Figure 3-20. Kinetic variation of reduced HEWL spectral response on mixing with DTAC. Fitted curves for (a) the CD signal at 222 nm and (b) the fluorescence intensity, where inset shows early time behavior (Fit as described in Figure 3-18).

3.3.7 Comparison with refolding of denatured/reduced HEWL by dilution and reformation of disulfide bonds

Previous papers have reported both equilibrium and kinetic studies on the refolding of denatured/reduced HEWL, under different conditions than we have studied. Native HEWL can be denatured by GdnHCl or urea and reduced by addition of DTT.⁽⁷⁸⁻⁸⁰⁾ The refolding process is accomplished by dilution of the denatured/reduced HEWL with added refolding buffer containing GSSG which can oxidize the Cys and allow reformation of the protein disulfide bonds. The idea behind those previous studies is to remove the effect of the denaturant and reform the disulfide bond. Our experiments are unique and different from these reported studies because we do not reoxidize and reform the disulfide but instead have added micelles which can provide an alternative pathway for structure formation that can then be compared to that including disulfide bonds in the same environment. These previous refolding studies reported three rate constants with k_1 and k_2 close to 0.06 min^{-1} and k_3 close to 0.002 min^{-1} which are all much slower than the rate constants we have obtained with surfactants, $k_1 \sim 250 \text{ s}^{-1}$ and $k_2 \sim 10 \text{ s}^{-1}$. The explanation for this difference is because it takes time for the eight cysteine residues in the sequence to locate each other, form disulfide bonds and then reshuffle to the correct configuration of -S-S- links. Our experiment does not require formation of disulfide bonds, so the kinetics are not limited by that rate. By contrast, we monitor the secondary structure refolding mechanism, under reducing conditions in the presence of micelles, which is occurring on a much faster time scale. Chaffotte et al. also studied refolding of denatured oxidized HEWL, which has already all disulfide

bonds pre-formed, by dilution with refolding buffer and reported a fast rate constant of $k_1 = 69.9 \text{ s}^{-1}$ and a slower rate constant of $k_2 = 2.74 \text{ s}^{-1}$.⁽⁷⁹⁾ These reported values are comparable with our kinetic results, but imply that micelles (which can solvate and access to the peptide chain) can provide faster secondary structure formation mechanisms than can disulfide bonds alone in water, even when the correct disulfide bonds are already present.

3.4 Conclusion

3.4.1 Interaction of reduced HEWL in surfactant micelles

Reduced HEWL interacts with anionic surfactants to regain a highly helical but non-native state. Above the CMC, the non-native state has more helical structure than that of the native HEWL but loses tertiary structure and enzymatic activity. In our studies, this non-native helical state of the reduced protein can not be distinguished from that of oxidized (originally native state) HEWL once they both interact with micelles since they have superimposable CD and fluorescence spectra and no enzymatic activity. Charge and hydrophobicity play important roles in this non-native refolding process, particularly since we are studying HEWL, which has a pI~10-11, at pH 4.6. More negative charge on the surfactant head groups helps micelles bind to the positive protein surface (of HEWL), effectively desolvating it. This is operative at low surfactant concentrations which encompass monomer interactions and induce the initial structure changes. A larger degree of hydrophobicity, where the differences are most evident under conditions of micelle formation, can induce even more helical structure (i.e.

favoring internal H-bond formation leading to stability). Reduced HEWL can only gain part of this degree of helicity when interacting with cationic surfactants above their CMC, since the surfactant has the same charge as the protein, leading to a binding or interaction that effectively only depends on the hydrophobic aspects of the surfactant. Our data suggest that the surfactant acts primarily to desolvate the peptide chain, which can allow those segments having a high helical propensity to reform structure. As such it suggests that the hydrophobic interactions are not sufficient to drive the protein to such a fully structured state, and that the framework needs an assist to build secondary structure, native or otherwise. This desolvation is supported by the parallel between surfactant and TFE influences on regaining helicity, however their fluorescence differences suggest that the terminal (tertiary at least) states are not the same. The preference for negative (anionic) surfactants suggests that neutralization of positive sidegroups can facilitate structure formation. This may be akin to creating hydrophobic interactions, or reducing charge repulsion, thereby reducing barriers to folding found in the just buffer-solvated, positively charged protein structure. Thus, although average secondary structure is similar in the two proteins interacting with SDS, native (oxidized) and reduced, it is possible and even likely that their detailed (especially tertiary) structures differ. The OSS mutant and reduced HEWL show similar structures in surfactant micelles, which indicates the replacement of non-crosslinked reduced cysteine residues with alanine residues does not have significant effect on the final reformed structure in micelles.

3.4.2 The role of disulfide bonds on the folding pathway of HEWL

From both equilibrium and kinetic studies of the reformation of secondary structure for reduced HEWL in surfactant micelles, we have shown that the reduced HEWL state, U_r , without disulfide bonds can be reconfigured to a compact state of higher helicity state, F_m , in micelles. This also behaves like the partially (tertiary structure) unfolded, but more helical state of native (oxidized) HEWL interacting with anionic surfactant micelles, where the micelles provide counteracting destabilizing (tertiary) and stabilizing (helicity) forces arising from as electrostatic and hydrophobic interactions, respectively. Both native and reduced HEWL in micelles have structural characteristics often associated with molten globules.

The formation of disulfide bonds early in protein folding clearly provides a restriction of conformational space, which can facilitate folding in, for example, a funnel mechanism. However, such disulfide links are not required to allow the reduced protein to find a compact state that has considerable secondary structure, although the tertiary structure may differ from that of the native (oxidized) state, as it does here for HEWL. This parallel of oxidized and reduced HEWL folding, when in surfactant micellar media, as found in both our equilibrium and dynamic studies using CD and fluorescence, suggests that disulfide bonds do not determine either the folding pathway or the final secondary structure of the protein at early stages of the folding process. Rather it suggests that disulfides can add stability to elements of secondary structures formed and contribute to the formation of tertiary structure.

4. Refolding of reduced and mutant lysozymes in vesicles. Impact of disulfide effects on refolding equilibria and dynamics

4.1 Introduction

Previous studies have shown that reduction of disulfide bonds decreases the stability of a native-state protein.⁽⁴³⁻⁴⁵⁾ As noted in chapter 3, disulfide bonds can have an important role in protein folding, forming either late in the process^(47, 48) or early to direct the path.⁽⁴⁹⁾ Still other studies found that a single specific disulfide bond out of a set of them in a protein can be eliminated without compromising the acquisition of secondary structure and the formation of native-like secondary structure.⁽⁸¹⁾ The effects of disulfide bond formation in the folding process remain unclear: does correct disulfide bond formation determine the folding pathway or just stabilize the elements of secondary structures formed and contribute to the formation of tertiary structure? What is the reason for the appearance of disulfide bonds during the evolution process?

Most previous studies of protein folding and the basic principles governing the folding process have been carried out using re-naturation of proteins with existing disulfide bonds. In a natural physiological folding process, the protein starts in the reduced form without the preformed disulfide bonds. As a result, to more closely mimic the physiological folding process, in this study we study the refolding of fully reduced hen egg white lysozyme (HEWL), as well as mutants, one of which also has no disulfide bonds (0SS) or one having only one disulfide bond left (1SS). By comparison, native HEWL has four disulfide bonds in the folded state. To initiate

refolding of these inherently destabilized HEWL forms, we have studied their spectral changes when mixed with model membrane vesicles with which they can interact and refold. Our previous studies reported in chapter 3, focused on induced folding of reduced HEWL mixed with surfactant micelles as a mimic of membrane interaction.⁽⁸²⁾ In this chapter, we extend our studies to HEWL interactions with lipid vesicles which can provide a mimic of cellular membranes to better model protein-membrane interactions. Our previous study showed that the unfolded states of reduced HEWL can regain helical secondary structure in the presence of detergents, but do not attain native tertiary folds.

The 0SS and 1SS mutants provide control systems that lack all or all but one of the four disulfide bonds but do not require additional reductant. The 1SS mutant, C64-C80, we use in this study has the disulfide bond left in the β domain, which is the only intra- β -domain disulfide bond in native HEWL. By studying the refolding process of the 1SS mutant with one intra- β -domain disulfide bond remaining intact, we can gain insight into the effects of this single disulfide bond and its role in the change to helical structure.

4.2 Experimental

4.2.1 Materials

Lysozyme from hen egg white (HEWL) was purchased from Sigma (catalog no. L6876), as were the reducing agent 1,4-dithio-DL-threitol (DTT), organic solvents (methanol and chloroform, spectral-grade) and sodium phosphate (analytical grade).

The lipids used: dimyristoylphosphatidylglycerol (DMPG), dimyristoylphosphatidylcholine (DMPC), dilauroylphosphatidylglycerol (DLPG), dioleoylphosphatidylglycerol (DOPG), distearoylphosphatidylglycerol (DSPG) and palmitoylphosphatidylglycerol (POPG) were purchased from Avanti Polar Lipids, Inc. (Alabaster, AL). The HEWL 0SS and 1SS mutants were prepared and kindly provided by our collaboration with the lab of Prof. Harald Schwalbe, Universität Frankfurt. Solution pH was measured with a HANNA HI 98180 pH meter. All the materials were used without further purification.

To prepare reduced lysozyme solution, the protein was dissolved (0.4 mg/mL) in 20 mM pH 4.6 phosphate buffer and incubated with 5 mM DTT for 24 hours at 65 °C. The reduction of the sample was quenched by rapid cooling and then storage at 5 °C. This procedure is a modification of a previously published method.⁽⁶⁸⁾ All samples were studied at pH 4.6 to enhance solubility of the reduced form with DTT reductant.

4.2.2 Lipid vesicles preparation

A weighed amount of lipid was dissolved in organic solvents (chloroform or chloroform/methanol mixture) in a glass vial, and the resulting lipid solutions were dried while being rotated under a small stream of dried air to form a relatively uniform thin film on the wall. The required volume of 20 mM pH 4.6 phosphate buffer was added to the vial to resuspend the dried film and form a multilamellar liposome suspension. The suspension was then sonicated (MICROSON XL2000 ultrasonic liquid processor, Qsonica, LLC) with 5-6W power for a few minutes until

the solution became clear. This freshly prepared SUV solution was then added to the protein solution and mixed well to form a protein-lipid complex with a final 0.2 mg/mL HEWL concentration. The average sizes of SUVs are around 50 nm as measured with dynamic light scattering (DLS).

4.2.3 CD measurements

CD spectra were measured from 185 nm to 250 nm with a 50 nm/min scanning rate, 2 s response time, 1 nm bandwidth as the average of 8 scans on a JASCO 810 spectrometer (Jasco, Inc.). For equilibrium measurements, the protein solutions were prepared at 0.2 mg/mL in 20 mM pH 4.6 phosphate buffer and measured in a 1 mm pathlength quartz cuvette (Starna, Inc) at room temperature. All sample spectra were corrected by subtraction of the corresponding spectrum of the buffer.

4.2.4 Fluorescence

Fluorescence spectra were measured on a Fluoromax-3 spectrofluorometer (Horiba Jobin Yvon Inc.) with the samples held in a 1 mm×1 cm quartz cell. The excitation wavelength was 295 nm and the emission spectra were collected from 300 nm to 500 nm. All the spectra were corrected by subtraction of the buffer spectrum.

4.2.5 Stopped-flow measurements

For stopped-flow mixing dynamics, a SFM-400 accessory (Bio-logic) and MPS-52 control console were connected to the Jasco-810 spectrometer. The Xe lamp in the CD spectrometer was changed to a Xe-Hg lamp to enhance far-UV intensity. The mixing dead time under our measurement conditions was ~ 10 ms, but instrument response was much faster and the signal change was large enough to allow determination of kinetics in the ms and longer time range. The CD signal channel was recorded with 1 KHz sampling for 5 s of the signal at 222 nm using a 4 nm bandwidth by means of standard JASCO kinetics methods. A fixed HV and computational normalization of the modulated signal by the detector current (in the software) was used to determine ΔA with a faster response. The total fluorescence signal was simultaneously collected on the same sample for all emission above 320 nm using a cut-off filter in front of a separate fluorescence detector which was located at right angles to the CD and excitation beam. The results were fit with multiple exponential functions using the Bio-Kin32 software.

4.2.6 Attenuated Total Reflectance Fourier Transform Infrared (ATR-FTIR)

The FTIR spectrometer (Bruker Vertex 80) was used with an attenuated total reflection technique (ATR) accessory fitted with a ZnSe crystal (PIKE MIRacle three reflection ATR). Samples were dried on the crystal surface to form a uniform thin film on the crystal surface. Sample absorbance spectra over the range 4500 cm^{-1} to 600 cm^{-1} were collected as an average of 512 scans (10 kHz scan speed with a DTGS

detector) and processed with 3-term Blackman-Harris apodization and zero filling of

2. Background spectra collected with same measurement parameters but without a sample on the ATR crystal surface were used as a reference for absorbance calculation. Polarized ATR spectra were collected with a wire grid polarizer placed in front of the ATR apparatus and oriented at 0° and 90° polarizations of the incident light beam. The dichroic difference spectra were obtained by subtracting the spectrum recorded at 0° from that recorded at 90° using a weight coefficient ratio, R_{iso} . R_{iso} is obtained by calculating the ratio of integrated absorbance of the lipid carbonyl band (1699 cm^{-1} to 1700 cm^{-1}) in spectra measured at 90° to the integrated absorbance of the spectra measured at 0° , so that this band integrates to zero in the difference spectra.⁽⁴²⁾

4.3 Results and discussion

4.3.1 Refolding of reduced HEWL with various lipid vesicles

HEWL reduced by addition of DTT loses all four disulfide bonds as confirmed by mass spectra that show the molecular weight to increase from the native/oxidized state value by eight mass units (see chapter 3).⁽⁸²⁾ The CD spectrum of reduced HEWL (Figure 4-1 red dash line) shows that it loses most of its helical structure and gains mainly unordered/unfolded structure after losing its four disulfide bonds, by comparison with the CD spectrum of native/oxidized HEWL (black solid line in Figure 4-1).

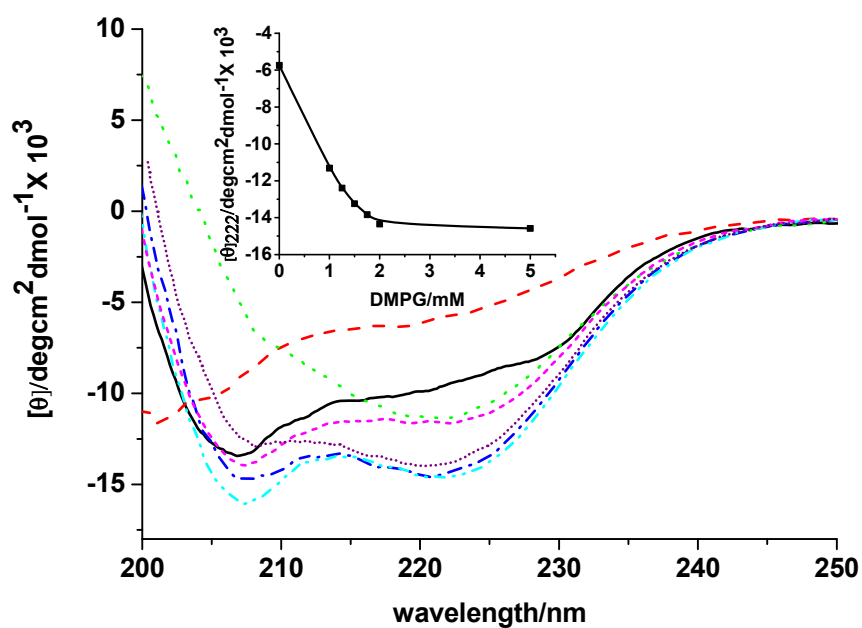


Figure 4-1. Far-UV CD spectra of native HEWL and reduced HEWL, and with addition of different concentrations of DMPG at pH 4.6.

Black solid line: native HEWL; magenta short dash line: native HEWL + 5 mM DMPG; red dash line: reduced HEWL; green dot line: reduced HEWL + 1 mM DMPG; purple short dot line: reduced HEWL + 1.75 mM DMPG; blue dash dot line: reduced HEWL + 2 mM DMPG; cyan dash dot dot line: reduced HEWL + 5 mM DMPG. The inset shows the variation of ellipticity at 222 nm with addition of DMPG.

To investigate the refolding of reduced HEWL which has lost most of its helical structure, it was mixed with varying concentrations of vesicles of a lipid DMPG, and the resultant CD spectra are overlaid in Figure 4-1. Lipids with negatively charged head groups were used, since the protein has a net positive charge under the conditions used. For comparison, the spectrum of oxidized HEWL in DMPG vesicles is also presented (Figure 4-1, magenta short dash line) to demonstrate the difference of interaction with lipid vesicles between reduced HEWL and oxidized HEWL, one with no disulfide bonds and one with four disulfide bonds. This may shed light on the effects of disulfide bonds on the folding process or the gain of secondary structure in this protein.

The CD spectra show that with the addition of DMPG vesicles, the reduced HEWL increases in helical structure up to a maximum, achieving a saturated state with ~5 mM DMPG. As indicated by the two negative CD bands at 208 nm and 222 nm characteristic of α -helices, the refolded state of reduced HEWL in 5 mM DMPG vesicles (Figure 4-1 cyan dash dot dot line) clearly has much more helical structure than does the oxidized/native HEWL (Figure 4-1 black solid line). The oxidized HEWL also gains helical structure with 5 mM DMPG vesicles (Figure 4-1 magenta short dash line) as compared to native HEWL in buffer only, but this change is less than achieved for the reduced HEWL in 5 mM DMPG vesicles.

Both the oxidized HEWL and reduced HEWL are positively charged under conditions used, so they can both bind to the negative head groups on the DMPG vesicle surface, and may insert into and thus interact with both the surface and bilayer interior of the DMPG vesicles. Since the oxidized HEWL has intact disulfide bonds and stable native secondary structure, it should be more difficult for it to insert into the vesicles. On the other hand, the reduced HEWL has no disulfide bonds, and in buffer solution loses most of its helical structure and probably all tertiary structure, which can be observed from the collapse of the reduced HEWL near-UV CD (Figure 4-2 red dash line). As a result, the reduced form is more flexible and can more easily insert into the interior hydrophobic environment of the vesicles which may induce even more helical structure formation.

HEWL has six tryptophan (Trp) residues and their intrinsic fluorescence emission can be used to monitor changes of their local environment as well as coupling to other Trp residues and thus can give information on the change of the protein tertiary structure. The intrinsic fluorescence intensity increases in the presence of DMPG vesicles (Figure 4-3 and Figure 4-4). Below 1 mM DMPG the fluorescence intensity reaches a maximum and then slightly falls back to a plateau at higher concentrations. Instead of the two-step change observed for the fluorescence intensity, the peak position blue shifts in a simpler one-step process: going from 351 nm in buffer to about 340 nm in the presence of DMPG vesicles, and is independent of the DMPG vesicle concentration above 0.5 mM. The blue shift of peak position and the increased fluorescence intensity indicates that as the reduced HEWL binds to the lipid

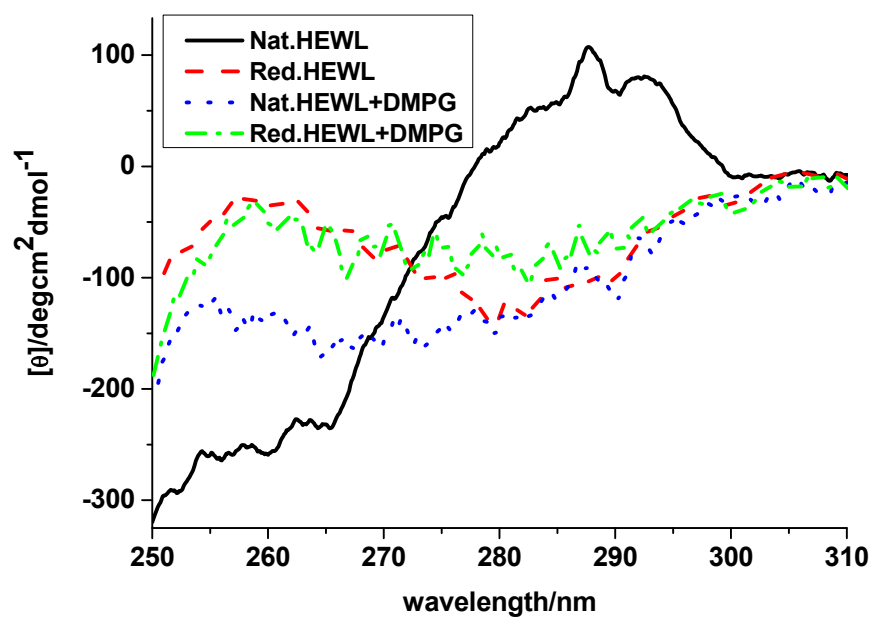


Figure 4-2. Near-UV CD spectra of native HEWL (black solid line), reduced HEWL (red dash line), native HEWL in 5 mM DMPG (blue dot line) and reduced HEWL in 5 mM DMPG (green dash dot line).

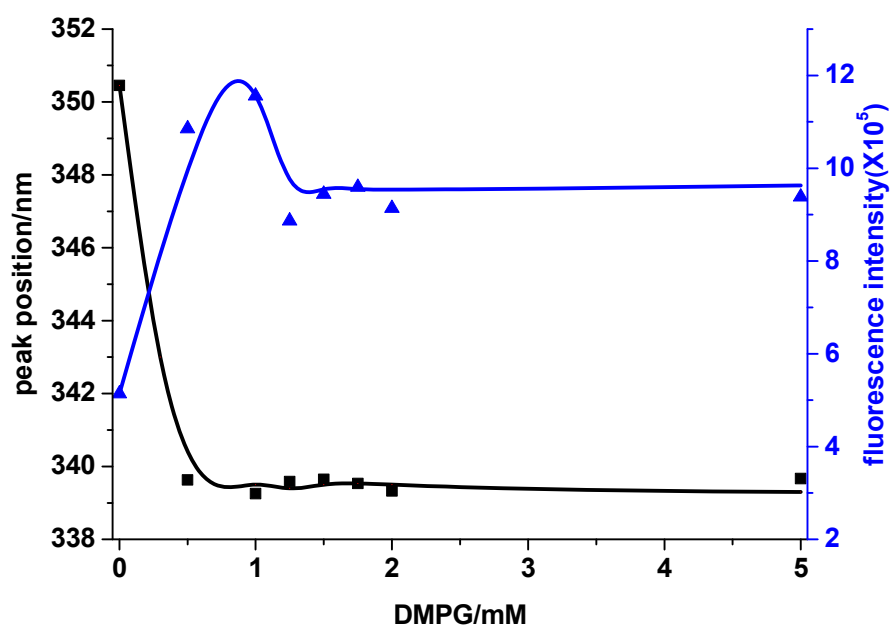


Figure 4-3. Variation of the integrated intrinsic fluorescence intensity (blue triangles) and peak position (black squares) of reduced HEWL with addition of DMPG vesicles.

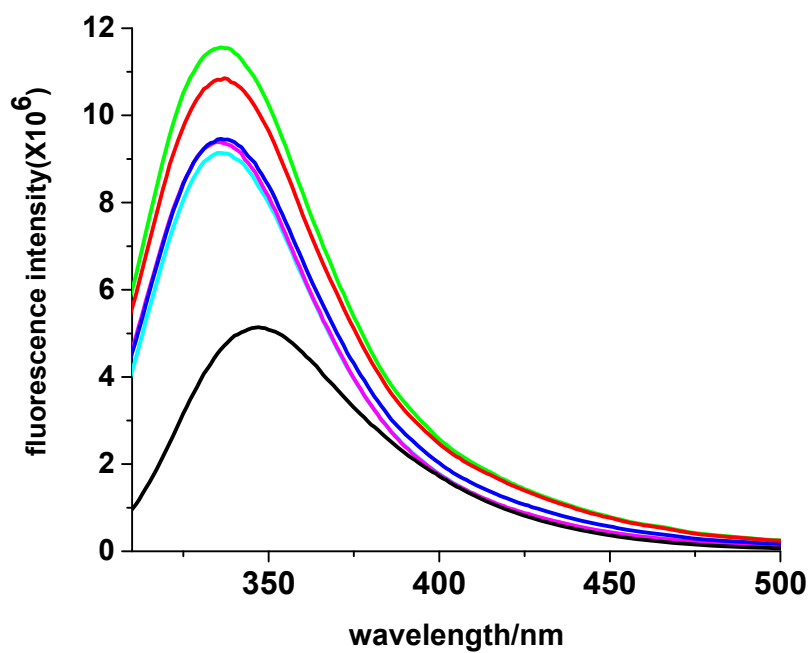


Figure 4-4. Fluorescence spectra of reduced HEWL (black line), and reduced HEWL with 0.5 mM (red line), 1 mM (green line), 1.5 mM (blue line), 2 mM (cyan line) and 5 mM (magenta line) DMPG vesicles.

vesicles, segments containing tryptophan residues are shielded from the solvent and at least those with higher quantum yield are moved into a hydrophobic environment, presumably the interior of the lipid bilayer. During that process lipid-bound reduced HEWL starts forming helical structures while the tryptophan residues become less exposed to solvent. With addition of more DMPG vesicles, the helicity of the reduced HEWL continues to grow, and the fluorescence intensity decreases to a stable state ($\sim 1.5\text{mM}$), even though the peak position no longer varies.

While lipid vesicles with negative head groups have coulomb attraction to the positively charged reduced HEWL protein (native HEWL has an isoelectric point of ~ 10.7 , but our measurements are at pH 4.6), it is interesting to explore the relationship between coulomb forces and hydrophobic interactions. We wish to determine whether attraction of opposite charges is a prerequisite for the insertion process, or if hydrophobic interactions alone could lead to the same structural transition. In contrast to its behavior with negative DMPG vesicles, reduced HEWL behaves differently with DMPC, which has zwitterionic head groups. The DMPC-HEWL complex induces some secondary structure in reduced HEWL but it does not significantly affect helicity, as shown by the CD spectra (Figure 4-5). The CD of the oxidized/native HEWL (Figure 4-5 black line) barely changes upon addition of DMPC (Figure 4-5 magenta short dash line) with the spectra being superimposable.

These results are similar to observations we reported comparing surfactant micelles (chapter 3), in that reduced HEWL can interact with cationic/zwitterionic surfactant micelles or lipid vesicles with positive/zwitterionic head groups, while the

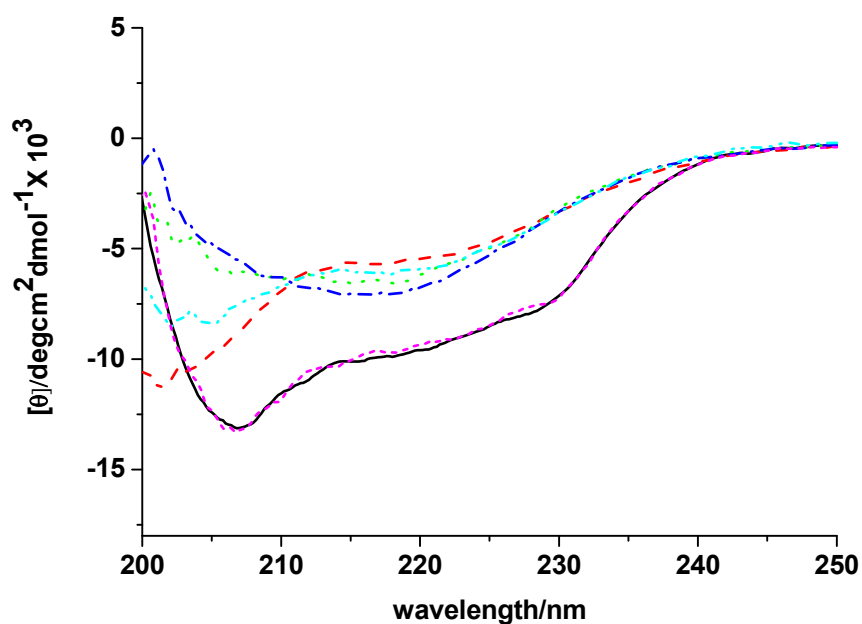


Figure 4-5. Far-UV CD spectra of native HEWL and reduced HEWL, and with addition of different concentrations of DMPC at pH 4.6.

Black solid line: native HEWL; magenta short dash line: native HEWL + 1.5 mM DMPC; red dash line: reduced HEWL; green dot line: reduced HEWL + 0.5 mM DMPC; blue dash dot line: reduced HEWL + 1 mM DMPC; cyan dash dot dot line: reduced HEWL + 1.5 mM DMPC.

oxidized HEWL has no obvious structure changes with cationic/zwitterionic surfactant micelles or lipid vesicles. Cationic/zwitterionic micelles can induce more structure changes for the reduced HEWL than do the DMPC vesicles with zwitterionic head groups. Micelles are smaller and can more easily attach to or occlude the reduced HEWL to affect its structure, while the DMPC vesicles are larger and more structured, so that the reduced HEWL may have more difficulty inserting into the lipid bilayer without electrostatic attractions holding it to the surface of the vesicles. The changes of reduced HEWL with DMPC vesicles indicate that there are still interactions, in the absence of coulomb attractions, presumably due to hydrophobic stabilization of parts of the HEWL sequence. The observed CD changes, together with the ATR spectra (Figure 4-6) showing increasing beta sheet peak (1627 cm^{-1}) intensity, suggest formation of beta sheet structure which may be on the lipid surface. When the protein is well-structured and more rigid, such as the case with oxidized/native HEWL, the binding between opposite charges from the protein and vesicle membrane can facilitate, and may be a prerequisite for, further insertion and hydrophobic interactions. The fluorescence spectra (Figure 4-7) show that, in the presence of DMPC, the peak position blue shifts from 351 nm to 348 nm and intensity increases, but both changes are smaller than with DMPG vesicles, suggesting less interaction with the hydrophobic interior of the bilayer than with DMPG.

It is reasonable to think that after the electrostatically mediated binding to and initial insertion into the lipid membrane bilayers, hydrophobic interactions play a more important role for further formation of helicity in reduced HEWL. As a result,

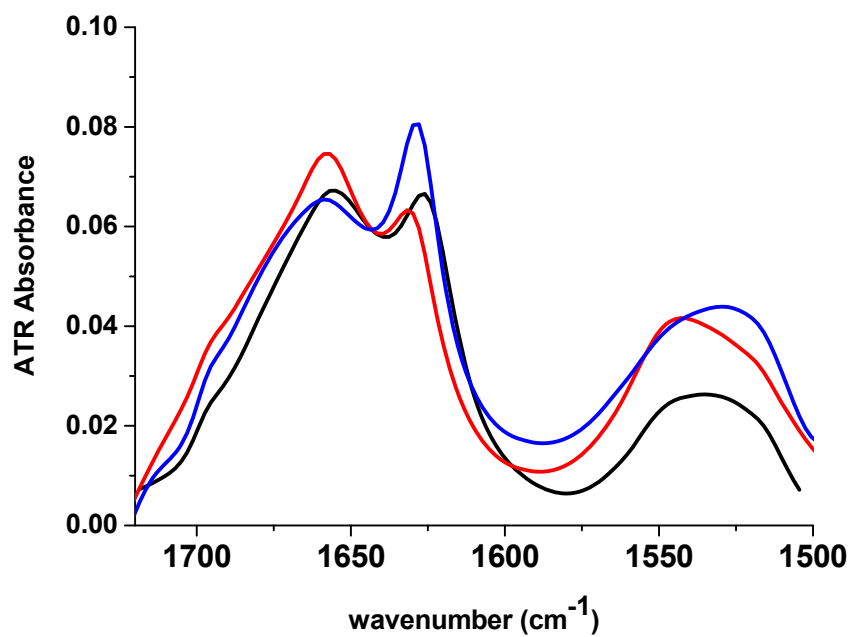


Figure 4-6. ATR spectra of reduced HEWL (black line), reduced HEWL with 5 mM DMPG (red line) and reduced HEWL with 1.5 mM DMPC (blue line).

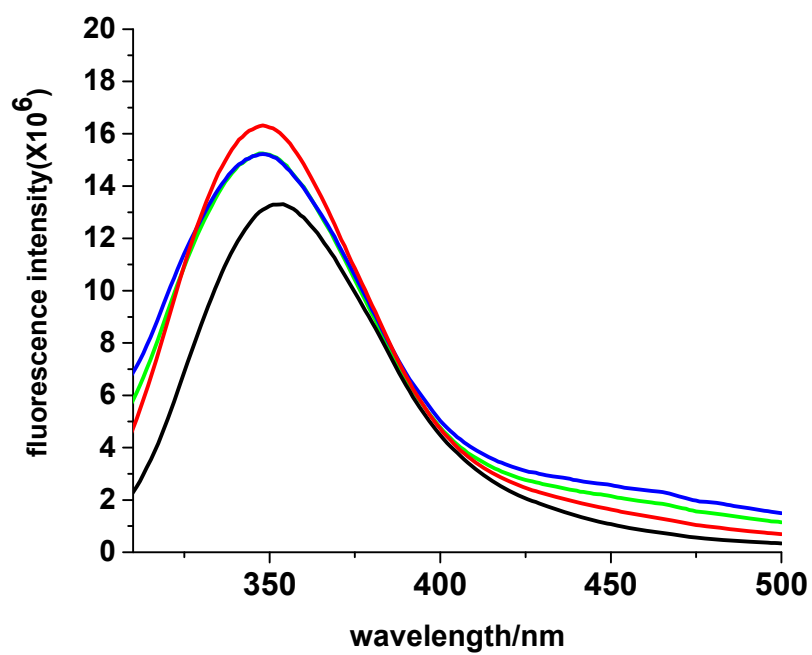


Figure 4-7. Fluorescence spectra of reduced HEWL (black line), and reduced HEWL with 0.5 mM (red line), 1 mM (green line) and 1.5 mM (blue line) DMPC vesicles.

the hydrophobicity and packing of the lipid vesicles could be two key factors for the formation of protein helicity with vesicles. Three other lipid vesicles were studied that have the same negative head groups as DMPG, but differ in hydrophobicity and/or packing of the lipid bilayers. DLPG aliphatic tails are only 12 carbons long, as compared to 14 for DMPG, and result in a lower liquid crystal phase transition at $T_m \sim -3^\circ\text{C}$. As seen with DMPG vesicles, reduced HEWL interacting with DLPG vesicles have more helicity than the oxidized/native HEWL in only buffer, but the final maximum helical content induced by DLPG vesicles is less than for DMPG vesicles. This suggests that the longer chains creating a larger hydrophobic interior in the lipid vesicle bilayers provides a better environment for the reduced HEWL to form helical structure. The reduced HEWL with 1 mM DLPG (Figure 4-8 blue dash dot line) is more helical than with 1 mM DMPG (Figure 4-1 green dot line), and it reaches its maximum plateau faster. One possible explanation is that the DLPG has higher fluidity, making it easier for the reduced HEWL to bind but the larger DMPG has higher capacity for helix insertion.

The other two lipid vesicles studied, POPG and DOPG, alter both the hydrophobicity and their packing properties. POPG has one 16 carbon chain and one 18 carbon chain with a double bond, and DOPG has two 18 carbon chains with a double bond on each. Both of them have longer hydrocarbon chains than DMPG, but lower transition temperatures since the packing properties of kinks induced by double bonds in the lipid bilayer are different. As demonstrated by the respective CD spectra in Figure 4-9 and Figure 4-10, despite their higher hydrophobicity, POPG and DOPG

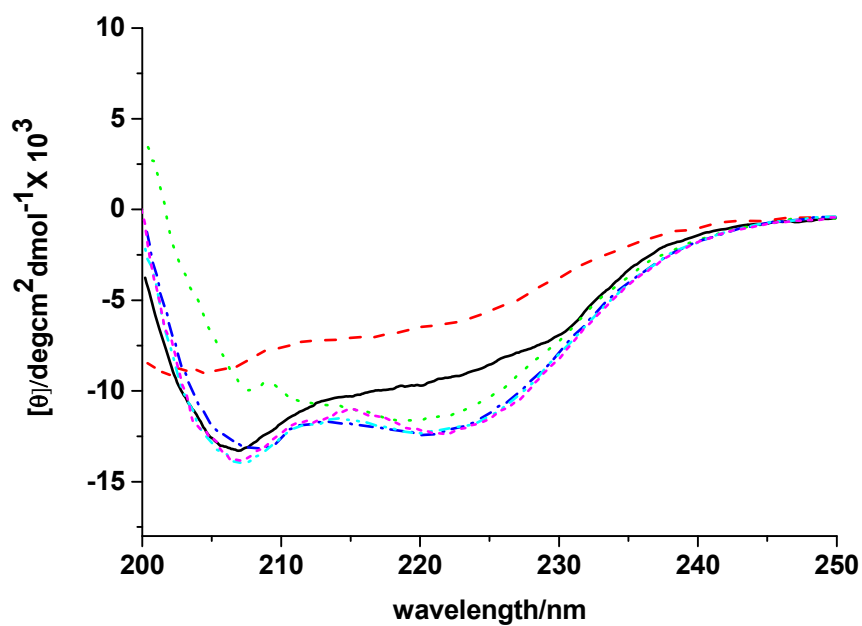


Figure 4-8. Far-UV CD spectra of native HEWL, and reduced HEWL with addition of different concentrations of DLPG at pH 4.6.

Black solid line: native HEWL; red dash line: reduced HEWL; green dot line: reduced HEWL + 0.5 mM DLPG; blue dash dot line: reduced HEWL + 1 mM DLPG; cyan dash dot dot line: reduced HEWL + 2 mM DLPG; magenta short dash line: reduced HEWL + 5 mM DLPG.

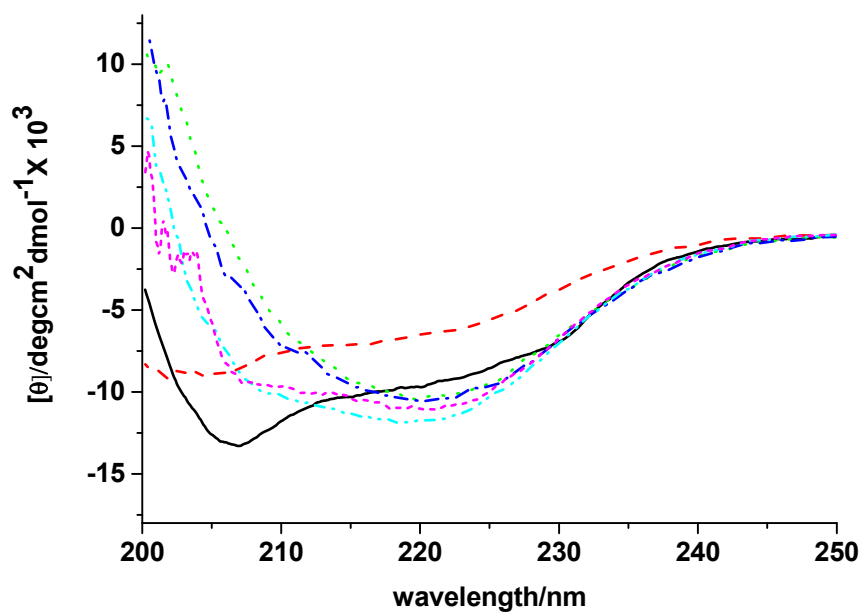


Figure 4-9. Far-UV CD spectra of native HEWL, and reduced HEWL with addition of different concentrations of POPG at pH 4.6.

Black solid line: native HEWL; red dash line: reduced HEWL; green dot line: reduced HEWL + 0.5 mM POPG; blue dash dot line: reduced HEWL + 1 mM POPG; cyan dash dot dot line: reduced HEWL + 2 mM POPG; magenta short dash line: reduced HEWL + 5 mM POPG.

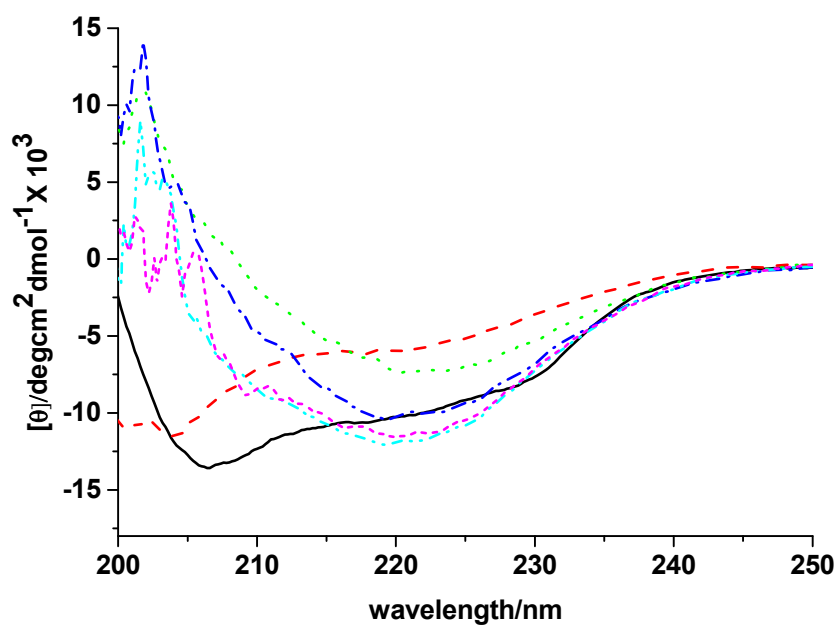


Figure 4-10. Far-UV CD spectra of native HEWL, and reduced HEWL with addition of different concentrations of DOPG at pH 4.6.

Black solid line: native HEWL; red dash line: reduced HEWL; green dot line: reduced HEWL + 0.5 mM DOPG; blue dash dot line: reduced HEWL + 1 mM DOPG; cyan dash dot dot line: reduced HEWL + 2 mM DOPG; magenta short dash line: reduced HEWL + 5 mM DOPG.

vesicles interact with reduced HEWL but induce less helicity than do DMPG vesicles, even less than DLPG vesicles. In this case, the degraded packing plays a more important role than the increase in hydrophobicity, as implied by their longer tails, for the folding and formation of helical structure. Both POPG and DOPG vesicles have double bonds, which cause kinks in the tails so that they do not pack as well, which may have consequences for insertion of a helical segment.

4.3.2 Refolding of HEWL mutants with DMPG vesicles

The 0SS mutant has all eight cysteines in HEWL replaced with alanines, and thus there are no disulfide bonds. The 1SS (64-80) mutant retains one single disulfide bond in the beta domain of the native HEWL, with the six other cysteine residues replaced with alanines. Since the Cys64-Cys80 disulfide bond is in the beta domain, its impact on structural changes that induce formation of helical structure inside vesicles is a more interesting question than for the other three disulfide bonds in HEWL. The CD spectra of 0SS (Figure 4-11) and 1SS (Figure 4-12) in the presence of DMPG vesicles show that they behave similarly as reduced HEWL, forming significantly more helical structure than does native HEWL in 5 mM DMPG. All three disulfide depleted HEWLs, 0SS, 1SS and reduced HEWL, form their maximum helical refolded state interacting with DMPG vesicles to attain apparently the same final secondary structure, as indicated by their superimposable CD spectra in the presence of 5 mM DMPG vesicles. Even though they achieve the same final state, the 1SS mutant behaves slightly differently from 0SS and reduced HEWL during the

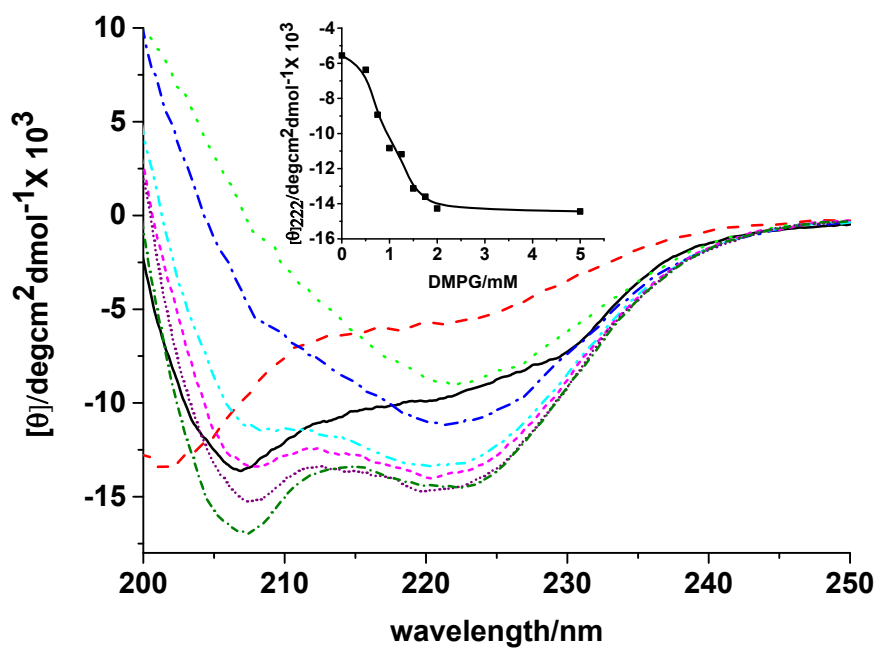


Figure 4-11. Far-UV CD spectra of native HEWL, and O5S mutant with addition of different concentrations of DMPG at pH 4.6.

Black solid line: native HEWL; red dash line: O5S mutant; green dot line: O5S + 0.75 mM DMPG; blue dash dot line: O5S + 1 mM DMPG; cyan dash dot dot line: O5S + 1.5 mM DMPG; magenta short dash line: O5S + 1.75 mM DMPG; purple short dot line: O5S + 2 mM DMPG; olive short dash dot line: O5S + 5 mM DMPG. The inset shows the variation of ellipticity at 222 nm with addition of DMPG.

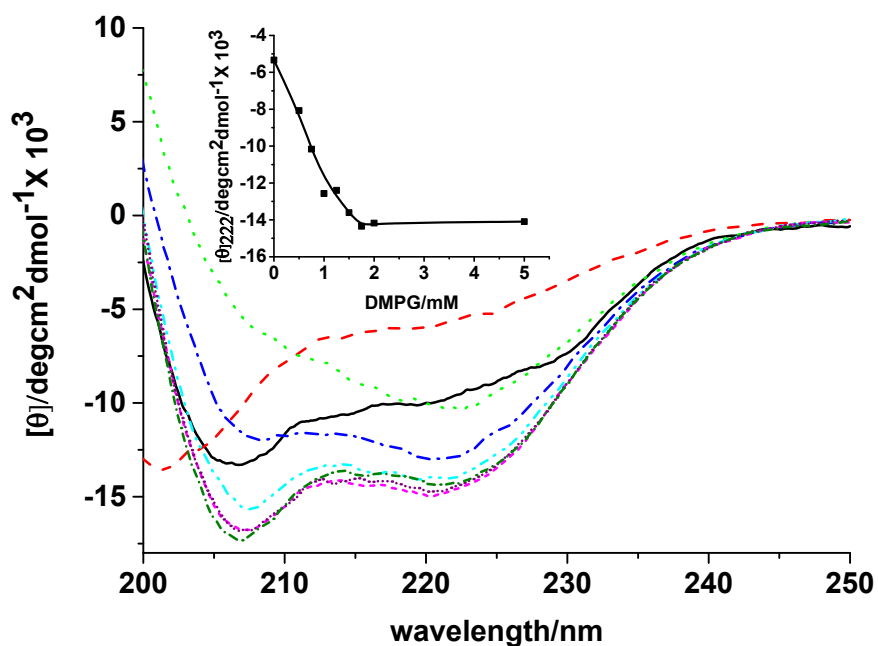


Figure 4-12. Far-UV CD spectra of native HEWL, and 1SS mutant with addition of different concentrations of DMPG at pH 4.6.

Black solid line: native HEWL; red dash line: 1SS mutant; green dot line: 1SS + 0.75 mM DMPG; blue dash dot line: 1SS + 1 mM DMPG; cyan dash dot dot line: 1SS + 1.5 mM DMPG; magenta short dash line: 1SS + 1.75 mM DMPG; purple short dot line: 1SS + 2 mM DMPG; olive short dash dot line: 1SS + 5 mM DMPG. The inset shows the variation of ellipticity at 222 nm with addition of DMPG.

refolding process. In the presence of 1.75 mM DMPG, the 1SS nearly achieves its maximum helicity (Figure 4-12 magenta short dash line), while the 0SS (Figure 4-11 magenta short dash line) and reduced HEWL (Figure 4-1 purple short dot line) require higher lipid vesicle concentrations (higher than 2 mM) before maximizing helicity. From our observations, the single disulfide bond Cys64-Cys80 in the 1SS mutant does not inhibit the ability of HEWL to form a final vesicle-bound secondary structure similar to the fully reduced and 0SS HEWLs, but this disulfide bond does affect the pathway or intermediate formation in the folding process. The disulfide bond can restrict the conformational distribution in the unfolded state, although the unfolded states of HEWL after losing three or all four disulfide bonds must be similar, since the CD spectra of unfolded 0SS and 1SS are so similar.

The intrinsic tryptophan fluorescence peak positions for both the 1SS and 0SS mutants undergo similar changes upon addition of DMPG vesicles, both showing blue shifts from 351 nm to about 340 nm in the presence of DMPG vesicles in what appears to be a one-step process (Figure 4-13, Figure 4-14, Figure 4-15 and Figure 4-16). Higher concentrations of DMPG vesicles do not affect the fluorescence peak position. However, the intrinsic fluorescence intensity of both 1SS and 0SS mutants have a different pattern of changes from that of reduced HEWL: the fluorescence intensity increases gradually and then reaches a plateau with addition of higher DMPG vesicle concentrations. This contrasts with reduced HEWL fluorescence which increased to a maximum at low vesicle concentration then stabilized back to a plateau with addition of more DMPG vesicles. The difference in fluorescence

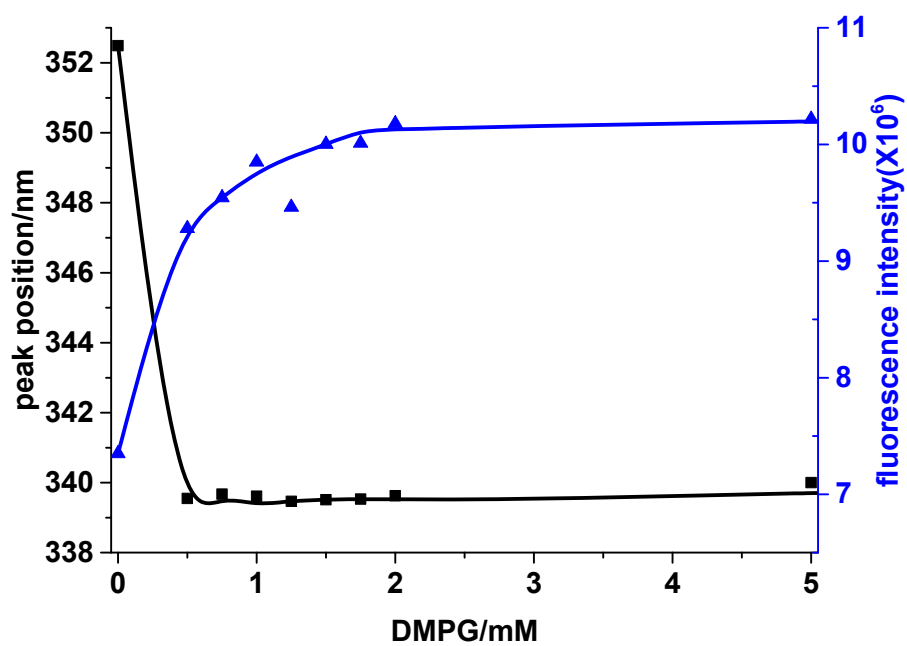


Figure 4-13. Variation of the integrated intrinsic fluorescence intensity (blue triangles) and peak position (black squares) of OSS mutant with addition of DMPG vesicles.

(no data for DMPG concentrations below 0.5 mM because of precipitation).

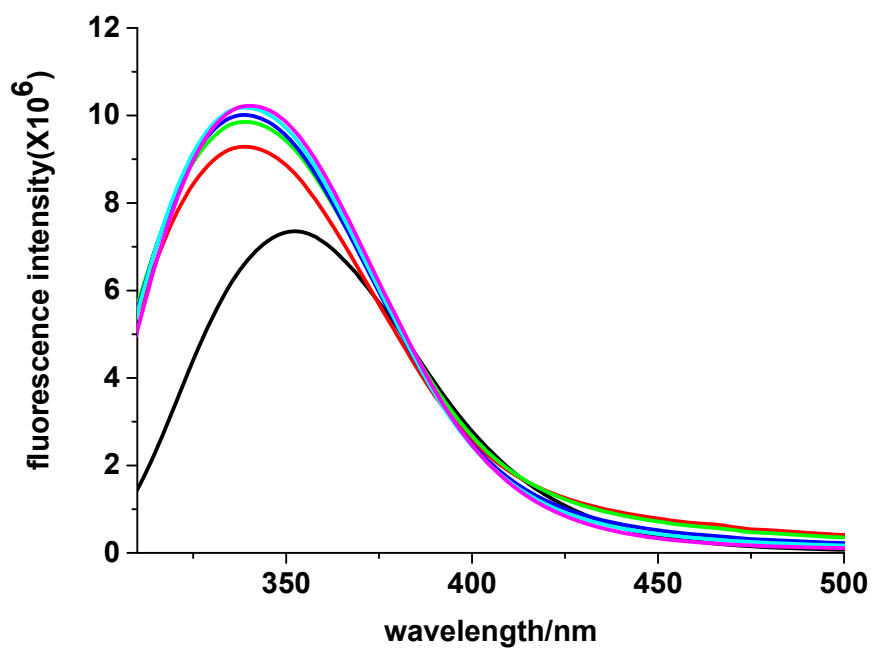


Figure 4-14. Fluorescence spectra of OSS mutant (black line), and OSS mutant with 0.5 mM (red line), 1 mM (green line), 1.5 mM (blue line), 2 mM (cyan line) and 5 mM (magenta line) DMPG vesicles.

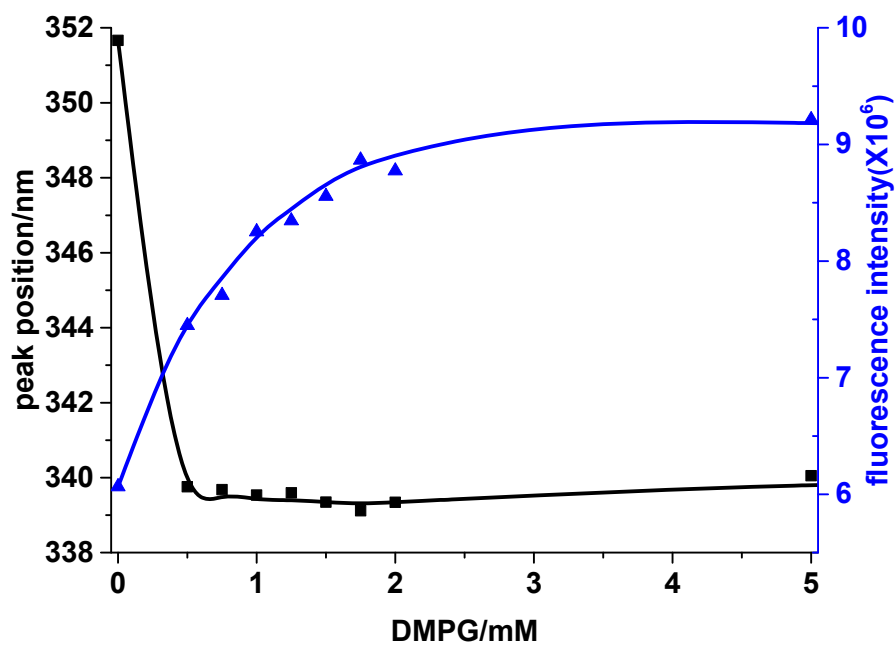


Figure 4-15. Variation of the integrated intrinsic fluorescence intensity (blue triangles) and peak position (black squares) of 1SS mutant with addition of DMPG vesicles.

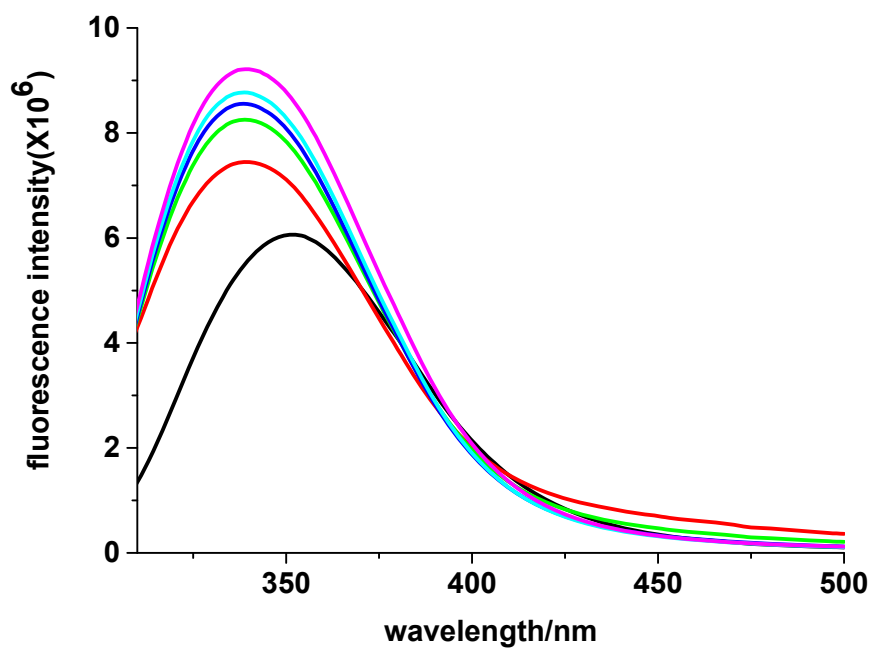


Figure 4-16. Fluorescence spectra of 1SS mutant (black line), and 1SS mutant with 0.5 mM (red line), 1 mM (green line), 1.5 mM (blue line), 2 mM (cyan line) and 5 mM (magenta line) DMPG vesicles.

intensity change does not originate from the presence of DTT for reduced HEWL and its absence for the mutants, because for HEWL samples with added DTT but without incubation at 65 °C either the peak position or the intensity of HEWL's fluorescence was not affected. As a result, the difference in fluorescence intensity changes for OSS in DMPG suggest that the reduced cysteine residues may affect the environment of some tryptophan residues, and this effect is modulated if the cysteines replaced by alanines in the mutants. From the native structure of HEWL, some of the cysteine residues are close to tryptophans and thus the charge and dipolar properties of cysteine residues as compared to alanine substitutes must have an influence on DMPG dependence of the tryptophan fluorescence.⁽⁸³⁾

4.3.3 Thermal stability studies

Thermal stability studies on both oxidized HEWL and reduced HEWL in DMPG vesicles (Figure 4-17) show a gradual decrease in magnitude for the far-UV CD (negative) ellipticity, corresponding to degree of helicity, with increasing temperatures. The lipid vesicles cause the native state HEWL to lose its normal cooperative thermal denaturation behavior ($T_m \sim 83^\circ\text{C}$), as seen for HEWL in buffer only (Figure 4-17, open triangles), and evidence only a broad transition at lower temperature ($T_m \sim 65^\circ\text{C}$). Even though the four disulfide bonds can have strong stabilizing effects on the structure of native/oxidized HEWL, they are not strong enough to resist the effects of lipid vesicle interaction as evidenced by loss of cooperativity in the structural stabilization. The more gradual change for the reduced

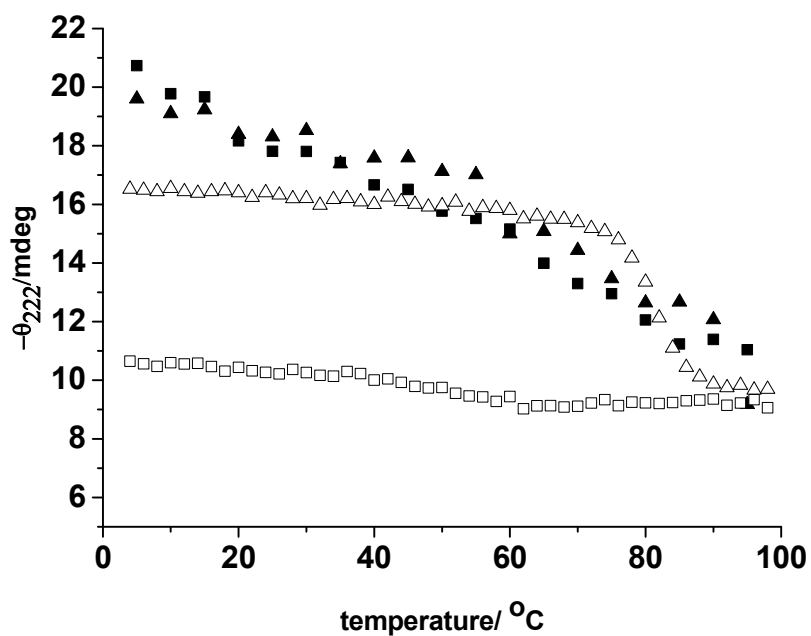


Figure 4-17. Thermal denaturation of oxidized HEWL (filled triangles) and reduced HEWL (filled squares) in DMPG vesicles, native HEWL in buffer only (open triangles) and reduced HEWL in buffer only (open squares).

HEWL-vesicle complex might be described as a molten globule state⁽⁷⁷⁾ which has substantial helical secondary structure but little tertiary structure.

4.3.4 Orientation of protein structures in the lipid bilayer

Polarized ATR-FTIR was employed to identify the orientations of component structures of refolded reduced HEWL, and the refolded 0SS and 1SS mutants with DMPG films on a surface. The polarized ATR-FTIR difference spectra (90° - 0° polarization) for reduced HEWL (red line), 0SS mutant (blue line) and 1SS mutant (black line) with DMPG vesicles are shown in Figure 4-18 and evidence similar characteristics. The transition dipole moment of the CH_2 scissoring modes of the lipid aliphatic tails is perpendicular to the hydrocarbon chains. In our spectra, it appears as a negative difference band at 1467 cm^{-1} , which, assuming the lipid chains are predominantly perpendicular to the normal of the plate after self-assembly, indicates that a negative difference corresponds to a transition dipole parallel to the plate surface. The positive band at 1655 cm^{-1} in the protein-containing films can be assigned to the α -helical amide I modes, which implies the α -helical amide I dipoles are mostly perpendicular to the plate surface and the lipid membrane surface. Thus, the helices are preferentially perpendicular to the lipid membrane and inserted into it. The positive band at 1629 cm^{-1} can be assigned to the β -sheet amide I modes, which are normal to the strands, and their positive sign suggests that they might lie on the membrane surface. Based on these polarized ATR-FTR results, we can conclude that the helical structure of the reduced HEWL, 0SS and 1SS mutant gained from the

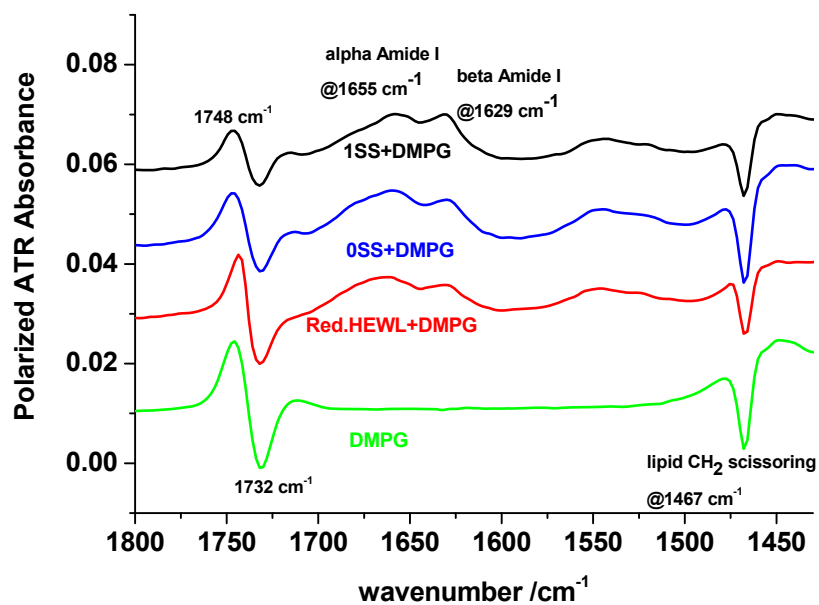


Figure 4-18. Polarized ATR-FTIR difference spectra (90°-0° polarization) of reduced HEWL (red line), 0SS mutant (blue line) and 1SS mutant (black line) with DMPG vesicles and DMPG only (green line).

interactions with vesicles is formed by incorporation of segments which can form helices and their insertion into the lipid vesicles.

4.3.5 Stopped-flow kinetic studies of reduced HEWL refolding with DMPG vesicles

The kinetics of the induced structural changes of reduced HEWL by interaction with DMPG vesicles were monitored with both changes in CD ellipticity at 222 nm and in total fluorescence intensity above 320 nm under stopped-flow mixing conditions.

The stopped-flow curves, $\phi(t)$, from the CD channel and total fluorescence intensity channel were fit with multiple exponential functions to determine rate constants in the structure reforming process using the following formula:

$$\phi(t) = at + b + \sum c_i \cdot e^{-k_i t} \quad (\text{eq.4-1})$$

where k_i and c_i are the rate constant and amplitude, respectively, of the i th exponential component and a and b represent linear baseline corrections. Figure 4-19a shows a sample kinetic trace and fit of the CD amplitude at 222 nm for reduced HEWL mixing with 5 mM DMPG vesicles, and Figure 4-19b shows the corresponding kinetic trace from the total fluorescence intensity above 320 nm with the inset indicating the very fast mixing step. We did not have sufficient OSS and ISS mutant samples for corresponding stopped-flow experiments. The kinetic parameters obtained from the fits to the kinetic traces are listed in Table 4-1.

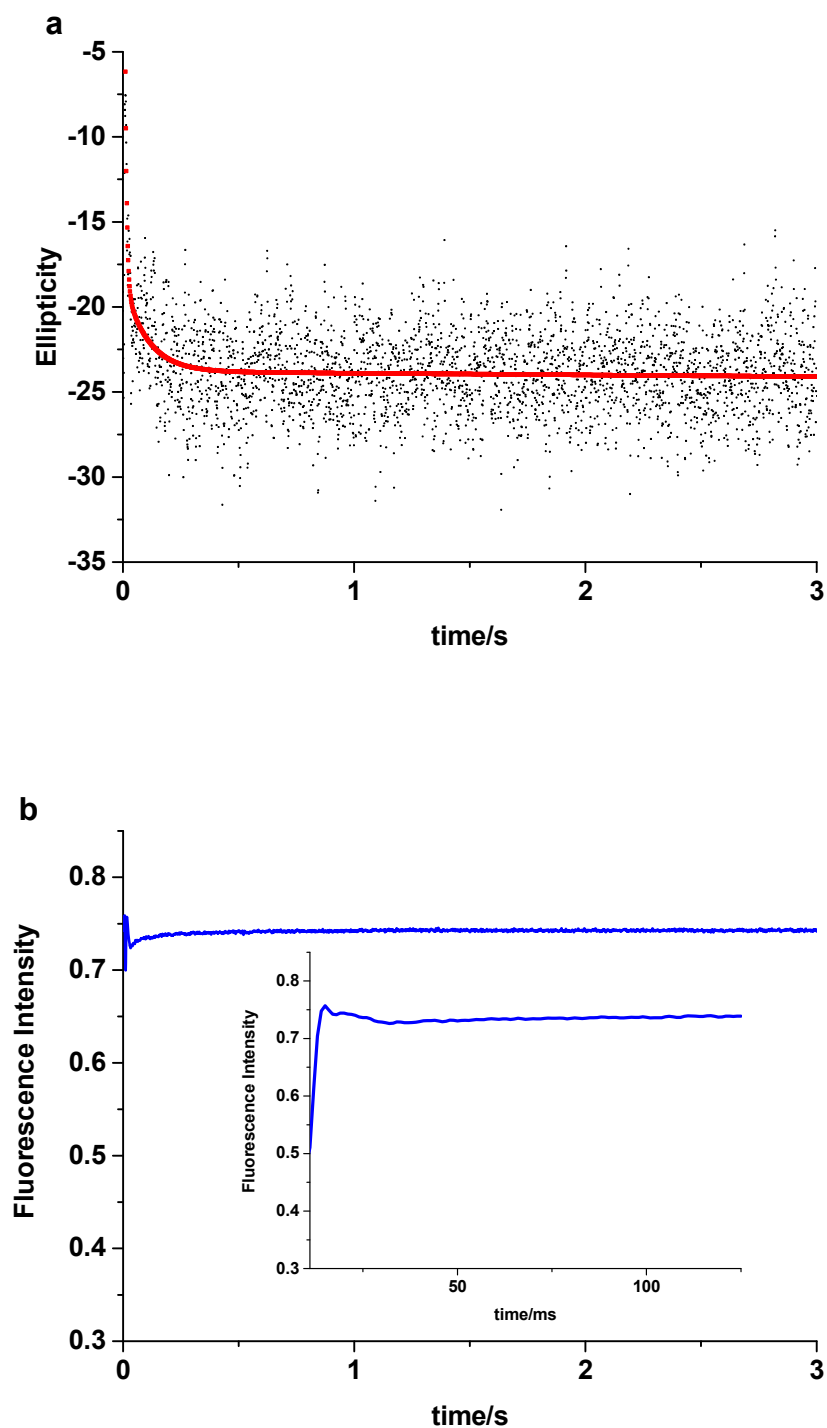


Figure 4-19. (a) The CD signal at 222 nm (black dots) and its fitted curve (red line) showing the kinetics of reduced HEWL mixing with 5 mM DMPG vesicles; (b) The total fluorescence intensity above 320 nm showing the kinetics of reduced HEWL mixing with 5 mM DMPG vesicles, where inset shows early time behavior.

Table 4-1. Stopped-flow kinetic parameters from ECD and fluorescence for reduced HEWL mixing with 5 mM DMPG vesicles.

	k_1/s^{-1}	c_1	k_2/s^{-1}	c_2	k_3/s^{-1}	c_3
ECD	146.1 ± 20.1	12.7	9.7 ± 0.9	4.9	-	-
Fluorescence	395.5 ± 60.5	-0.29	18.5 ± 1.9	-0.02	1.8 ± 0.3	-0.02

* errors are calculated with the results of three trials

The stopped-flow kinetic trace for the ellipticity change at 222 nm on mixing reduced HEWL with 5 mM DMPG vesicles shows a biexponential behavior. There is a fast phase, $k_1[\text{CD, vesicle}] \sim 146 \text{ s}^{-1}$, resulting in a large gain in helical secondary structure, followed by a slower phase, $k_2[\text{CD, vesicle}] \sim 9.7 \text{ s}^{-1}$ corresponding to a smaller increase of helical structure. The fluorescence traces show an initial large burst increase, $k_1[\text{fluorescence, vesicle}] \sim 395.5 \text{ s}^{-1}$, which is followed by two much slower increase steps with rate constants, $k_2[\text{fluorescence, vesicle}] \sim 18.5 \text{ s}^{-1}$ and $k_3[\text{fluorescence, vesicle}] \sim 1.8 \text{ s}^{-1}$. Between the fast and slower steps is an overshoot and recovery that we did not attempt to fit in our analysis. Consequently, the fast fluorescence increase ($k_1[\text{fluorescence, vesicle}]$) was fit separately from the other two constants $k_2[\text{fluorescence, vesicle}]$ and $k_3[\text{fluorescence, vesicle}]$.⁽⁸³⁾ Even though the first fast fluorescence rate constant $k_1[\text{fluorescence, vesicle}]$ is 2-3 times larger than the fast CD rate constant $k_1[\text{CD, vesicle}]$, the fast CD and fluorescence spectral changes at the very early stages of folding may occur in the same process or kinetic

step. The CD data is quite noisy and consequently is more limited in time resolution than the fluorescence data. During this step, to the ability we can resolve it, the polypeptide chain appears to collapse, as monitored by fluorescence, in the same time frame as the major secondary structure change occurs, as monitored by CD. Following the fast step, the two slower fluorescence rate constants bracket the slower CD rate constant. These slower rate constants may represent best fits to different processes resulting from one or multiple sequential mechanistic steps, but for the fluorescence they represent smaller spectral changes.

Based on these kinetic parameters, we propose that the first step of the folding of reduced HEWL with vesicles is a process involving both binding and partial insertion, during which there are major changes for both secondary and tertiary structure. The fast (burst) fluorescence change is within the mixing time and indicates the tryptophan environment is altered immediately either due to the electrostatic interactions with the lipid head groups or to the overall change in environment. For the first binding and insertion step, the electrostatic attractions of the opposite charges on protein and vesicles define this interaction. In subsequent steps after binding, the protein can rearrange its structure, continue to refold helical structure and equilibrate to the more hydrophobic interior of the lipid bilayer.

4.3.6 Comparison with micelle refolding

Our previous study reported the results of similar studies with surfactant micelles such as SDS.⁽⁸²⁾ The rate constants for reduced HEWL with SDS micelles

were shown, $k_1[\text{CD, micelle}] \sim 250 \text{ s}^{-1}$ and $k_2[\text{CD, micelle}] \sim 10 \text{ s}^{-1}$ while, $k_1[\text{fluorescence, micelle}] \sim 150 \text{ s}^{-1}$ and $k_2[\text{fluorescence, micelle}] \sim 0.7\text{-}1.8 \text{ s}^{-1}$. The rate constants from DMPG vesicles are similar to those from micelles, suggesting they represent intrinsic reduced protein folding properties more than lipid control. Previous papers have reported both equilibrium and kinetic studies on the refolding of denatured/reduced HEWL, under different conditions than we have studied. One study tried to refold the denatured but still oxidized form of HEWL containing all disulfide bonds by removing the effect of the denaturant, and reported two rate constants $k_1 \sim 69.9 \text{ s}^{-1}$ and $k_2 \sim 2.74 \text{ s}^{-1}$.⁽⁷⁹⁾ Another used reduced HEWL but then reformed the disulfide bonds by addition of oxidizing agent, and reported three very slow rate constants with k_1 and k_2 close to 0.06 min^{-1} and k_3 close to 0.002 min^{-1} .⁽⁷⁸⁻⁸⁰⁾ The rate constants for refolding reduced HEWL and reforming four disulfide bonds are much slower than our results with vesicles or micelles, because it takes much longer for the cysteine residues to come together and form the correct disulfide bonds. By contrast, interaction with lipids does not require formation of disulfide bonds but does not form native structure. The rate constants from the refolding of the denatured HEWL with all disulfide bonds intact by removing denaturant are closer but still slower than our results with vesicles or micelles, which indicates that vesicle or micellar medium can facilitate secondary structure formation independent of disulfide bonds, even faster than in buffer with conformational constraints due to preformed disulfide bonds.

Despite being similar, the rate constants of refolding reduced HEWL with DMPG vesicles are different from those with SDS micelles. The fast CD step, representing initial helical formation, is slower with DMPG than with SDS micelles. This may be due to the micelles being smaller and easier for reduced HEWL to access, or it may represent micellular interaction with just parts of the unfolded HEWL based on the beads on a chain model.⁽⁵⁹⁾ The slower step for reduced HEWL interacting with DMPG is almost the same as with SDS micelles, suggesting the slower steps after the initial binding and insertion are similar for DMPG vesicles and SDS micelles. Even though the first binding and insertion step is slower, vesicles can eventually induce more helical structure than micelles for the reduced HEWL, as shown by comparing our equilibrium studies. This indicates that the bilayer structure of the DMPG vesicles with their highly hydrophobic interior can support final membrane bound states with more helical structure than do SDS micelles. It suggests that hydrophobic effects provide a driving force to the subsequent refolding steps after the first binding and insertion step in DMPG vesicles. As a result, only selected lipids can refold reduced HEWL to attain even more helical structure than in native HEWL, due to the lipid hydrophobic and packing properties, while for micelles, several negative surfactants can refold reduced HEWL.

For the fluorescence kinetics, the fast step in DMPG vesicles is much faster than with micelles, and the slower steps for DMPG are (combined) faster than for the single micelles' rate. The differences of the rate constants from fluorescence kinetics are opposite in sense from the CD data and suggest that the secondary and tertiary

structure changes are not fully coordinated. These differences demonstrate that the hydrophobic interactions of DMPG vesicles are different from that of SDS micelles. The vesicles have larger sizes and a bilayer interior, resulting in higher hydrophobicity than micelles. We can also see that the fluorescence rate constants are larger than the CD ones, but by contrast, the SDS fluorescence rate constants are smaller than the CD ones. Fluorescence changes reflect local conformational changes around the tryptophan residues and tertiary structure (interaction and quenching) changes. The DMPG SUV vesicles have a radius of ~ 30 nm, while both HEWL and micelles have a radius of ~ 2 nm. Due to their larger size, the DMPG vesicles can provide larger and more unified surface for the binding with reduced HEWL and thus may lead to faster local conformational changes for the tryptophan residues, even though any transport-limited binding may be slower for vesicles than for micelles, due to their larger size. A more hydrophobic environment in vesicles is consistent with the fluorescence peak position changes for reduced HEWL in the presence of DMPG vesicles and micelles. In DMPG vesicles, the fluorescence peak position blue shifts to the final value right away, while in micelles, the blue shift shows a more gradual transition process to its final value.

4.4 Conclusion

4.4.1 Effects of charges, hydrophobicity and membrane packing

Reduced HEWL can be largely refolded to a highly helical non-native state with bilayer vesicles composed of lipids having negative head groups. Our data

cannot determine which part of HEWL forms the new helices. Possibly the terminal parts can insert into the membrane and form helices with the sheets laying on the membrane surface. The first step of the refolding process involves both the binding and reconfiguration of the protein on the vesicles, whereby the majority of helical structure is formed. The binding between the protein and vesicle surface appears to be driven by electrostatic attraction of opposite charges on protein and vesicles. This interaction with the surface apparently stabilizes an intermediate that can facilitate the formation of helical secondary structure and insertion in to the bilayer. The intermediate formation is suggested by the differences in kinetic fast steps detected by fluorescence and CD in the process.

Electrostatic attractions drive the attraction between protein and vesicles, but are not a prerequisite for interaction of a flexible unfolded protein with the membrane. When the protein chain is flexible enough, such as for reduced HEWL, the strong hydrophobic interactions can bring the protein and vesicles together and possibly result in a change of conformation and eventual insertion of protein segments into vesicle membrane. Whether the helix develops prior to insertion or in some concerted multistep process is not defined by our data. Subsequent steps after the binding and insertion process allow the protein to rearrange structure further, continue to gain helical content and adjust packing of tryptophan residues, for which the hydrophobic interactions are the major driving forces. When the protein chain is rigid, or more constrained by a stable fold, such as for native/oxidized HEWL, it can barely insert into the membrane of DMPC vesicles in the absence of electrostatic attractions.

Vesicles with higher hydrophobicity can induce more helical structure but the packing of lipids in the vesicle also plays an important role in the insertion process. When the lipids have double bonds in the tails, these create kinks and thus do not pack well. This appears to create a barrier or destabilization condition for helix insertion, and consequently the protein exhibits less structural change. DMPG SUV vesicles with sizes around 50 nm and DMPG LUV vesicles with sizes around 120 nm can induce the same amount of helical content for reduced HEWL, which suggests that the size of vesicles or planarity of the bilayer surface does not have a significant effect on the refolding.⁽⁸⁴⁾

4.4.2 Micelles and vesicles as mimics of membrane

Our equilibrium studies show that vesicles can induce more helical structure for the reduced HEWL than do micelles, which may indicate that vesicles have more space for helical development and higher hydrophobicity in the bilayer than do micelles. The comparison of the kinetics of refolding with vesicles and micelles also reveal that there are other differences between vesicles and micelles during the binding, insertion and post-insertion steps. These could originate from the differences of sizes, curvatures, compositions, and hydrophobicity between micelles and vesicles. Although, lipid vesicles provide a better mimic of membrane in cells, comparison of results with both micelles and vesicles can give useful insight into the interaction of proteins with cellular membranes.

4.4.3 Role of disulfide bonds on protein folding

Equilibrium studies of the interactions of reduced HEWL, OSS mutant and native/oxidized HEWL with vesicles with negative or zwitterionic head groups indicate that the set of four disulfide bonds has a huge effect on the refolding process in vesicle membrane. The reduced HEWL and OSS mutant without disulfide bonds undergoes larger structural changes in lipid bilayers than does the native/oxidized HEWL with four disulfide bonds. The reason is that the disulfide bonds can reduce the protein chain flexibility and its accessible configurational space. In this case, the set of four disulfide bonds determines a specific folding pathway and leads to the final folded state. For the 1SS mutant interacting with lipid vesicles, with a single disulfide bond, a terminal state with the same secondary structure as formed for reduced HEWL and OSS in vesicles is formed, but it requires lower vesicle concentrations to reach the final state. So the single disulfide bond Cys64-Cys80 in the 1SS mutant does affect the mechanism, perhaps by favoring an on-path intermediate in the folding process achieved by stabilizing and conformationally constraining the starting structure, and thus facilitates folding with vesicles. In this case, the single disulfide bond does affect an early stage of folding, but its effects are overshadowed in the final stage when there are stronger hydrophobic stabilizing forces from the bilayer.

This example helps illustrate that disulfide bonds can be used to alter the stability, or flexibility of a protein, which may be one reason for their evolutionary development. Flexibility is an important aspect for protein folding and activity, and disulfide bonds can be a manipulating tool for altering the protein flexibility, and thus

to improve protein activity during the evolution process. In addition, altering the number of disulfide bonds and incorporating mutations of other residues provides an engineering method to change the stability or flexibility of the whole or some part of the protein.

5. Spectroscopic study on Collagen-collagen interactions mediated by plant-derived proanthocyanidins

This chapter contains work done in collaboration with the UIC college of Dentistry which has been submitted for publication by that group (Vidal, Cristina and Bedran-Russo, Ana submitted). The study involves multiple techniques, but only my results are presented here unless explicitly noted.

5.1 Introduction

Type I collagen is the most abundant structural protein in human body and is the major component of connective tissues such as skin, tendons, bone, and dentin. Collagen molecules are assembled extracellularly to form microfibrils and fibrils. A cascade of reactions initiated by lysyl oxidase cleavage of lysine and hydroxylysine aminoacids at the telopeptide regions of the collagen molecules results in the formation of inter-, and intra-molecular and inter-microfibrillar cross-linking.⁽⁸⁵⁻⁸⁸⁾ Such enzymatically mediated cross-links provide a foundation for stability, strength and function. The types and amount of cross-links vary among tissues and change due to physiological and pathological conditions.

Collagen cross-links have inspired novel approaches for tissue repair and regeneration with ultimate goal to restore function. In dentistry, mimicking cross-linking in mature dentin collagen matrix through non-enzymatic chemical reactions enhances the native tissue's biomechanics and can reduce enzymatic breakdown.⁽⁸⁹⁻⁹²⁾ Synthetic chemicals such as glutaraldehyde and carbodiimides were explored as non-enzymatic chemical cross-linkers.^(91, 93, 94) Carbodiimide compounds (EDC) are

functional coupling reagents that induce cross-linking by activating carboxylic acid groups of glutamic or aspartic acid residues to form stable amide bonds with amines of lysine and hydroxylysine residues in the presence of N-hydroxysuccinimide (NHS).⁽⁹⁵⁾ Glutaraldehyde (GA) effectively cross-links the tissue by forming covalent binding of two amine groups of (hydroxy)-lysine residues with its aldehyde groups, which will further react to form pyridinium compounds.⁽⁹⁵⁾ EDC/NHS and GA induce cross-links even in highly cross-linked tissue such as dentin;⁽⁹¹⁾ however clinical usage remains problematic due to cytotoxic reactions.⁽⁹⁴⁾

Plant-derived agents exhibit comparable or higher activity with biological tissue when compared to synthetic agents.⁽⁹⁴⁾ In specific, biocompatible proanthocyanidins (PACs) are considered one of the most important classes of secondary metabolites in the plant kingdom, offering a renewable source of raw material. Natural extracts containing oligomeric PACs enhance the mechanical properties and decrease degradation of dentin via interaction with type I collagen.^(90, 96) The specific mechanisms of interaction between PACs-type I collagen to convert from triple helices to fibrils remains largely speculative. The complexity of interactions between PACs and proline rich proteins yielded reports of their dependence on formation of a variety of molecular bonds, including hydrogen and covalent bonds, hydrophobic interactions and formation of hydrophobic pockets.⁽⁹⁷⁻¹⁰⁰⁾

To elucidate the mechanism of interaction of PACs with collagen-rich tissues, we have undertaken spectroscopic analyses in purified type I collagen and correlated them to changes in the spectroscopic analysis of collagen-rich dentin matrices induced

by chemical and natural cross-linkers. The well-described mechanisms of cross-linking between EDC and GA with collagen-rich tissues were used as a reference to determine the chemical interactions of PACs with dentin collagen. The hypothesis tested was that the interactions with PACs would be of similar nature and intensity of the cross-linking induced by synthetic agents.

5.2 Experimental

5.2.1 Materials

Cross-linking agents used in this study included: grape seed extract [(GSE), *Vitis vinifera*, total proanthocyanidins (PACs) concentration >94%, Lot#31492514-01, MegaNatural Polyphenolics, Madera, CA]; 1-ethyl-3-[3-dimethylaminopropyl] carbodiimide hydrochloride (EDC, Pierce/Thermo Scientific, Rockford, IL), N-hydroxysuccinimide (NHS, Pierce Thermo Fisher Scientific Inc.), and glutaraldehyde (GA, 25% stock solution, Fisher Scientific, Pittsburgh, PA). Type I collagen extracted from rat tail tendon and solubilized in acetic acid (BDTM Biosciences, San Jose, CA) was used to evaluate the structural impact of the interaction between cross-linking agents and collagen and to determine collagen-collagen interactions.

5.2.2 Fluorescence analysis

Fluorescence experiments were carried out at room temperature with excitation at 276 nm using a FluoroMax 3 fluorescence spectrophotometer (Horiba Scientific,

Edison, New Jersey, NJ) and a 1 cm path length quartz cuvette. Spectra were measured in triplicate by incubating 0.5 g/L of type I collagen with a range of different concentrations of GSE, EDC/NHS and GA: from 0.0065% to 0.065% (w/v) GSE, from 0.0575% to 0.575% (w/v) for EDC with 0.014% to 0.14% (w/v) NHS, and from 0.005% to 0.5% (w/v) GA. Cross-linking solutions were prepared in distilled water (DW) and pH was adjusted to 7.2. Reference spectra of solubilized collagen and of the cross-linking solutions were also recorded. CD measurements of collagen with cross-linkers could only be carried out for low concentrations due to interference from light scattering of particles. Consequently, no CD data is presented.

5.2.3 ATR-FTIR analysis

Interactions of type I collagen and dentin collagen (in demineralized dentin) with cross-linkers were analyzed using an ATR accessory (single reflection diamond, PIKE MIRacle ATR, Madison, WI) mounted in an FTIR spectrometer (Bruker Vertex 80, Billerica, MA). Solubilized type I collagen (1 mg/ml) was incubated at room temperature for 1 hour with either 0.065% (w/v) GSE, 5.75% (w/v) EDC/1.4% (w/v) NHS or 5% (v/v) GA freshly prepared in DW as described above. Because relatively high concentrations of GSE, EDC or GA were used, resulting in strong cross-linking, after mixing the collagen with the cross-linkers the solution became more viscous, and eventually a gel phase formed separate from a supernatant liquid phase, especially for the GSE. Since the liquid phase transmission IR spectrum showed mostly peaks from the cross-linkers, ATR-IR spectra were measured for the gel phase to assess changes in

the collagen. For that, the gel was pressed onto the ATR plate using a pressure clamp to obtain better contact with the diamond surface. Spectra over the range 4500 cm^{-1} to 600 cm^{-1} were collected as an average of 512 scans (10 kHz scan speed with a DTGS detector) and processed with a 3-term Blackman-Harris apodization and zero filling of 2. Background transmission spectra with no sample on the ATR crystal surface were collected with same measurement parameters and used to compute absorbance spectra. Repeated spectra were collected until the collagen gels were completely dried and the results were consistent. The ATR absorbance spectra of GSE, EDC/NHS and GA solutions were measured by applying $10\text{ }\mu\text{l}$ of each solution on the crystal surface and drying with a mild flow of nitrogen gas to form a homogenous thin film.

The evaluation of collagen cross-linking in the dentin organic matrix was performed as described for purified type I collagen. Dental samples were all prepared in the UIC college of Dentistry by our colleague Cristina Vidal. Five freshly extracted human molar teeth were collected and stored at $-20\text{ }^{\circ}\text{C}$ (IRB, University of Illinois at Chicago, protocol # 2006-0229). Crowns were cut off using a low speed diamond saw (Buehler, Lake Bluff, IL) to obtain dentin specimens with 0.5 mm thickness x 1.5 mm width x 1.5 mm length. Dentin specimens were completely demineralized with 10% phosphoric acid (Ricca Chemical Company, Arlington, TX) for 5 h under agitation.⁽⁹⁰⁾ Water-rinsed specimens were pressed onto the diamond crystal surface to better cover the active area and ATR spectra of dentin only were obtained. After that, dentin specimens ($n = 3$) were re-hydrated and treated with: 6.5 % GSE, 5.75% EDC/1.4% NHS or 5% GA, prepared in DW (pH 7.0). Each dentin specimen was treated with 200

μl of fresh cross-linking solution for 1 h at room temperature and washed before re-measurement with ATR-FTIR to obtain a spectrum of cross-linked dentin from the same dentin surface. Reference ATR spectra of the GSE, EDC/NHS, and GA solutions were measured as described above.

Difference spectra were obtained by subtracting the spectra of untreated from treated collagen or dentin samples with cross-linking agents. Subtraction factors were adjusted to minimize the amide I and amide II bands from collagen (in practice the collagen peaks could not be fully eliminated without introducing baseline artifacts into the difference spectra). Spectra from cross-linked collagen or dentin and/or cross-linking solutions were scaled and plotted along with difference spectra for evaluation and comparison. Data were plotted using Origin software (OriginLab, Northampton, MA).

5.3 Results

5.3.1 Fluorescence results

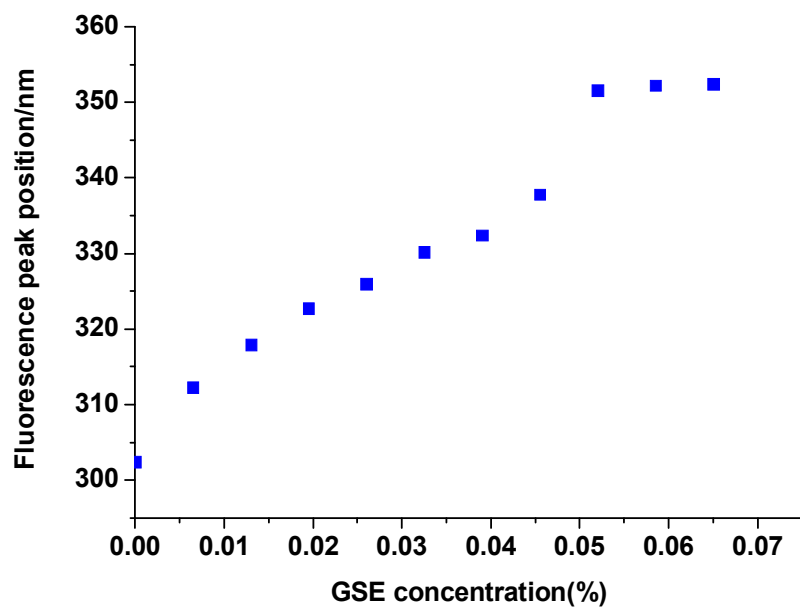
Collagen fluorescence spectra obtained from three repetitions were similar, so results from only one representative sample are presented. When excited at 276 nm, collagen exhibited emission with a maximum at ~ 303 nm, characteristic for tyrosine fluorescence.⁽³⁸⁾ Fluorescence intensity with 276 nm excitation of GSE, EDC and GA solutions alone were much lower than for collagen (not shown), so we could monitor the changes in collagen fluorescence after interaction with such cross-linkers without

interference from the fluorescence of those cross-linkers. The absorbance of tyrosine from collagen did not shift upon adding cross-linking agent so the same excitation wavelength of 276 nm was used for all samples. When treated with cross-linking agents, collagen fluorescence intensity decreased, with the most prominent reduction observed for addition of GSE (Figure 5-1b). A large red shift from 303 nm to 352 nm can be seen as GSE concentration increases (Figure 5-1a). With addition of low concentrations of GSE, the fluorescence intensity shows an initial increase before falling off. With higher concentrations of GSE, a gel was formed, which impaired the measurements due to higher light scatter. By contrast, collagen fluorescence after cross-linking with EDC and GA showed only very small red shifts, ~1-2 nm (not shown). Somewhat varying from GSE, fluorescence intensity steadily decreased with added EDC and GA, although the latter evidenced a stable intensity for GA additions up to ~0.05 % (Figures 5-1c and 5-1d).

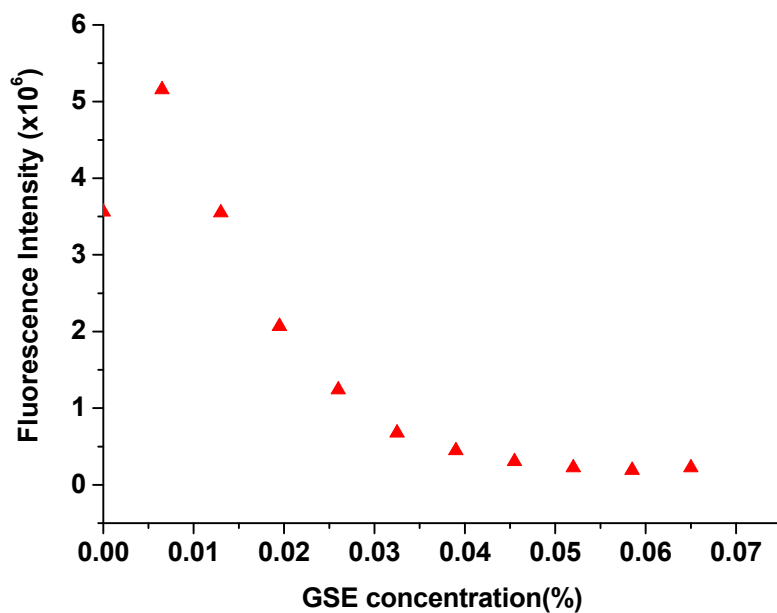
5.3.2 ATR-FTIR analysis

Representative ATR-FTIR spectra for cross-linked type I collagen and dentinal collagen are presented in Figures 5-2 and 5-3. Both collagen and dentin spectra for all specimens showed typical peaks for collagen, such as C=O stretching at $\sim 1632\text{ cm}^{-1}$ (amide I), out-of-phase combination of N-H bending and C-N stretching at $\sim 1544\text{ cm}^{-1}$ (amide II), CH₂ scissoring at $\sim 1450\text{ cm}^{-1}$ and some contribution from the mix of C α -H deformation and N-H bending and C-N stretching between 1350 and 1200 cm^{-1} (C α -H and amide III) (Figures 5-2 and 5-3).

(a)



(b)



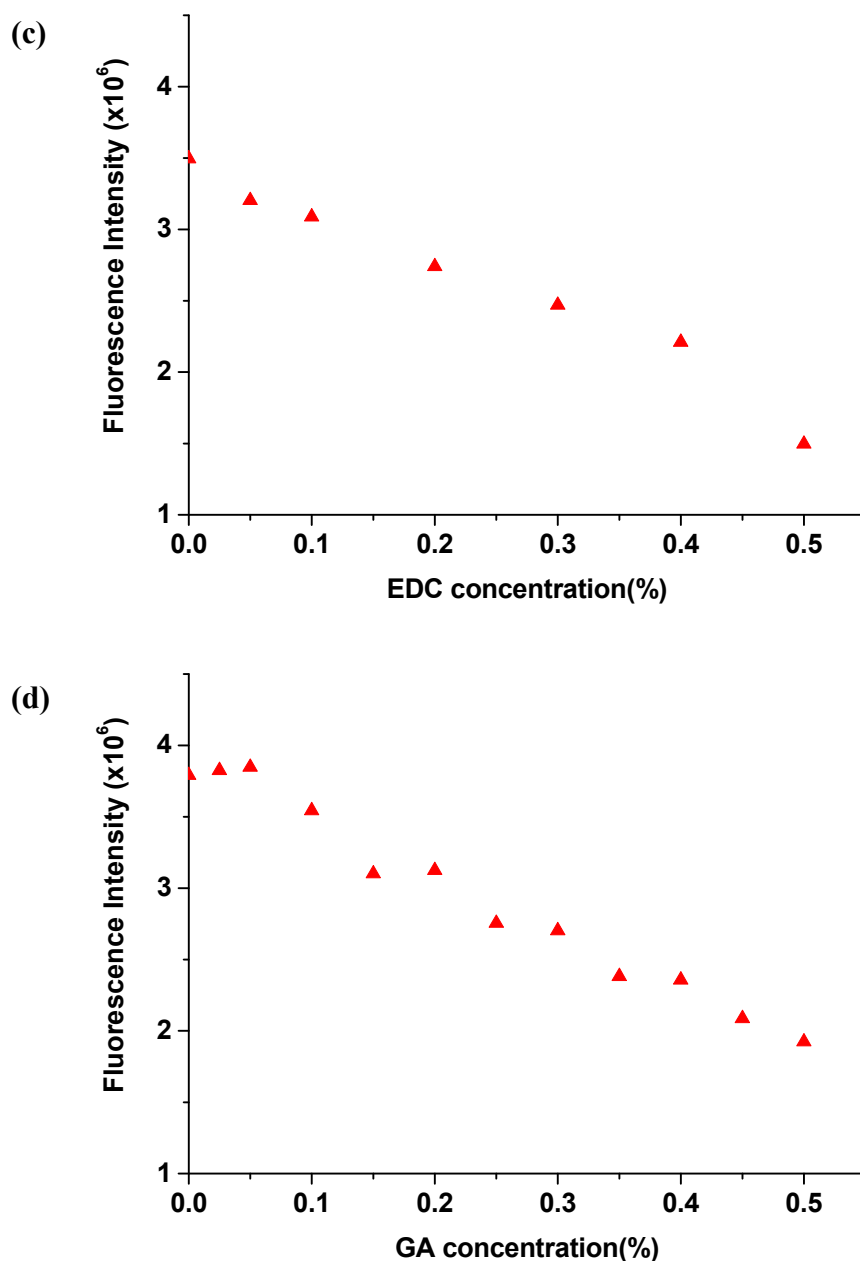
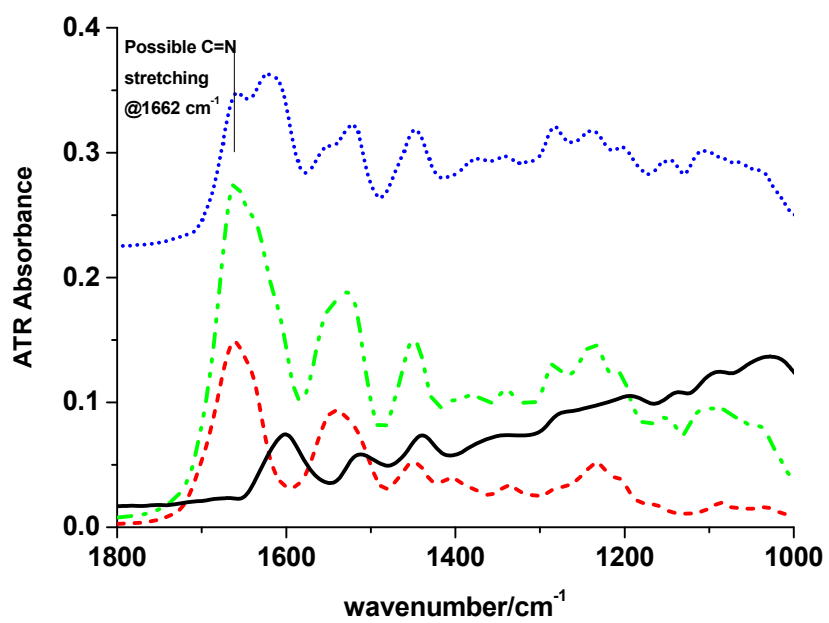
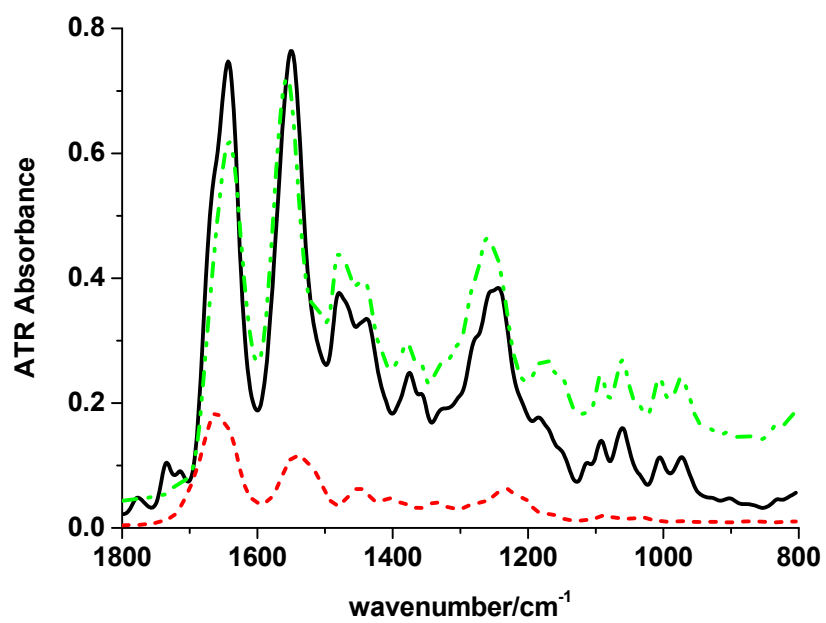


Figure 5-1. Collagen fluorescence changes in peak position and fluorescence intensity when treated with different concentrations of GSE, EDC/NHS and GA. **(a)** Collagen fluorescence peak positions and **(b)** fluorescence intensities when incubated with 0.0065 - 0.065% GSE. **(c)** Collagen fluorescence intensities after incubation with 0.0575 - 0.575% EDC containing 0.014 - 0.14% NHS. **(d)** Fluorescence intensities when collagen was incubated with 0.005 - 0.5% GA.

(a)



(b)



(c)

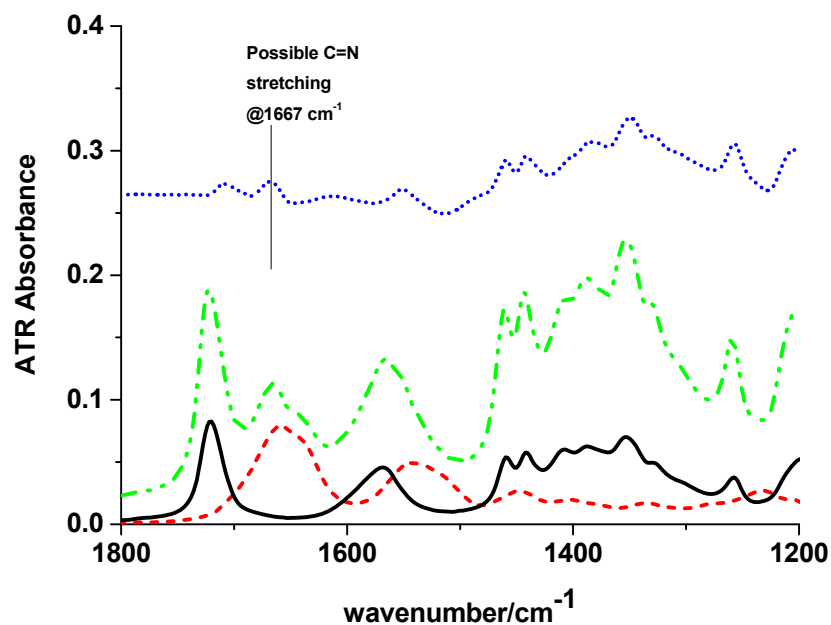
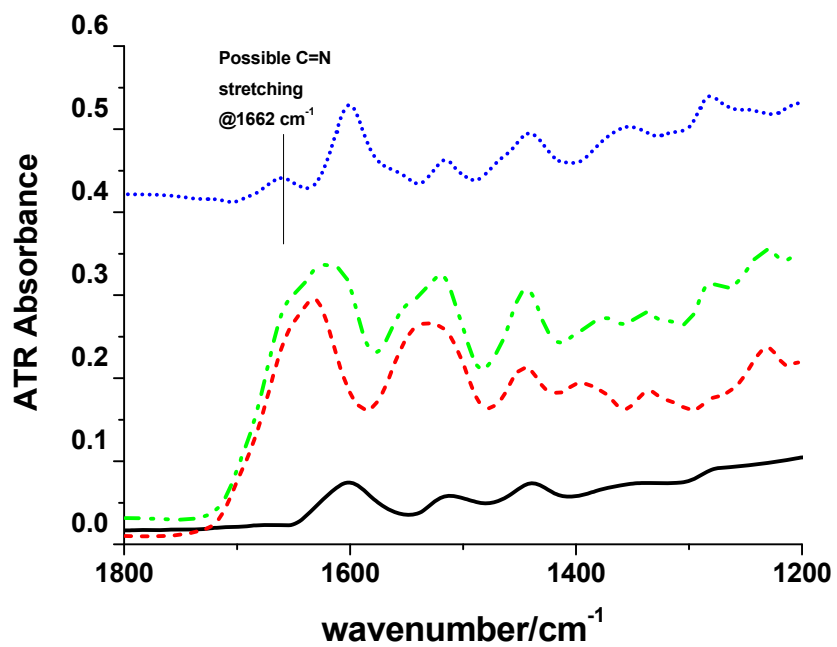
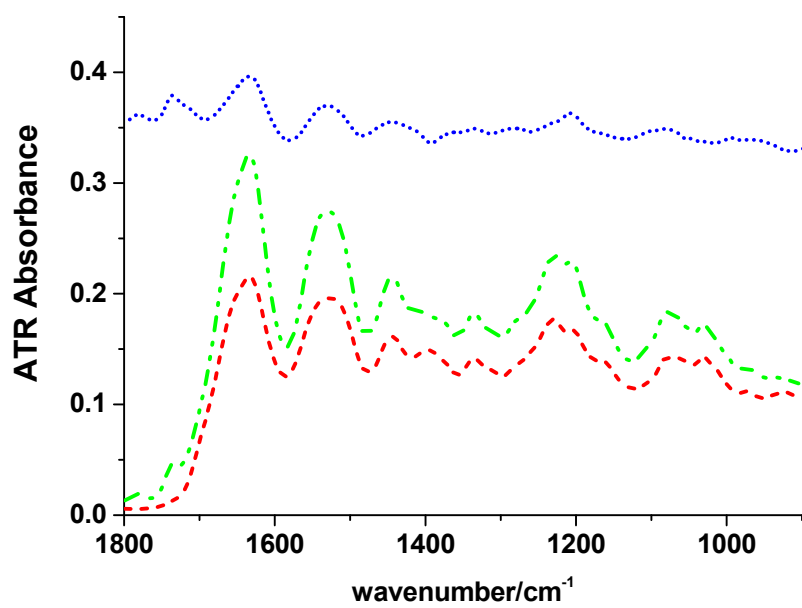


Figure 5-2. (a) ATR-FTIR spectra of type I collagen treated with 0.065% GSE. Black solid line: GSE; red short dash line: collagen; green dash dot line: collagen + GSE; blue short dot line: difference spectrum. (b) ATR-FTIR spectra type I collagen treated with 5.75% EDC/1.4% NHS. Black solid line: EDC/NHS; red short dash line: collagen; green dash dot line: collagen + EDC/NHS. (c) ATR-FTIR spectra type I collagen treated with 5% GA. Black solid line: 5% GA; red short dash line: collagen; green dash dot line: collagen + GA; blue short dot line: difference spectrum.

(a)



(b)



(c)

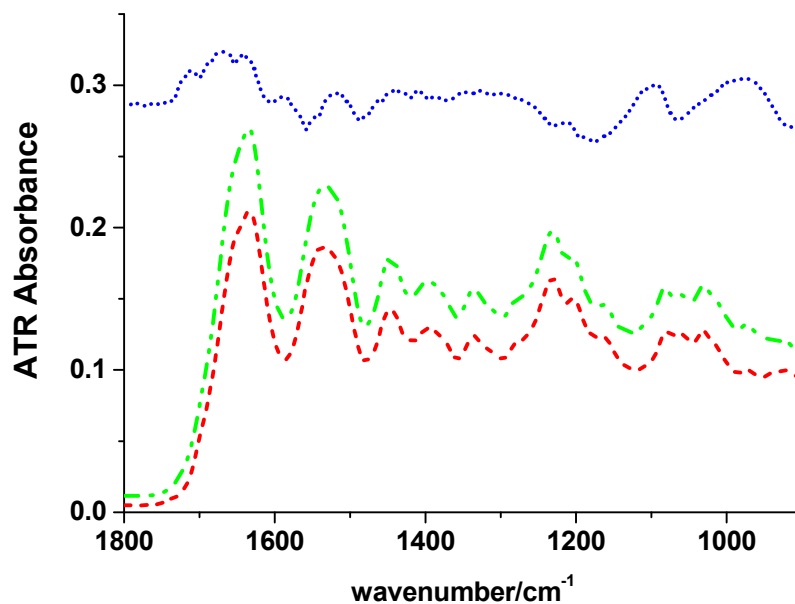


Figure 5-3. (a) ATR-FTIR spectra of dentin treated with GSE. Black solid line: 6.5% GSE; red short dash line: dentin; green dash dot line: dentin + GSE; blue short dot line: difference spectrum. (b) ATR-FTIR spectra of dentin treated with 5.75% EDC/1.4% NHS. Red short dash line: dentin; green dash dot line: dentin + EDC/NHS; blue short dot line: difference spectrum. (c) Dentin treated with 5% GA. Red short dash line: dentin; green dash dot line: dentin + GA; blue short dot line: difference spectrum (multiplied by three).

In GSE-treated collagen, GSE peaks are aromatic ring C-C stretching at $\sim 1600\text{ cm}^{-1}$ and $\sim 1517\text{ cm}^{-1}$ and at 1450 cm^{-1} (red dash, Figure 5-2a). A possibly new feature is observed in the difference spectrum, a peak at 1662 cm^{-1} (blue dots, Figure 5-2a). For the spectra of EDC-treated collagen (Figure 5-2b), the gel phase formed after mixing collagen and EDC solution (Figure 5-2b, green dash-dot) still evidences most of the peaks from EDC/NHS and shows only minor intensity and frequency variations. There are small relative variations in intensities for the mixture as compared to the spectrum of EDC/NHS, however, due to the higher concentrations of EDC/NHS used, our ability to detect its impact on collagen is poor for this ATR-IR test. Similar to EDC-treated collagen, for the interaction of GA and collagen the difference spectrum is again dominated by the peaks from GA. By using a double difference, subtracting both collagen and GA from the mix, a new peak is clearly evident at 1667 cm^{-1} in this case (Figure 5-2c, blue dot). In all these cross-linked collagen solution spectra, elimination of the protein spectral bands by simple subtraction should leave behind residual cross-linker plus any new products. Since the added cross-linker is in excess and difficult to separate after reaction, sensitivity to new features in the difference spectra so dominated by cross linker bands is limited.

In GSE-treated dentin, GSE peaks are similar to the ones described for collagen. Besides the new feature at 1662 cm^{-1} , changes at ~ 1350 and 1250 cm^{-1} are observed due to GSE-collagen interaction, which are most evident in the difference spectrum as compared to the spectrum of GSE (Figure 5-3a). EDC/NHS-treated dentin IR spectrum is almost identical in shape to that of dentin, with the exception of two weak peaks at

1734 cm^{-1} and 1776 cm^{-1} (Figure 5-3b). In addition, there are small absorption increases at 1200 cm^{-1} and 1079 cm^{-1} and decrease at 1395 cm^{-1} when compared to the spectrum of untreated dentin and in the difference spectrum. When dentin was treated with GA, none of the peaks from GA are evident and a very small shoulder at 1658 cm^{-1} was observed (Figure 5-3c), which is most obvious in the difference spectrum. The spectra also show a weak feature at $\sim 1715 \text{ cm}^{-1}$, which could be from GA. Other than that, GA peaks are not evident in the difference spectrum and no comparison between difference spectrum and spectrum of GA is made.

5.4 Discussion

The present study showed significant changes in the collagen spectroscopic patterns after interaction with the cross-linkers. Pronounced modifications in collagen fluorescence upon interaction with natural and synthetic cross-linking agents were observed, indicating collagen conformational modifications promoted by the cross-linkers. Moreover, the mechanism of interaction with the collagen molecule seems to be different for each cross-linker as shown by ATR-FTIR experiments, although some similarities can be seen for GSE and GA.

Collagen was solubilized at pH 7.2, since a precipitate was formed at pH higher than 7.4, probably due to fibril or other aggregate formation. After mixing with cross-linking solutions, the pH was dropped to 6.0, so the fluorescence assay could be performed without any distortions from aggregation. With excitation at 276 nm, there was no interference from any of the cross-linking agents. Also, we can clearly observe

the tyrosine (Tyr) fluorescence change, since tryptophan is not present in type I collagen.^(101, 102) Our results showed a decrease in collagen fluorescence intensity when any of the cross-linkers were added at relatively high concentrations, with GSE inducing the greatest intensity loss. There were also red shifts of the peak frequencies, but these latter changes were significant only for GSE. Red shifts in protein/Tyr fluorescence generally indicate an increase in solvation or a less hydrophobic environment. The red-shifted tyrosine emission observed for all cross-linkers is not fully understood. One possibility might be that ionization of the phenolic hydroxyl group of Tyr leads to tyrosinate formation and red shift in the emission spectrum, but this seems unlikely at the pH values we used. Another possibility is that the Tyr residue may get trapped in a local conformation and participate in events like excited state proton transfer, leading to a red-shifted fluorescence emission.⁽³⁸⁾ Since the frequency shift is only significant with GSE, one might assume that the Tyr side chains interact with the aromatic rings of the polyphenolic components of GSE⁽¹⁰³⁾ which could result in a red shift, or that the extended linkage exposed the fluorescent Tyr on the collagen telopeptide segments to more solvation.

The fact that the shift is much smaller with EDC/NHS or GA implies that those cross-linked structures are different, and possibly more tightly packed, at least in the regions of the sequence with a significant Tyr fraction. That would also seem to argue against an aromatic interaction of the PAC with the protein to drive collagen cross-linking with GSE. Some difference in mechanism is indicated here. Loss of intensity is more dependent on quencher availability close by in the sequence. For GSE, there is a

gain in intensity at low concentration added, followed by a much larger loss. Charged amino acids such as lysine, aspartic acid, glutamic acid and histidine can quench the fluorescence of tyrosine when they are close. In the sequence of collagen, about 50% of the intensity of the fluorescence is found within the mapped cross-link domain (containing cross-linking sites such as lysine).⁽¹⁰⁴⁾ After addition of low concentrations of cross-linker, many of the lysines become cross-linked (thus no longer charged), which could allow the tyrosine fluorescence intensity to increase, as seen with GSE, and possibly, but less so, with GA. This again might argue for a chemical linkage, and not just H-bonding, but could alternatively suggest some aromatic interaction altering quantum yield, although one would expect the PAC to quench Tyr, acting as an acceptor. With higher concentrations of any of the cross-linkers, gel formation causes loss of tyrosine fluorescence intensity due to scatter. The GSE shows a stronger cross-linking effect on the tyrosine fluorescence than GA, as demonstrated from the larger amplitude of tyrosine fluorescence increase at low cross-linker concentrations and decrease at high cross-linker concentrations. On the other hand, the mechanism of cross-linking for EDC is described as “zero-length” since the carbodiimide does not become part of the cross-linked protein.⁽⁹⁵⁾ Possibly, the resulting minimal modifications in collagen structure with EDC were reflected in relatively small changes in collagen fluorescence. Exposure of type I collagen and its microfibrils to cross-linking agents induced stronger chemical bonding interactions than physiologic ones.

To better understand the specific mechanisms of interactions between dentin collagen and cross-linking agents, we performed ATR-FTIR analysis using both type I

collagen and demineralized dentin. The IR spectra of collagen shows its specific feature, the amide bands, which are characteristic of its triple helix conformation. The GSE-treated collagen spectrum shows a combination of IR peaks from the collagen and the GSE spectra, but the difference spectra show evidence for new bands at 1662 cm^{-1} and possibly 1350 and 1280 cm^{-1} , for example (Figure 5-2a), which provide evidence of GSE incorporation and interaction with collagen. Similar results were observed for dentin cross-linked with GSE (Figure 5-3a). A peak at 1450 cm^{-1} and a loss of intensity at 1400 cm^{-1} can be noted in the difference spectrum and confirms previous results.⁽¹⁰⁵⁾

Recent studies have suggested that hydrogen bonding is the main mechanism of interaction between hydroxyl groups present in PACs and amino and amide groups of collagen.^(98, 106) However, hydrophobic interactions were also proposed to explain the binding of polyphenols to proteins, which might occur through the association of their aromatic rings with proline residues.^(107, 108) In the present study, the comparison of the difference spectrum both for dentin and type I collagen to the GSE ATR spectrum shows the changes after treatment more clearly: the new feature at 1662 cm^{-1} seen in the difference spectrum (top traces, blue dots, Figure 5-2a and 5-3a). This peak may be assigned to a possible C=N stretching, plus an enhancement of the CH₂ bending at 1442 cm^{-1} , the above noted 1400 cm^{-1} band, as well as an ester C-O stretching at 1283 cm^{-1} and a phenol and ether C-C, C-O stretching at 1198 cm^{-1} and 1038 cm^{-1} . Moreover, this new feature can be an indication of covalent or covalent-like bond formation, i.e. Schiff base, between GSE and collagen.

EDC couples carboxyl groups to primary amines forming amide bonds,⁽¹⁰⁹⁾

whose spectral contributions would be obscured by overlap with the collagen amide bands. Moreover, our ATR-FTIR data corroborate with absence of significant changes in collagen fluorescence since EDC induces the formation of inter- and intra-molecular amide bonds in collagen with no additional chemical features. However, it has been speculated that EDC does not cross-link collagen only by creating amide bonds, but also by additional ester bonds formed between carboxyl and hydroxyl groups.⁽¹¹⁰⁾ Interestingly, both the EDC treated collagen and dentin spectra show peaks at ~ 1740 and 1780 cm^{-1} , which could correspond to the ester C=O group stretch. The asymmetrical and symmetrical stretching frequencies of the C-O ester groups between large molecules are expected in the region of $1185\text{-}1277\text{ cm}^{-1}$ and $1050\text{-}1116\text{ cm}^{-1}$.⁽¹¹¹⁾ While we see intensity changes in this region, overlap with dentin modes makes determination difficult. These ester bonds can be also created with the hydroxyl groups of carbohydrate in glycosaminoglycans,⁽¹¹²⁾ which are also present in dentin organic matrix, although in a much smaller amount when compared to collagen. Two weak peaks that differ between EDC/NHS-treated dentin IR spectrum and dentin, are the peaks at 1734 cm^{-1} and 1776 cm^{-1} . The relative intensities of these features do not correspond to the peak distribution in the EDC/NHS spectrum, so their origin is unclear. They might correspond to impurities, excess of EDC (as seen in EDC/NHS solution Figure 5-2b, black trace) or ester formation.

The treatment of dentin with GA showed a new peak at 1667 cm^{-1} , which can be seen as a small shoulder in the difference spectrum. The absence of GA peaks in the difference spectrum is probably because GA was completely washed away from the

dentin specimen and only the induced changes to dentin could be observed. The mechanism of GA cross-linking is by a reaction of its aldehyde groups with free amino groups of lysine or hydrolysine residues, forming Schiff base intermediates. While we see evidence for a new band at 1664 cm^{-1} in the collagen plus GA spectrum, this is less evident in the dentin plus GA spectrum. This may be due to the complex structure of collagen in dentin that may inhibit more extensive incorporation of the GA linkage as compared to the solubilized collagen. A large variety of further reactions can occur forming secondary or tertiary amine groups or pyridinium compounds.⁽⁹⁵⁾ However, the mechanism of interaction limits the formation of large polymeric networks, since it is dependent on the availability of amino groups.

The AFM analysis conducted by our collaborator demonstrates that interaction forces between collagen fibrils after treatment with GSE, EDC and GA increase, which is more evident for GSE and is an indication of formation of strong covalent-bond-like interactions (mean force $\sim 700\text{ pN}$), and that biostability and biomechanical properties in dentin are increased by PACs through strong cross-linking, supporting the ATR-FTIR data for GSE-treated collagen and dentin.

5.5 Conclusion

Using spectroscopic analyses, together with the AFM analysis from our collaborator, interactions of PACs with collagen were characterized. Our study provides evidence for covalent-like bond formation between collagen and PACs. The specific mechanism of interaction exposed in the present study will drive further research of bioactive compounds of natural PAC-rich extracts based on the mechanism of their interaction with collagen-rich tissues.

CITED LITERATURE

1. Gad, S. C. (2007) *Handbook of Pharmaceutical Biotechnology*, Wiley, Hoboken, N.J.
2. Ramachandran, G. N., Ramakrishnan, C., and Sasisekharan, V. (1963) Stereochemistry of polypeptide chain configurations, *J. Mol. Biol.* 7, 95-99.
3. Pauling, L., Corey, R. B., and Branson, H. R. (1951) The Structure of Proteins: Two Hydrogen Bonded Helical Configurations of the Polypeptide Chain, *Proc. Natl. Acad. Sci.* 37, 205-211.
4. Saleman, F. R. (1983) Structural Properties of Protein beta-sheets, *Prog. Biophys. Mol. Biol.* 42, 95-133.
5. Colossi, M., Kover, K. E., Holly, S., and Fasman, G. D. (1987) beta-Turns in serine-containing linear and cyclic models, *Biopolymers* 26, 1527-1553.
6. Bernal, J. D., and Crowfoot, D. (1934) X-Ray photographs of crystalline pepsin, *Nature* 133, 794-795.
7. Smyth, M. S., and Martin, J. H. J. (2000) X ray crystallography, *J. Clin. Pathol: Mol. Pathol.* 53, 8-14.
8. Drenth, J. (2007) *Principles of protein x-ray crystallography*, 3 ed., Springer Science and Business Media LLC, New York.
9. Wuthrich, K. (1986) *NMR of Proteins and Nucleic Acids*, Wiley, New York.
10. Clore, G. M., and Gronenborn, A. M. (1991) Two-, three-, and four-dimensional NMR methods for obtaining larger and more precise three-dimensional structures of proteins in solution, *Ann. Rev. Biophys. Biophys. Chem.* 20, 29-63.
11. Clore, G. M., and Gronenborn, A. M. (1991) Structures of larger proteins in solution: three- and four-dimensional heteronuclear NMR spectroscopy, *Science* 252, 1390-1399.
12. Alberts, B., Alexander, J., Julian, L., Martin, R., Keith, R., and Peter, W. (2002) *The Shape and Structure of Proteins*, Garland Science, New York and London.
13. Jeremy, M. B., John, L. T., and Lubert, S. (2002) *Protein Structure and Function*, W. H. Freeman, San Francisco.
14. Dennis, J. S. (2003) Folding proteins in fatal ways, *Nature* 426, 900-904.
15. Luheshi, L. M., Crowther, D. C., and Dobson, C. M. (2008) Protein misfolding and disease: from the test tube to the organism, *Chemical Biology* 12, 25-31.
16. Jackson, S. E. (1998) How do small single-domain proteins fold?, *Fold Des* 3, 81-91.
17. Kubelka, J., Hofrichter, J., and Eaton, W. A. (2004) The protein folding speed limit, *Curr. Opin. Struct. Biol.* 14, 76-88.
18. Levinthal, C. (1968) Are there pathways for protein folding?, *J. Chim. Phys.* 65, 44-45.
19. Dill, K. A., and Chan, H. S. (1997) From Levinthal to pathways to funnels,

- Nature Structural Biology* 4, 10-19.
20. Fersht, A. R. (2008) From the first protein structures to our current knowledge of protein folding: delights and scepticisms, *Nat Rev Mol Cell Biol.* 9, 650-654.
 21. Englander, S. W., Mayne, L., and Krishna, M. M. G. (2007) Protein folding and misfolding: mechanism and principles, *Q Rev Biophys* 40, 287-326.
 22. Ptitsyn, O. B. (1994) Kinetic and Equilibrium Intermediates in Protein Folding, *Protein Engineering* 7, 593-596.
 23. Ptitsyn, O. B. (1987) Protein Folding: Hypotheses and Experiments, *J. Protein Chem.* 6, 273-293.
 24. Agashe, V. R., Shastry, M. C. R., and Udgaonkar, J. B. (1995) Initial hydrophobic collapse in the folding of barstar, *Nature* 377, 754-757.
 25. Dolgikh, D. A., Gilmanshin, R. I., Brazhnikov, E. V., Bychkova, V. E., Semisotnov, G. V., Venyaminov, S. Y., and Ptitsyn, O. B. (1981) Alpha-lactalbumin: Compact State with Fluctuating Tertiary Structure?, *FEBS Lett.* 136, 311-315.
 26. Leopold, P. E., Montal, M., and Onuchic, J. N. (1992) Protein folding funnels: a kinetic approach to the sequence-structure relationship, *Proc. Natl. Acad. Sci.* 89, 8721-8725.
 27. Hartl, F. U., and Hayer-Hartl, M. (2009) Converging concepts of protein folding in vitro and in vivo, *Nat Struct Mol Biol.* 16, 574-581.
 28. Mamathambika, B. S., and Bardwell, J. C. (2008) Disulfide-linked protein folding pathways, *Annu. Rev. Cell Dev. Biol.* 24, 211-235.
 29. Tanford, C. (1980) *The Hydrophobic Effect. Formation of Micelles and Biological Membranes*, Wiley, New York, NY.
 30. Rahman, A., and Brown, C. W. (1983) Effect of pH on the critical micelle concentration of sodium dodecyl sulphate, *Journal of Applied Polymer Science* 28, 1331-1334.
 31. Otzen, D. (2011) Protein–surfactant interactions: A tale of many states, *Biochimica et Biophysica Acta* 1814, 562-591.
 32. Magdassi, S. (1996) *Surface activity of proteins-chemical and physicochemical modifications*, Marcel Dekker, Inc., New York, Basel, Hong Kong.
 33. White, S. H., Ladokhin, A. S., Jayasinghe, S., and Hristova, K. (2001) How Membranes Shape Protein Structure, *Journal of Biological Chemistry* 276, 32395-32398.
 34. Lowry, T. M. (1964) *Optical Rotary Power*, Dover, New York.
 35. Greenfield, N. J., and Fasman, G. D. (1969) Computed circular dichroism spectra for the evaluation of protein conformation, *Biochemistry* 8, 4108-4116.
 36. Sreerama, N., and Woody, R. W. (2000) *Circular Dichroism of Peptides and Proteins*, Wiley-VCH, New York.
 37. Berova, N., Nakanishi, K., and Woody, R. W. (2000) *Circular Dichroism Principles and Applications*, Wiley-VCH, New York.
 38. Ross, J. B. A., Laws, W. R., Rousslang, K. W., and Wyssbrod, H. R. (2002) *Topics in Fluorescence Spectroscopy*, Vol. 3, Springer US.
 39. Susi, H. (1972) Infrared Spectroscopy Conformation, *Methods Enzymol* 26,

- 455-472.
40. Stuart, B. H. (2000) *Infrared Spectroscopy of Biological Application*, John Wiley & Sons Ltd, Chichester.
 41. Ramer, G., and Lendl, B. (2013) *Attenuated Total Reflection Fourier Transform Infrared Spectroscopy. Encyclopedia of Analytical Chemistry.*, Wiley.
 42. Goormaghtigh, E., Raussens, V., and Ruyschaert, J.-M. (1999) Attenuated total reflection infrared spectroscopy of proteins and lipids in biological membranes, *Biochimica et Biophysica Acta 1422*, 105-185.
 43. Ryota, K., Inaka, K., Taniyama, Y., Kidokoro, S., Matsushima, M., Kikuchi, M., and Yutani, K. (1992) Enthalpic destabilization of a mutant human lysozyme lacking a disulfide bridge between cysteine-77 and cysteine-95, *Biochemistry 31*, 8323-8328.
 44. Radford, S. E., Woolfson, D. N., Martin, S. R., Lowe, G., and Dobson, C. M. (1991) A three-disulphide derivative of hen lysozyme. Structure, dynamics and stability., *Biochem J. 273*, 211-217.
 45. Privalov, P. L., Tiktopulo, E. I., Venyaminov, S. Y., Griko, Y. V., Makhatadze, G. I., and Khechinashvili, N. N. (1989) Heat capacity and conformation of proteins in the denatured state *J. Mol. Biol. 205*, 737-750.
 46. Creighton, T. E. (1988) Disulphide bonds and protein stability, *BioEssays 8*, 57-63.
 47. Creighton, T. E. (1975) Interactions between cysteine residues as probes of protein conformation: The disulphide bond between Cys-14 and Cys-38 of the pancreatic trypsin inhibitor, *J. Mol. Biol. 96*, 767-776.
 48. Jaenicke, R., and Buchner, J. (1993) Protein folding: From “unboiling an egg” to “catalysis of folding.”, *Chemtracts-Biochem. & Mol. Biol. 4*, 1-30.
 49. Goldberg, M. E., and Guillou, Y. (1994) Native disulfide bonds greatly accelerate secondary structure formation in the folding of lysozyme, *Protein Sci. 3*, 883-887.
 50. Jones, M. N., and Manley, P. (1980) Interaction between lysozyme and n-alkyl sulphates in aqueous solution., *J. Chem. Soc., Faraday Trans. 1 76*, 654–664.
 51. Gelamo, E. L., Silva, C. H. T. P., Imasato, H., and Tabak, M. (2002) Interaction of bovine (BSA) and human (HSA) serum albumins with ionic surfactants: spectroscopy and modelling, *Biochim. Biophys. Acta 1594*, 84-99.
 52. Gelamo, E. L., and Tabak, M. (2000) Spectroscopic studies on the interaction of bovine (BSA) and human (HSA) serum albumins with ionic surfactants, *Spectrochim. Acta A 56*, 2255-2271.
 53. Lapanje, S. (1978) *Physicochemical aspects of protein denaturation.*, Wiley Interscience Publications, New York
 54. Jones, M. N. (1975) *Biological interfaces: An introduction to the surface and colloid science of biochemical and biological system*, Elsevier Scientific Pub. Co., Amsterdam.
 55. Turro, N. J., Lei, X.-G., Ananthapadmanabhan, K. P., and Aronson, M. (1995) Spectroscopic probe analysis of protein-surfactant Interactions: The BSA/SDS system, *Langmuir 11*, 2525–2533.

56. Moriyama, Y., and Takeda, K. (1999) Re-formation of the helical structure of human serum albumin by the addition of small amounts of sodium dodecyl sulfate after the disruption of the structure by urea. A comparison with bovine serum albumin, *Langmuir* 15, 2003–2008.
57. Duggan, E. L., and Luck, J. M. (1948) The combination of organic anions with serum albumin: IV. Stabilization against urea denaturation, *J. Biol. Chem.* 172, 205-220.
58. Xu, Q., and Keiderling, T. A. (2006) Stop-flow kinetics studies of the interaction of surfactant, sodium dodecyl sulfate, with acid-denatured cytochrome c, *Proteins: Struct., Funct., Bioinf.* 63, 571–580.
59. Xu, Q., and Keiderling, T. A. (2004) Effect of sodium dodecyl sulfate on folding and thermal stability of acid-denatured cytochrome c: A spectroscopic approach, *Protein Sci.* 13, 2949–2959.
60. Ge, N., Zhang, X., and Keiderling, T. A. (2010) Kinetic studies of the interaction of β -Lactoglobulin with model membranes: Stopped-flow CD and fluorescence studies, *Biochemistry* 49, 8831-8838.
61. Zhang, X., and Keiderling, T. A. (2006) Lipid-Induced Conformational Transitions of β -Lactoglobulin, *Biochemistry* 45, 8444-8452.
62. Creamer, L. K. (1995) Effect of sodium dodecyl sulfate and palmitic acid on the equilibrium unfolding of bovine β -lactoglobulin, *Biochemistry* 34, 7170-7176.
63. Takeda, K., Takahashi, K., and Batra, P. P. (1985) Kinetic aspects of the interaction of horse heart cytochrome c with sodium dodecyl sulfate, *Arch. Biochem. Biophys.* 236, 411-417.
64. Das, T. K., Mazumdar, S., and Mitra, S. (1998) Characterization of a partially unfolded structure of cytochrome c induced by sodium dodecyl sulphate and the kinetics of its refolding., *Eur. J. Biochem.* 254, 662–670.
65. Wild, P., Gabrieli, A., Schraner, E. M., Pellegrini, A., Thomas, U., Frederik, P. M., Stuart, M. C. A., and Fellenberg, R. V. (1997) Reevaluation of the effect of lysozyme on *Escherichia coli* employing ultrarapid freezing followed by cryoelectronmicroscopy or freeze substitution, *Microsc. Res. Tech.* 39, 297–304.
66. Ibrahim, H. R., Higashiguchi, S., Koketsu, M., Juneja, L. R., Kim, M., Yamamoto, T., Sugimoto, Y., and Aoki, T. (1996) Partially unfolded lysozyme at neutral pH agglutinates and kills gram-negative and gram-positive bacteria through membrane damage mechanism, *J. Agric. Food Chem.* 44, 3799–3806.
67. Ibrahim, H. R., Higashiguchi, S., Juneja, L. R., Kim, M., and Yamamoto, T. (1996) A structural phase of heat-denatured lysozyme with novel antimicrobial action, *J. Agric. Food Chem.* 44, 1416–1423.
68. Ristow, S. S., and Wetlaufer, D. B. (1973) Evidence for nucleation in the folding of reduced hen egg lysozyme, *Biochem. Biophys. Res. Commun.* 50, 544-550.
69. Domínguez, A., Fernández, A., González, N., Iglesias, E., and Montenegro, L. (1997) Determination of Critical Micelle Concentration of Some Surfactants by Three Techniques, *J. Chem. Educ.* 74, 1227-1231.
70. Sreerama, N., and Woody, R. W. (2004) Computation and analysis of protein circular dichroism spectra, *Methods Enzymol* 383, 318-351.

71. Lad, M. D., Ledger, V. M., Briggs, B., Green, R. J., and Frazier, R. A. (2003) Analysis of the SDS-lysozyme binding isotherm, *Langmuir* 19, 5098-5103.
72. Huibers, P. D. T. (1999) Quantum-chemical calculations of the charge distribution in ionic surfactants, *Langmuir* 15, 7546–7550.
73. Rashid, F., Sharma, S., Baig, M. A., and Bano, B. (2006) Molten globule state of human placental cystatin (HPC) at low pH conditions and the effects of trifluoroethanol (TFE) and methanol, *Biochem. Cell Biol.* 84, 126-134.
74. Gast, K., Zirwer, D., Müller-Frohne, M., and Damaschun, G. (1999) Trifluoroethanol-induced conformational transitions of proteins: Insights gained from the differences between α -lactalbumin and ribonuclease A, *Protein Sci.* 8, 625-634.
75. Buck, M., Schwalbe, H., and Dobson, C. M. (1995) Characterization of conformational preferences in a partly folded protein by heteronuclear NMR spectroscopy: Assignment and secondary structure analysis of hen egg-white lysozyme in trifluoroethanol, *Biochemistry* 34, 13219-13232.
76. Buck, M., Radford, S. E., and Dobson, C. M. (1993) A partially folded state of hen egg white lysozyme in trifluoroethanol: structural characterization and implications for protein folding, *Biochemistry* 32, 669-678.
77. Ohgushi, M., and Wada, A. (1983) 'Molten-globule state': a compact form of globular proteins with mobile side-chains, *FEBS Lett.* 164, 21-24.
78. Buswell, A. M., and Middelberg, A. P. J. (2002) Critical Analysis of Lysozyme Refolding Kinetics, *Biotechnol. Prog.* 18, 470-475.
79. Roux, P., Delepierre, M., Goldberg, M. E., and Chaffotte, A.-F. (1997) Kinetics of Secondary Structure Recovery during the Refolding of Reduced Hen Egg White Lysozyme, *J. Biol. Chem.* 272, 24843-24849.
80. Raman, B., Ramakrishna, T., and Rao, C. M. (1996) Refolding of Denatured and Denatured/Reduced Lysozyme at High Concentrations, *J. Biol. Chem.* 271, 17067-17072.
81. Acharya, A. S., and Taniuchi, H. (1977) Formation of the four isomers of hen egg white lysozyme containing three native disulfide bonds and one open disulfide bond, *Proc. Natl. Acad. Sci.* 74, 2362-2366.
82. Zhu, W., and Keiderling, T. A. (2013) Interaction of reduced lysozyme with surfactants. Disulfide effects on reformed structure in micelles, *Biochimica et Biophysica Acta* 1834, 593-600.
83. Guez, V., Roux, P., Navon, A., and Goldberg, M. E. (2002) Role of individual disulfide bonds in hen lysozyme early folding steps, *Protein Science* 11, 1136-1151.
84. Chong, S. Y., Taneva, S. G., Lee, J. M. C., and Cornell, R. B. (2014) The Curvature Sensitivity of a Membrane-Binding Amphipathic Helix Can Be Modulated by the Charge on a Flanking Region, *Biochemistry* 53, 450-461.
85. Bertassoni, L. E., Orgel, J. P. R., Antipova, O., and Swain, M. V. (2012) The dentin organic matrix - limitations of restorative dentistry hidden on the nanometer scale, *Acta Biomaterialia* 8, 2419-2433.
86. Orgel, J. P. R. O., C., I. T., Miller, A., and Wess, T. J. (2006) Microfibrillar

- structure of type I collagen in situ, *Proc Natl Acad Sci U S A* 103, 9001-9005.
87. Knott, L., and Bailey, A. J. (1998) Collagen cross-links in mineralizing tissues: a review of their chemistry, function, and clinical relevance, *Bone* 22, 181-187.
 88. Rivera, E. M., and Yamauchi, M. (1993) Site comparisons of dentine collagen cross-links from extracted human teeth, *Archives of Oral Biology* 38, 541-546.
 89. Bedran-Russo, A. K., Castellan, C. S., Shinohara, M. S., Hassan, L., and Antunes, A. (2011) Characterization of biomodified dentin matrices for potential preventive and reparative therapies, *Acta Biomaterialia* 7, 1735-1741.
 90. Castellan, C. S., Pereira, P. N., Grande, R. H. M., and Bedran-Russo, A. K. (2010) Mechanical characterization of proanthocyanidin-dentin matrix interaction, *Dental Materials* 26, 968-973.
 91. Bedran-Russo, A. K. B., Vidal, C. M. P., Dos Santos, P. H., and Castellan, C. S. (2010) Long-term effect of carbodiimide on dentin matrix and resin-dentin bonds, *Journal of Biomedical Materials Research Part B: Applied Biomaterials* 94, 250-255.
 92. Bedran-Russo, A. K. B., Pashley, D. H., Agee, K., Drummond, J. L., and Miescke, K. J. (2008) Changes in stiffness of demineralized dentin following application of collagen crosslinkers, *Journal of Biomedical Materials Research Part B: Applied Biomaterials* 86, 330-334.
 93. Sung, H.-W., Chang, W.-H., Ma, C.-Y., and Lee, M.-H. (2003) Crosslinking of biological tissues using genipin and/or carbodiimide, *Journal of Biomedical Materials Research Part A* 64, 427-438.
 94. Han, B., Jaurequi, J., Tang, B. W., and Nimni, M. E. (2003) Proanthocyanidin: a natural crosslinking reagent for stabilizing collagen matrices, *Journal of Biomedical Materials Research Part A* 65, 118-124.
 95. Damink, L. H. H. O., Dijkstra, P. J., van Luyn, M. J. A., van Wachem, P. B., Nieuwenhuis, P., and Feijen, J. (1996) Cross-linking of dermal sheep collagen using a water-soluble carbodiimide, *Biomaterials* 17, 765-773.
 96. Aguiar, T. R., Vidal, C. M. P., Phansalkar, R. S., Todorova, I., Napolitano, J. G., McAlpine, J. B., Chen, S. N., Pauli, G. F., and Bedran-Russo, A. K. (2014) Dentin Biomodification Potential Depends on Polyphenol Source, *J Dent Res* 93, 417-422.
 97. Liu, Y., Chen, M., Yao, X., Xu, C., Zhang, Y., and Wang, Y. (2013) Enhancement in dentin collagen's biological stability after proanthocyanidins treatment in clinically relevant time periods, *Dental Materials* 29, 485-492.
 98. He, L., Mu, C., Shi, J., Zhang, Q., Shi, B., and Lin, W. (2011) Modification of collagen with a natural cross-linker, procyanidin, *International Journal of Biological Macromolecules* 48, 354-359.
 99. Siebert, K. J. (1999) Effects of protein-polyphenol interactions on beverage haze, stabilization, and analysis, *J. Agric. Food Chem.* 47, 353-362.
 100. Spencer, C. M., Cai, Y., Martin, R., Gaffney, S. H., Goulding, P. N., Magnolato, D., Lilley, T. H., and Haslam, E. (1988) Polyphenol complexation-some thoughts and observations, *Phytochemistry* 27, 2397-2409.
 101. Nuytinck, L., Tukel, T., Kayserili, H., Apak, M. Y., and Paepe, A. D. (2000)

- Glycine to tryptophan substitution in type I collagen in a patient with OI type III: a unique collagen mutation, *J Med Genet* 37, 371-375.
102. Eastoe, J. E. (1955) The amino acid composition of mammalian collagen and gelatin, *Biochem J.* 61, 589-600.
 103. Quideau, S., Deffieux, D., Douat-Casassus, C., and Pouységu, L. (2011) Plant polyphenols: chemical properties, biological activities, and synthesis, *Angewandte Chemie International Edition* 50, 586-621.
 104. Lutz, V., attler, M. S., Gallinat, S., Wenck, H., Poertner, R., and Fischer, F. (2012) Impact of collagen crosslinking on the second harmonic generation signal and the fluorescence lifetime of collagen autofluorescence, *Skin Research and Technology* 18, 168-179.
 105. Liu, Y., and Wang, Y. (2013) Proanthocyanidins' efficacy in stabilizing dentin collagen against enzymatic degradation: MALDI-TOF and FTIR analyses, *J Dent* 41, 535-542.
 106. Canon, F., Giuliani, A., Paté, F., and Sarni-Manchado, P. (2010) Ability of a salivary intrinsically unstructured protein to bind different tannin targets revealed by mass spectrometry, *Analytical and Bioanalytical Chemistry* 398, 815-822.
 107. Hagerman, A. E., Rice, M. E., and Ritchard, N. T. (1998) Mechanisms of Protein Precipitation for Two Tannins, Pentagalloyl Glucose and Epicatechin₁₆ (4→8) Catechin (Procyanidin), *J. Agric. Food Chem.* 46, 2590-2595.
 108. Baxter, N. J., Lilley, T. H., Haslam, E., and Williamson, M. P. (1997) Multiple interactions between polyphenols and a salivary proline-rich protein repeat result in complexation and precipitation, *Biochemistry* 36, 5566-5577.
 109. Zeeman, R., Dijkstra, P. J., van Wachem, P. B., van Luyn, M. J. A., Hendriks, M., Cahalan, P. T., and Feijen, J. (1999) Successive epoxy and carbodiimide cross-linking of dermal sheep collagen, *Biomaterials* 20, 921-931.
 110. Everaerts, F., Torrianni, M., Hendriks, M., and Feijen, J. (2008) Biomechanical properties of carbodiimide crosslinked collagen: influence of the formation of ester crosslinks, *Journal of Biomedical Materials Research Part A* 85, 547-555.
 111. Socrates, G. (2004) *Infrared and Raman characteristic group frequencies: tables and charts*, 3 ed., John Wiley and Sons, Ltd.
 112. Gratzer, P. F., and Lee, J. M. (2001) Control of pH alters the type of cross-linking produced by 1-ethyl-3-(3-dimethylaminopropyl)-carbodiimide (EDC) treatment of acellular matrix vascular grafts, *Journal of Biomedical Materials Research* 58, 172-179.

APPENDIX

LICENSE PERMISSION

ELSEVIER LICENSE
TERMS AND CONDITIONS

Oct 21, 2015

This is a License Agreement between WEIYING ZHU ("You") and Elsevier ("Elsevier") provided by Copyright Clearance Center ("CCC"). The license consists of your order details, the terms and conditions provided by Elsevier, and the payment terms and conditions.

All payments must be made in full to CCC. For payment instructions, please see information listed at the bottom of this form.

Supplier	Elsevier Limited The Boulevard, Langford Lane Kidlington, Oxford, OX5 1GB, UK
Registered Company Number	1982084
Customer name	WEIYING ZHU
Customer address	933 W 32ND ST CHICAGO, IL 60608
License number	3733841216971
License date	Oct 21, 2015
Licensed content publisher	Elsevier
Licensed content publication	Biochimica et Biophysica Acta (BBA) - Proteins and Proteomics
Licensed content title	Interaction of reduced lysozyme with surfactants Disulfide effects on reformed structure in micelles
Licensed content author	Weiyong Zhu, Timothy A. Keiderling
Licensed content date	February 2013
Licensed content volume number	1834
Licensed content issue number	2
Number of pages	8
Start Page	593
End Page	600
Type of Use	reuse in a thesis/dissertation
Portion	full article
Format	both print and electronic
Are you the author of this Elsevier article?	Yes
Will you be translating?	No
Title of your thesis/dissertation	Spectroscopic Studies on Refolding of Reduced and Mutant Lysozymes, and Collagen/Dentin Crosslinking

APPENDIX (CONTINUED)

Expected completion date	Feb 2016
Estimated size (number of pages)	147
Elsevier VAT number	GB 494 6272 12
Permissions price	0.00 USD
VAT/Local Sales Tax	0.00 USD / 0.00 GBP
Total	0.00 USD
Terms and Conditions	

INTRODUCTION

1. The publisher for this copyrighted material is Elsevier. By clicking "accept" in connection with completing this licensing transaction, you agree that the following terms and conditions apply to this transaction (along with the Billing and Payment terms and conditions established by Copyright Clearance Center, Inc. ("CCC"), at the time that you opened your Rightslink account and that are available at any time at <http://myaccount.copyright.com>).

GENERAL TERMS

2. Elsevier hereby grants you permission to reproduce the aforementioned material subject to the terms and conditions indicated.
3. Acknowledgement: If any part of the material to be used (for example, figures) has appeared in our publication with credit or acknowledgement to another source, permission must also be sought from that source. If such permission is not obtained then that material may not be included in your publication/copies. Suitable acknowledgement to the source must be made, either as a footnote or in a reference list at the end of your publication, as follows:
 "Reprinted from Publication title, Vol /edition number, Author(s), Title of article / title of chapter, Pages No., Copyright (Year), with permission from Elsevier [OR APPLICABLE SOCIETY COPYRIGHT OWNER]." Also Lancet special credit -
 "Reprinted from The Lancet, Vol. number, Author(s), Title of article, Pages No., Copyright (Year), with permission from Elsevier."
4. Reproduction of this material is confined to the purpose and/or media for which permission is hereby given.
5. Altering/Modifying Material: Not Permitted. However figures and illustrations may be altered/adapted minimally to serve your work. Any other abbreviations, additions, deletions and/or any other alterations shall be made only with prior written authorization of Elsevier Ltd. (Please contact Elsevier at permissions@elsevier.com)
6. If the permission fee for the requested use of our material is waived in this instance, please be advised that your future requests for Elsevier materials may attract a fee.
7. Reservation of Rights: Publisher reserves all rights not specifically granted in the combination of (i) the license details provided by you and accepted in the course of this licensing transaction, (ii) these terms and conditions and (iii) CCC's Billing and Payment terms and conditions.
8. License Contingent Upon Payment: While you may exercise the rights licensed immediately upon issuance of the license at the end of the licensing process for the transaction, provided that you have disclosed complete and accurate details of your proposed use, no license is finally effective unless and until full payment is received from you (either by publisher or by CCC) as provided in CCC's Billing and Payment

VITA

NAME: Weiyong Zhu

EDUCATION: B.S., Chemistry, Peking University, Beijing, China, 2006
M.S., Chemistry, University of Illinois at Chicago, Chicago, IL 2011
Ph.D., Chemistry, University of Illinois at Chicago, Chicago, IL 2015

PROFESSIONAL
MEMBERSHIP: Society of Applied Spectroscopy

PUBLICATIONS: “Refolding of reduced and mutant lysozymes in vesicles. Impact of disulfide effects on refolding equilibria and dynamics”, Weiyong Zhu, Timothy A. Keiderling, Robert Silvers and Harald Schwalbe. (submitted)

“Collagen-collagen interactions mediated by plant-derived proanthocyanidins: a spectroscopic and atomic force microscopy study”, Cristina M. P. Vidal, Weiyong Zhu, Suresh Manohar, Berdan Aydin, Timothy Keiderling, Phillip B. Messersmith and Ana Bedran-Russo. (under review of *Acta Biomaterialia*)

“Interaction of reduced lysozyme with surfactants: Disulfide effects on reformed structure in micelles”, Weiyong Zhu and Timothy A. Keiderling. *Biochimica et Biophysica Acta*, 2013, 1834, 593–600

POSTER
PRESENTATION: "The effects of micelles, vesicles and lipids on the structure of reduced lysozyme", Weiyong Zhu and Timothy Keiderling, 5th Midwest Conference on Protein Folding, Assembly and Molecular Motions (2010)